

LEO SATELLITES: DYNAMIC MODELLING, SIMULATIONS AND SOME
NONLINEAR ATTITUDE CONTROL TECHNIQUES

A THESIS SUBMITTED TO
THE GRADUATE SCHOOL OF NATURAL AND APPLIED SCIENCES
OF
MIDDLE EAST TECHNICAL UNIVERSITY

BY

SONER KARATAŞ

IN PARTIAL FULFILLMENT OF THE REQUIREMENTS
FOR THE DEGREE OF MASTER OF SCIENCE
IN
ELECTRICAL AND ELECTRONICS ENGINEERING

APRIL 2006

Approval of the Graduate School of Natural and Applied Sciences.

Prof. Dr. Canan ÖZGEN
Director

I certify that this thesis satisfies all the requirements as a thesis for the degree of Master of Science.

Prof. Dr. İsmet ERKMEN
Head of Department

This is to certify that we have read this thesis and that in our opinion it is fully adequate, in scope and quality, as a thesis for the degree of Master of Science

Prof. Dr. Erol KOCAOĞLAN
Supervisor

Examining Committee Members

Prof. Dr. Kemal LEBLEBİCİOĞLU	(METU,EE)	_____
Prof. Dr. Erol KOCAOĞLAN	(METU,EE)	_____
Prof. Dr. Mübeccel DEMİREKLER	(METU,EE)	_____
Prof. Dr. Aydan ERKMEN	(METU,EE)	_____
Gökhan YÜKSEL M.Sc.	(BILTEN)	_____

I hereby declare that all information in this document has been obtained and presented in accordance with academic rules and ethical conduct. I also declare that, as required by these rules and conduct, I have fully cited and referenced all material and results that are not original to this work.

Name, Last name : Soner KARATAŞ

Signature :

ABSTRACT

LEO SATELLITES: DYNAMIC MODELLING, SIMULATIONS AND SOME NONLINEAR ATTITUDE CONTROL TECHNIQUES

KARATAŞ, Soner

Msc., Department of Electrical and Electronics Engineering

Supervisor : Prof. Dr. Erol KOCAOĞLAN

April 2006, 95 pages

In this thesis nonlinear control method techniques are investigated to control the attitude of Low Earth Orbit satellites. Nonlinear control methods are compared with linear control methods. Simulations are done using Matlab and Simulink software and BILSAT-1 parameters are used in the simulations. Reaction wheels are used as the actuator.

Keywords: Attitude Control, Satellite, LEO, BILSAT-1

ÖZ

ALÇAK YÖRÜNGE UYDULARI : DİNAMİK MODELLEME,
SİMÜLASYONLAR VE KİMİ DOĞRUSAL OLMAYAN KONUM DENETİM
TEKNİKLERİ

KARATAŞ, Soner

Yüksek Lisans, Elektrik-Elektronik Mühendisliği Bölümü

Tez Yöneticisi : Prof. Dr. Erol KOCAOĞLAN

Nisan 2006, 95 sayfa

Bu tezde düşük yörüngeli bir uydunun davranış hareketini kontrol etmek amacıyla doğrusal olmayan denetleçlerin sistem üzerindeki etkisi incelenmiştir. Bu bağlamda elde edilen doğrusal olmayan denetleçlerin performansları doğrusal denetleçler kullanılarak elde edilenlerle karşılaştırılmıştır. Benzetimler Matlab ve Simulink yazılımları ile yapılmış olup BILSAT-1 uydusunun parametreleri uygulanmıştır. Tetikleyici olarak tepki tekerleri kullanılmıştır.

Anahtar Kelimeler: Davranış Denetimi, Uydu, Düşük Yörünge Uydusu, BILSAT-1

ACKNOWLEDGEMENTS

The author wishes to express his deepest gratitude to his supervisor Prof. Dr. Erol KOCAOĞLAN and Gökhan YUKSEL (M.Sc., BILTEN-TUBITAK) for their guidance, advices, criticism, encouragements and insight throughout the study.

TABLE OF CONTENTS

PLAGIARISM	iii
ABSTRACT	iv
ÖZ	v
ACKNOWLEDGEMENTS	vi
TABLE OF CONTENTS	vii
LIST OF TABLES	x
LIST OF FIGURES	xi
GLOSSARY	xiii
ABBREVIATIONS	xiv

CHAPTER 1)- INTRODUCTION

1.1 Background	1
1.2 Literature Survey	2
1.3 BILSAT-1	2
1.4 This Report	5
1.5 Contributions Of This Thesis	5
1.6 Outline Of The Thesis	6
1.7 Tools	6

CHAPTER 2)- SENSORS AND ACTUATORS OF BILSAT-1

2.1 Sensors	8
2.1.1 Sun Sensor.....	8
2.1.2 Magnetometer.....	8
2.1.3 Star Camera.....	9
2.1.4 Gyroscope.....	10
2.1.5 Sensor Summary.....	10
2.2 Actuators	11
2.2.1 Reaction Wheels	11

2.2.2 Magnetic Torquers.....	11
2.2.3 Gravity Gradient Boom.....	12
2.2.4 Actuator Summary.....	13

CHAPTER 3)- DEFINITIONS AND NOTATIONS

3.1 Reference Frames	14
3.1.1 Earth Centered Inertia Frame.....	14
3.1.2 Earth Centered Earth Fixed Frame.....	15
3.1.3 Orbit Frame.....	16
3.1.4 Body Frame.....	16
3.2 Rotation Matrix	17
3.3 Angular Velocity	18
3.4 Attitude Representation	19
3.4.1 Euler Angles	20
3.4.2 Unit Quaternions.....	22
3.5 The Inertia Matrix	24

CHAPTER 4)- MATHEMATICAL MODELLING

4.1 Satellite Model	25
4.1.1 Dynamics For Satellite Model.....	25
4.1.2 Kinematics For Satellite Model.....	28
4.2 Magnetic Torque	29
4.3 Reaction Wheel Torque	30
4.4 Gravity Gradient Torque	31
4.5 Disturbance Torques	33
4.5.1 Solar Radiation.....	33
4.5.2 Aerodynamic Torque.....	34
4.6 Reference Model	34

CHAPTER 5)- MODELLING OF REACTION WHEELS

5.1 Control Allocation	36
5.2 Control Allocation For Satellite	37

5.3 Configuration Of Reaction Wheels	38
CHAPTER 6)- CONTROLLER DESIGN AND SIMULATIONS	
6.1 Quaternion Feedback Controller	41
6.1.1 Stabilization Analysis.....	42
6.1.2 Energy Considerations.....	42
6.1.2.1 Kinetic Energy.....	42
6.1.2.2 Potential Energy	42
6.1.2.3 Total Energy	43
6.2 Sliding Mode Regulator	45
6.3 Simulations.....	48
6.3.1 Quaternion Feedback Controller.....	48
6.3.2 Sliding Mode Regulator.....	54
6.3.3 Actual Results Taken From Tübitak-Bilten For BILSAT-1.....	62
CHAPTER 7)- CONCLUSIONS AND FUTURE WORK	64
REFERENCES.....	67
APPENDIX A – SIMULINK DIAGRAMS.....	69
APPENDIX B – MATLAB SOURCE CODES.....	84
APPENDIX C – TETRAHEDRAL CONFIGURATION ANGLE.....	94

LIST OF TABLES

Table – 2.1 Comparison table of attitude determination sensors.....	10
Table – 2.2 Comparison table of attitude control actuators	13
Table – 3.1 Comparison table of attitude representation	20
Table – 4.1 Effect of ω_n on system response.....	35
Table – 6.1 General BILSAT-1 parameters.....	48
Table – 6.2 Simulation parameters of Quaternion Feedback Controller.....	48
Table – 6.3 Simulation parameters of the Sliding Mode Regulator.....	54
Table – 6.4 Time and command table for the BILSAT-1.....	62
Table – 7.1 Simulation result of controllers.....	65

LIST OF FIGURES

Figure – 1.1 Project team of BILSAT-1	3
Figure – 1.2 General view of BILSAT-1.....	3
Figure – 1.3 BILSAT-1 was launched in Russia	3
Figure – 1.4 Block diagram of BILSAT-1.....	4
Figure – 1.5 Block diagram of ADCS	4
Figure – 1.6 Image of BILSAT-1 from Manyas Lake , Ulubat Lake Bandirma Turkey	5
Figure – 2.1 Block diagram of ADCS	7
Figure – 2.2 Processing unit of star camera	9
Figure – 2.3 Star camera head	9
Figure – 2.4 Reaction Wheels in a tetrahedral configuration	11
Figure – 2.5 Slewing about pitch axis	11
Figure – 2.6 Stowed Boom	12
Figure – 2.7 Deployed Boom	12
Figure – 3.1 Earth-Centered Inertial (ECI) frame	15
Figure – 3.2 ECEF and ECI frames	15
Figure – 3.3 Orbit frame	16
Figure – 3.4 Body frame	16
Figure – 3.5 Euler Angles.....	21
Figure – 4.1 Translational Motion.....	28
Figure – 4.2 Gravity gradient parameters.....	31
Figure – 5.1 General Control Design For Reaction Wheels.....	36
Figure – 5.2 Tetrahedral Configuration Of Reaction Wheels.....	38
Figure – 6.1 Functions.....	47
Figure – 6.2 System response of QFC without noise.....	49

Figure – 6.3 Output from regulator and wheels without noise	49
Figure – 6.4 System response for QFC with noise.....	50
Figure – 6.5 Output from regulator and wheels with noise.....	50
Figure – 6.6 System response for the QFC without noise and reaction Wheel-2 was disabled	51
Figure – 6.7 Output from regulator and wheels without noise and reaction Wheel-2 was disabled.....	51
Figure – 6.8 System response for the QFC without noise and reaction wheels-2, 4 were disabled.....	52
Figure – 6.9 Output from regulator and wheels without noise and reaction wheels-2, 4 were disabled.....	52
Figure – 6.10 System response for the QFC without noise and desired euler angles are $[\phi \ \theta \ \psi]=[0 \ 30 \ 0]$	53
Figure – 6.11 Output from regulator and wheels without noise desired euler angles are $[\phi \ \theta \ \psi]=[0 \ 30 \ 0]$	53
Figure – 6.12 System response for the SMR without noise.....	55
Figure – 6.13 Output from regulator and wheels without noise.....	55
Figure – 6.14 System response for the sliding mode regulator with noise.....	56
Figure – 6.15 Output from regulator and wheels with noise	56
Figure – 6.16 System response for the SMR without noise and reaction Wheel-2 was disabled.....	57
Figure – 6.17 Output from regulator and wheels without noise and reaction Wheel-2 was disabled.....	57
Figure – 6.18 System response for the sliding mode regulator without noise and reaction wheel-2, 4 were disabled.....	58
Figure – 6.19 Output from regulator and wheels without noise and reaction Wheel-2, 4 were disabled.....	58
Figure – 6.20 System response for the sliding mode regulator without noise and desired euler angles are $[\phi \ \theta \ \psi]=[0 \ 30 \ 0]$	59
Figure – 6.21 Output from regulator and wheels without noise desired euler angles are $[\phi \ \theta \ \psi]=[0 \ 30 \ 0]$	59
Figure – 6.22 System response of SMR without aerodynamic torque.....	60

Figure – 6.23 Output from regulator and wheels without aerodynamic torque...	60
Figure – 6.24 System response of SMR with $K = 2 * 1_{3 \times 3}$	61
Figure – 6.25 Output from regulator and wheels with $K = 2 * 1_{3 \times 3}$	61
Figure – 6.26 Actual pitch axis maneuver of BILSAT-1	62
Figure – 6.27 Actual pitch axis maneuver of BILSAT-1 (Zoomed).....	63

GLOSSARY

Space Terminology

- **Apogee** is the point at which a satellite in orbit around the Earth reaches its farthest distance from the Earth.
- **Attitude** of a spacecraft is its orientation in a certain coordinate system.
- **Center of Mass** is a point in an isolated system that moves at a constant velocity in accordance to Newton's laws of motion
- **Eclipse** is a transit of the Earth in front of the Sun, blocking all or a significant part of the Sun's radiation.
- **Ecliptic** is the mean plane of the Earth's orbit around the Sun.
- **Ellipse** is a shape that looks like a squashed circle that is produced by cutting a cone at an angle.
- **Gravity** is a property of matter which produces a mutual attraction between all the bodies present.
- **Latitude** is the angular distance on the Earth measured north or south of the equator along the meridian of a satellite location.
- **Longitude** is the angular distance measured along the Earth's equator from the Greenwich meridian to the meridian of a satellite location.
- **Orbit** is the path that an astronomical body follows as it moves around another astronomical body.
- **Orbital rate** is the mean angular velocity of the satellite rotation about the Earth.
- **Roll, Pitch and Yaw** are the angles describing satellite attitude. Roll is referred to the rotation about the x-axis of a reference coordinate system, pitch to the y-axis, and yaw to the z-axis.
- **Perigee** is the point at which a satellite in orbit around the Earth most closely approaches the Earth.
- **Vernal Equinox** is the point where the ecliptic crosses the Earth equator going from South to north.

ABBREVIATIONS

ACS	Attitude Control Subsystem
ADCS	Attitude Determination Control System
BILTEN	Information Technologies and Electronics Research Institute
CS	Coordinate System
COBAN	Imaging system developed and added as payload to BILSAT-1 by BILTEN.
DEM	Digital Elevation Map
ECI	Earth Centered Inertial Frame
ECEF	Earth Centered Earth Fixed Frame
GEZGIN	Image Compression and Data Processing Card produced by BILTEN
GPS	Global Positioning System
IAGA	International Association of Geomagnetism and Aeronomy
IGRF	International Geomagnetic Reference Field
LEO	Low Earth Orbit
METU	Middle East Technical University
NTNU	Norwegian University of Science and Technology
OBC	On-Board Computer
QFC	Quaternion Feedback Controller
SMR	Sliding Mode Regulator
SSDR	Solid State Data Recorder
SSTL	Surrey Satellite Technology Limited
TUBITAK	The Scientific And Technological Research Council Of Turkey
UHF	Ultra High Frequency
VHF	Very High Frequency
rpm	Revolutions Per Minute
w.r.t	With Respect To

CHAPTER 1

INTRODUCTION

In this chapter, information about satellites ADCS systems, literature survey on attitude controller types and information about BILSAT-1 satellite are briefly introduced. Properties of BILSAT-1 project are presented. Furthermore, the work done in this Master thesis is introduced. Finally, the outline of the thesis is given.

1.1 Background

Attitude control is required for nearly all space missions. Mission objectives of satellites may be severely disrupted without correct attitude control. The attitude control consists of two areas called attitude stabilization and attitude maneuver control. The first is the process of maintaining an existing orientation, while the latter has to do with controlling the reorientation of the spacecraft from one attitude to another.

This thesis describes the design, analysis and development of attitude control systems for the Low Earth Orbit (LEO) satellites. The purpose of this thesis is to apply nonlinear control methods to control the attitude maneuver of a Low Earth Orbit (LEO) satellite using reaction wheels and compare their performance with those of linear controller. The nonlinear mathematical model of a satellite is derived, and BILSAT-1's parameters are used in this model in realizing the simulations.

In recent years there has been an increasing interest in space-related activities in Turkey. It is hoped that this thesis will contribute to increase the already existing knowledge and interest in satellites.

1.2 Literature Survey

This section presents the recent literature on attitude dynamics and control of satellites. Wertz, Hughes (1986) and Wie (1998) are standard references on spacecraft dynamics. Concerning attitude control of spacecraft, Wie, Weiss and Arapostathis (1989) show that a PD controller stabilizes a spacecraft. Hall (2000) has studied spacecraft attitude control using several reaction wheels as actuators. The use of Euler parameters or unit quaternions in attitude control problems is treated by Fjellstad and Fossen (1994), but the results are applied to underwater vehicles. Derman (1999) has developed PD controller and linear state feedback controller for the TURKSAT-1B using thrusters. Based on the methods of Musser and Ebert, and Wisniewski, magnetic control laws using both a proportional-derivative controller and linear quadratic regulator have been developed by Makovec, (2001). Ytrehus (2003) has investigated linear and non-linear control techniques on NSAT when reaction wheels were chosen as actuator. Fauske (2003) has studied feedback stabilization of the attitude. A time varying periodic controller has been proposed for the angular velocity stabilization problem by Fauske. Topland (2004) has developed linear and nonlinear controller methods of ESEO spacecraft using thrusters and reaction wheels. Three of four nonlinear controllers rely on cancellation of system nonlinearities, while the fourth is a sliding mode controller. Overby (2004) has developed energy based controllers and linear quadratic controller methods of NCUBE satellite using magnetic coils. The stability analysis of the nonlinear controller was performed using energy considerations and Lyapunov methods by Overby. Uslu (1997), Bak (1999), Ose (2004) and Svartveit (2003) have worked on attitude determination of the satellites.

1.3 BILSAT-1

BILSAT-1 is the first Low Earth Orbit (LEO) satellite of Turkey. Project was started in August 2001 within the framework of an agreement between Surrey Satellite Technology Limited (SSTL) and The Scientific and Technological Research Council of Turkey (TUBITAK-BILTEN). The BILSAT-1 microsatellite was launched from Russia on September 27, 2003, into an orbit of 686km distance from the surface of the Earth. The spacecraft is a highly optimized satellite with a mass of 129 kg. BILSAT-1 has an average orbit period of about 97.7 minutes. This orbit

gives the Turkish ground station and the satellite a contact time of about 10 minutes per pass, with an average of four passes per day.

BILSAT-1 project had many aims. They are design, manufacture and launch of one Enhanced SSTL microsatellite platform, one engineering model for use in Turkey and the training of engineers in all aspects of the spacecraft design. Remote sensing is the main mission of the BILSAT-1. To prepare a Digital Elevation Map (DEM) of Turkey is one of the aims of the project team. To realize this mission objective, it is aimed to take as many pictures of Turkey as possible.



Figure-1.1: Project team of BILSAT-1

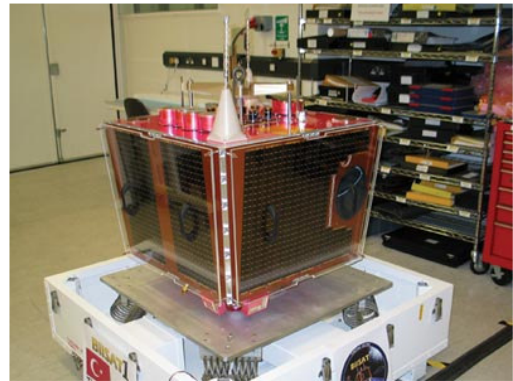


Figure-1.2: General view of BILSAT-1



Figure-1.3: BILSAT-1 was launched from Russia

The spacecraft consists of different units. Imager unit is the main payload and is used for remote sensing. For this aim BILSAT-1 uses two imagers, Pan-chromatic and Multispectral imagers. The multispectral imager is composed of four individual cameras with a ground sampling distance of 26 m. The panchromatic camera has a ground sampling distance of 12 m. Attitude Determination and Control Subsystem (ADCS) unit includes sun sensors, rate sensors, magnetometers, GPS receiver and star trackers for attitude determination, gravity gradient boom, torque rods and reaction wheels for attitude control. UHF/VHF system and an S-band system constitute the communication unit of BILSAT-1. On-Board Computers (OBC) unit consists of three main components. They are one Intel 80186 based OBC (16 MB of memory) and two Intel 80386 based OBC (32 MB of memory each). Two solid state data recorders (SSDRs) are used for storing large amounts of data on board. Body-mounted solar panels supply the needed power of BILSAT-1. To connect different subsystems of the spacecraft CAN (Control Array Network) network is used.

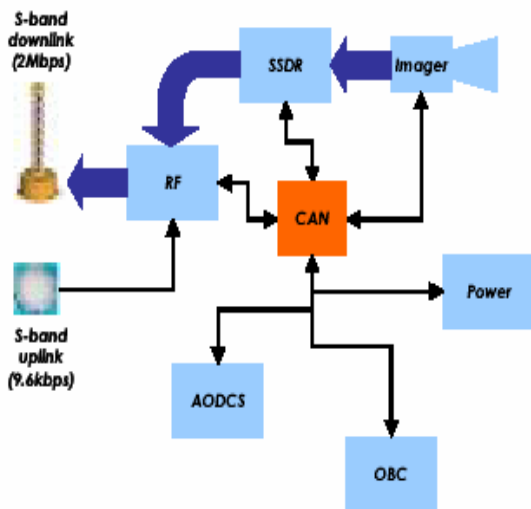


Figure-1.4: Block diagram of BILSAT-1

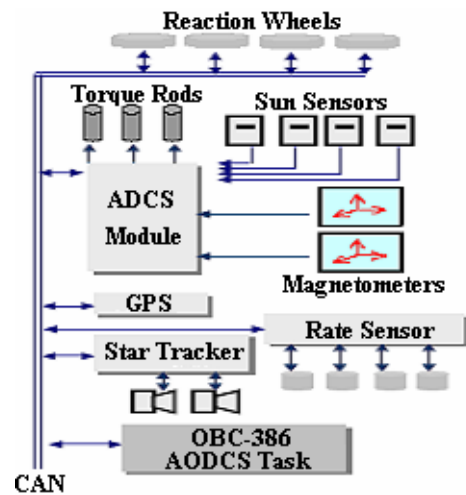


Figure-1.5: Block diagram of ADCS

The pictures taken from the satellite are used for study in miscellaneous areas like disaster monitoring, monitoring the urban areas and vegetation. BILSAT-1 also accommodates a store and forward type communications payload. As a part of the know how training and transfer (KHTT) programme, a multi spectral camera (COBAN) and a real time JPEG2000 image compression DSP (Digital Signal Processing) card (GEZGIN) were developed by Turkish engineers to be accommodated on the satellite.



Figure-1.6: Image of BILSAT-1 from Manyas Lake, Ulubat Lake Bandirma Turkey

Further information on BILSAT-1 can be found in references [1] and [2].

1.4 This Report

Attitude control (angular orientation) is needed so that the optical system covers the programmed ground area at all times. However, the satellite tends to change its orientation due to torque produced by the environment (drag of the residual atmosphere on the solar array, solar radiation pressure, etc.) or by itself (due to movement of mechanical parts, etc.). In this thesis some nonlinear controller methods which are suitable for BILSAT-1 are studied. Applications of nonlinear control methods are given and the results obtained are compared with linear method which is presented in the Ceren Kaplan's master thesis [20]. Finally conclusion of the thesis is given and suggestions for future work are presented.

1.5 Contributions of this Thesis

- An extensive list of references on the subject of attitude determination and control of satellites are compiled. This will serve as an excellent starting point for further study.
- An other contribution of this thesis is the complete design, implementation and test of an attitude control system for a low orbit satellite.
- Attitude dynamics of LEO satellites are investigated.
- Simulations codes are developed to simulate the maneuver performance of the BILSAT-1 satellite using reaction wheels.

1.6 Outline of the Thesis

BILSAT-1 uses different sensors for attitude determination and actuators for attitude control. In chapter 2 all these sensors and actuators are described. Also comparison tables of these sensors and actuators are given.

Definitions and notations used in studying satellites are described in chapter 3. The chapter also gives the mathematical background on which the mathematical modelling of the following chapter is based.

Mathematical modelling of the satellite is given in chapter 4. Mathematical model of both the dynamics of the satellite and its kinematics is derived here. Also satellite's environmental conditions and disturbing torques are mentioned in this section.

In chapter 5 mathematical model of reaction wheels is derived. Information about tetrahedral configuration is given and allocation problem is expressed in detail.

Chapter 6 covers nonlinear control methods which are used in the simulations. Matlab and Simulink simulation results are given using BILSAT-1 parameters.

For future work, some suggestions and recommendations are presented in chapter 7 together with conclusions.

1.7 Tools

This thesis is written in Microsoft Word 2002. Also MathType Editor 5.2c is used for mathematical equations. The controllers are designed and simulated in Simulink6.0R14 and Matlab7.0R14.

CHAPTER 2

SENSORS and ACTUATORS of BILSAT-1

The attitude determination subsystem of BILSAT-1 is composed of four sun sensors, four rate sensors, two magnetometers and two star cameras. Four reaction wheels, three torque rods and a gravity gradient boom constitute the attitude controller actuators. Figure-2.1 shows the block diagram of ADCS. In this chapter all of these sensors and actuators are described in detail. Furthermore accuracy, advantages and disadvantages of these sensors and actuators are given in the comparison tables.

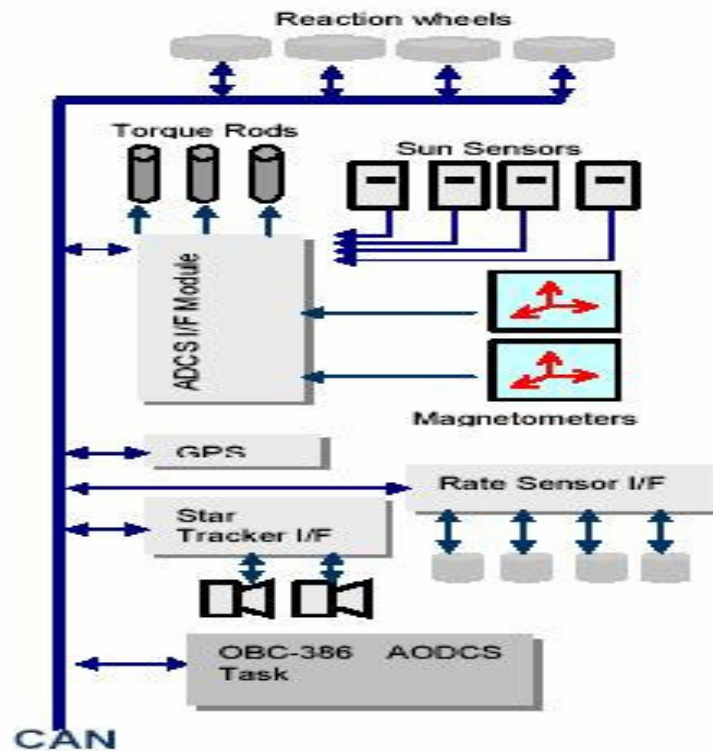


Figure-2.1: Block diagram of ADCS

2.1 Sensors

There are basically two classes of sensors commonly used in attitude determination of satellites [5].

- Reference Sensors
- Inertial Sensors

Reference sensors measure the direction of a known vector e.g. the Sun pointing vector. The vector measurement is a function of spacecraft attitude, making it attractive for attitude determination. Minimum two measurements are required for complete attitude information. Sun sensors, magnetometers and star cameras are the reference sensors of BILSAT-1.

Inertial sensors measure rotational and/or translational acceleration relative to an inertial frame. The sensors are subject to drift and bias errors and errors are not bounded. In order to provide an absolute attitude, regular updates are performed, based on references such as the Sun, stars or the Earth. Rate sensors of BILSAT-1 are known as inertial sensors.

2.1.1 Sun Sensor

Sun sensors are the most widely used sensor type; one or more varieties have flown on nearly every satellite. There are three basic classes of sun sensors [3].

- **Analogue sensors** have an output signal that is a continuous function of the Sun angle.
- **Sun presence sensors** provide a constant output signal whenever the Sun is in the fields of view.
- **Digital sensors** provide an encoded, discrete output which is a function of the Sun angle.

2.1.2 Magnetometer

The magnetometer measures the strength and direction of the Earth's magnetic field with its three orthogonal sensor elements. Magnetic field is strong and well modelled in orbits close to earth. Therefore magnetometers are mostly used in

the Low Earth Orbit (LEO) satellites. There are different models to compute the Earth's magnetic field. International Geomagnetic Reference Field (IGRF) created by the IAGA (International Association of Geomagnetism and Aeronomy) is the common and wide-spread model for this aim. Every fifth year it is revised by IAGA. Magnetometers accuracy is affected by three factors [5].

- Disturbance fields due to spacecraft electronics
- Modelling errors in the reference field model
- External disturbances such as ionospheric currents

Producers release different types of magnetometers. However main principles and missions are the same for all of these types. The different types are;

- Induction Coil Magnetometer
- Fluxgate Magnetometer
- Squid Magnetometer
- Magnetoresistive Gaussmeter

2.1.3 Star Camera

Star camera produces an image of the stars and this image is compared with an on board catalogue of the starry sky to determine the attitude. The location of two or more stars in the sensors field of view is enough to determine the attitude of the satellite. It is the most accurate attitude sensor on the satellites, with accuracies down to a few thousands of a degree. However it is heavy and big for small satellites.



Figure-2.2: Processing unit of star camera



Figure-2.3: Star camera head

2.1.4 Gyroscope

Gyroscope is an instrument which uses a rapidly spinning mass to sense and respond to changes in the inertial orientation of its spin axis. There are three basic classes of gyroscopes [3].

- **Rate Gyros (RG)** measure spacecraft angular rates and are frequently part of a feedback system for either spin rate control or attitude stabilization.
- **Rate Integrating Gyros (RIG)** measure spacecraft angular displacement directly.
- **Control Moment Gyros (CMG)** are used to generate attitude control torque. Therefore they are not attitude sensors like RGs or RIGs.

Due to drift in the gyroscopes it is necessary to use attitude sensors to compensate for this effect and to determine precise attitude.

2.1.5 Sensor Summary

As it is mentioned above, BILSAT-1 uses four types of attitude determination sensors. Among these sensors, magnetometers have low accuracy properties. Furthermore sun sensors are the most widely used sensor type because of its cheapness and enough accuracy. Star cameras are the most accurate sensors. Heaviness and expensiveness are the main disadvantages of star cameras for the small satellites. Due to drift and bias errors gyroscopes need some other sensors. In the table given below, accuracies, properties and constraints of sensors are demonstrated [4].

Table-2.1: Comparison table of attitude determination sensors

Sensor	Accuracy [degree]	Properties	Constraints
Sun Sensor	0.1	Cheap, simple, reliable	No measurement in eclipse
Magnetometer	1	Cheap, continuous coverage	Low altitude only
Star camera	0.001	Very accurate	Expensive, heavy complex
Gyroscope	0.01/hour	High bandwidth	Expensive, drifts with time

2.2 Actuators

2.2.1 Reaction Wheels

Reaction wheels use the rotational variant of Newton's third law. If the motion speeds up a wheel which is inside the satellite, the satellite speeds up just as much in the opposite direction. Normally, three reaction wheels are used to control a satellite, with the wheel axes aligned with the body principal axes. Using redundant fourth wheel is also a common practice in some satellites. Reaction wheels are the most accurate attitude control actuator for satellites. On the other hand, large weight is main disadvantage of reaction wheels.

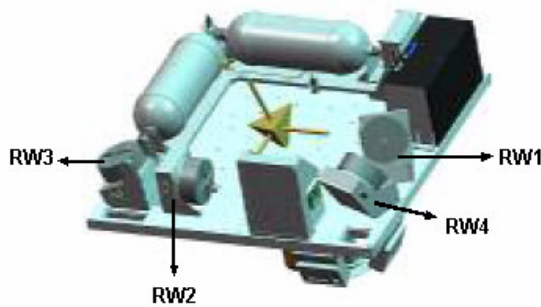


Figure-2.4: Reaction Wheels in a tetrahedral configuration

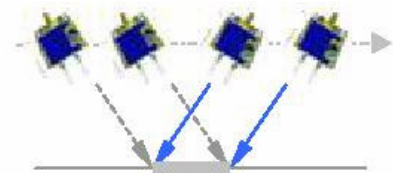


Figure-2.5: Slewing about pitch axis

2.2.2 Magnetic Torquers

Magnetic torquers are used to generate magnetic dipole moment for attitude control. They apply a torque on the satellite by producing a magnetic field which interacts with the earth's magnetic field. Magnetic torquers are generally a long copper wire, wound up into a coil or a piece of metal with very high permeability.

Magnetic torquers produce a momentum which is given in [6] as;

$$\mathbf{T} = \mathbf{B} \times \mathbf{M} = \mathbf{B} \times i N \mu A,$$

where

- \mathbf{B} : Earths magnetic field
- i : Current in the coil
- N : Number of windings in the coil
- μ : Permeability
- A : Area spanned by the coil.

2.2.3 Gravity Gradient Boom

Gravity gradient boom is deployed from the satellite when passive control is needed. While a boom with a tip mass is deployed from the satellite, the innermost of two masses is in a lower orbit and pull on the outermost [4]. Thus it is possible to control the attitude of the satellite pointing nadir surface. Deployment and construction are the difficulties of the boom.

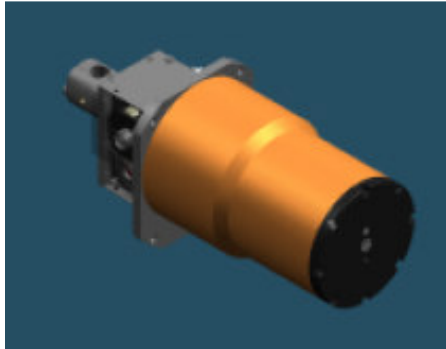


Figure-2.6: Stowed Boom



Figure-2.7: Deployed Boom

2.2.4 Actuator Summary

Three types of attitude control actuators are mentioned above. Among them, reaction wheels are the most accurate actuators. But they have the disadvantages because of their heaviness. Furthermore, magnetic torquer's response is slow and accuracy is better than gravity-gradient boom. On the other hand; gravity gradient booms do not need any energy for attitude control (passive control). Deployment and construction are the difficulties of the boom. In the table given below, accuracies, properties and constraints of actuators are demonstrated [4].

Table-2.2: Comparison table of attitude control actuators

Actuator	Accuracy [degree]	Properties	Constraints
Gravity gradient boom	1-5	Passive, simple Cheap	Central body oriented
Magnetic torquers	1-2	Cheap	Slow, lightweight, LEO only
Reaction Wheels	0.001-1	Expensive, precise, faster slew	Weight

CHAPTER 3

DEFINITIONS AND NOTATIONS

The orientation of the satellite and its mathematical model can be derived in different frames. This chapter presents some definitions and notations used throughout the thesis. The expressions used are based on [6], [7], [8] and [9].

3.1 Reference Frames

Several coordinate frames are described to determine and control the attitude in three dimensional spaces. Rotation from one frame to another frame must be well defined. Therefore concept of frame is described in detail in this section. Reference frame is denoted by \mathcal{F}_a , where the index a denotes which system is considered.

3.1.1 Earth-Centered Inertial (ECI) Frame

The Earth Centered Inertial (ECI) frame is a non-rotating reference frame in which the laws of Newton apply. This frame is fixed in space and the origin of the frame is located at the center of the earth. The x_i -axis points towards vernal equinox, Υ , the y_i axis is 90° east in the equatorial plane, and the z_i axis extends through the North Pole. It can be seen in Figure 3-1. The frame is denoted by \mathcal{F}_i .

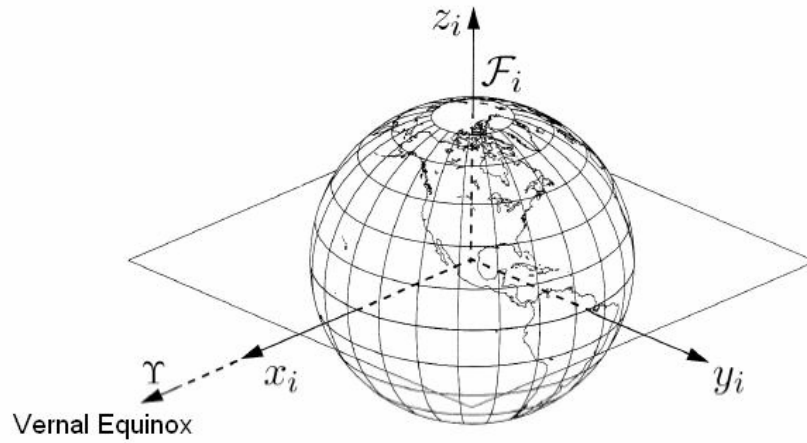


Figure3-1: Earth-Centered Inertial (ECI) frame, \mathcal{F}_i

3.1.2 Earth-Centered Earth Fixed (ECEF) Frame

The Earth Centered Earth Fixed (ECEF) frames origin is also located at the center of the earth. However the x_e and y_e axes rotate with the hemisphere relative to the ECI frame. z_e axis extends through the North Pole and the rotation is about the z_e axis. The x_e axis points toward the intersection between the Greenwich meridian and the Equator, which is at 0° longitude and 0° latitude. The y_e axis completes the right handed system. The ECEF frame is denoted \mathcal{F}_e and \mathcal{F}_e rotates relative to \mathcal{F}_i with a constant angular velocity $\omega_e = 7.2921 \cdot 10^{-5} \text{ rad/s}$ due to the daily rotation of the earth.

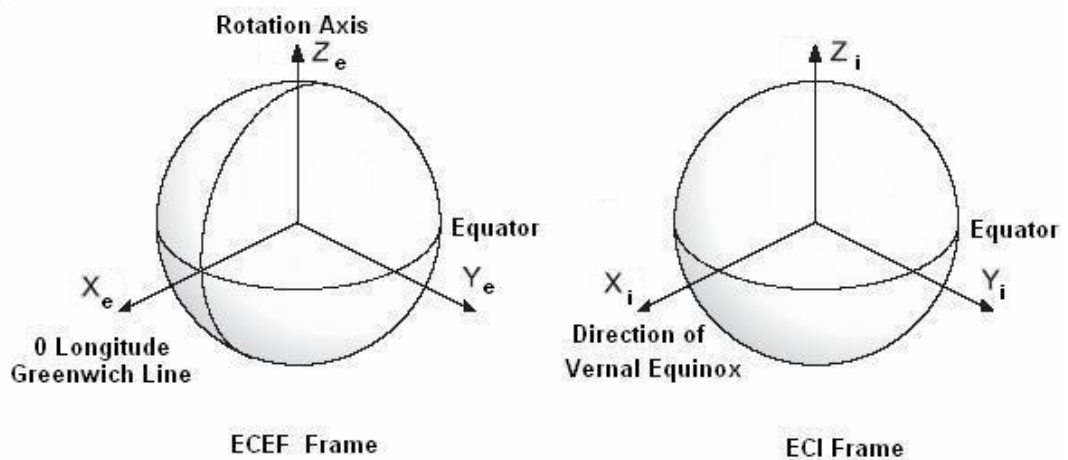


Figure3-2: ECEF and ECI frames, $\mathcal{F}_e - \mathcal{F}_i$

3.1.3 Orbit Frame

The origin of orbit frame coincides with the center of mass of the satellite. The z_o axis is always nadir pointing (center of earth). The x_o axis points in the direction of motion tangentially to the orbit and also x_o is perpendicular to z_o . The y_o axis completes the right hand system, as shown in Figure 3-3. The Orbit frame is denoted by \mathcal{F}_o .

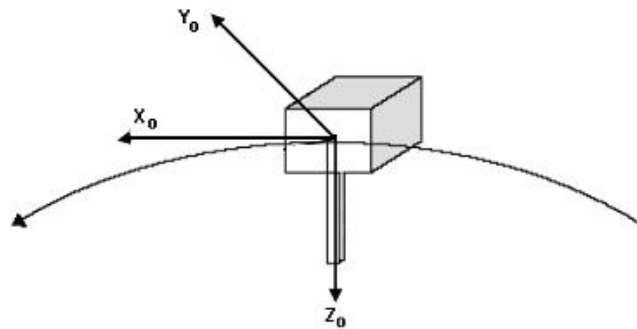


Figure3-3: Orbit frame, \mathcal{F}_o

3.1.4 Body Frame

The origin of body frame also coincides with the center of mass of the satellite. This frame is fixed with the satellite body. The nadir side of the satellite is in the z_b axis direction; x_b axis and y_b axis coincide with the orbit frames axes when the satellite has an attitude of 0° in roll, pitch and yaw. This frame is denoted \mathcal{F}_b .

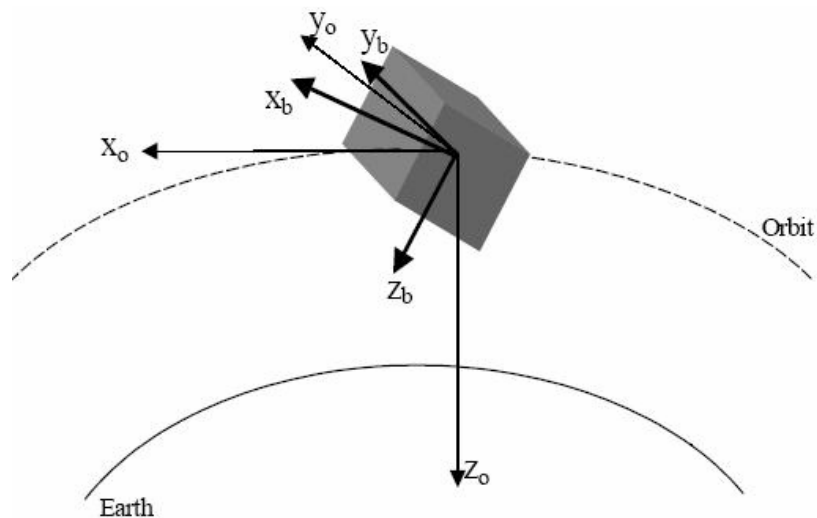


Figure3-4: Body frame

3.2 Rotation Matrix

Rotation matrix is a description of the rotational relationship between two reference frames. Rotation matrix (*direction cosine matrix*) has three statements [8]:

- Rotates a vector within a reference frame.
- Transforms vectors represented in one reference frame to another.
- Describes the mutual orientation between two coordinate frames, where the column vectors are cosines of the angles between the two frames.

The rotation matrix R from frame a to b is denoted R_a^b . Rotation of a vector from one frame to another frame can be given using R_a^b as;

$$\mathbf{v}^{to} = \mathbf{R}_{from}^{to} \mathbf{v}^{from} \quad (3.1)$$

Rotational matrices belongs to the set of matrices denoted by $SO(3)$ [6], which is defined as

$$SO(3) = \{ \mathbf{R} \mid \mathbf{R} \in R^{3 \times 3}, \mathbf{R}^T \mathbf{R} = \mathbf{1}_{3 \times 3} \text{ and } \det \mathbf{R} = 1_{3 \times 3} \} \quad (3.2)$$

Here $R^{3 \times 3}$ is the set of all 3×3 matrices with real elements, $\mathbf{1}_{3 \times 3}$ is the 3×3 identity matrix.

The orientation of the satellite is described using a rotation matrix R_O^B , which is denoted as

$$R_O^B = \begin{bmatrix} c_{11} & c_{12} & c_{13} \\ c_{21} & c_{22} & c_{23} \\ c_{31} & c_{32} & c_{33} \end{bmatrix} \quad (3.3)$$

Each of the elements c_{ij} is named directional cosines and column vectors can be arranged as;

$$c_1 = \begin{bmatrix} c_{11} \\ c_{21} \\ c_{31} \end{bmatrix} \quad c_2 = \begin{bmatrix} c_{12} \\ c_{22} \\ c_{32} \end{bmatrix} \quad c_3 = \begin{bmatrix} c_{13} \\ c_{23} \\ c_{33} \end{bmatrix} \quad (3.4)$$

Moreover, rotation matrix R_O^B is orthogonal and because of the orthogonality c_1 , c_2 and c_3 are orthonormal. Therefore below equations are valid for column vectors.

$$c_1 \times c_2 = c_3 \quad c_2 \times c_3 = c_1 \quad c_3 \times c_1 = c_2 \quad (3.5)$$

The rotation matrix satisfies the following properties;

$$R_B^A = (R_A^B)^{-1} = (R_A^B)^T. \quad (3.6)$$

$$R_B^A R_A^B = 1_{3 \times 3} \quad (3.7)$$

3.3 Angular Velocity

Angular velocity, ω_{AB}^A is defined as the rate at which a rotation matrix changes. It is used to study the angular displacements that occur over time. Angular velocities are dependent on the reference frames and ω_{AB}^A indicates the angular velocity of \mathcal{F}_a relative to \mathcal{F}_b in \mathcal{F}_a .

When the angular velocities are in the same reference frame, they can be added. For example, the following relation is valid

$$\omega_{BI}^B = \omega_{BO}^B + \omega_{OI}^B \quad (3.8)$$

If angular velocities are in the different reference frames, rotation matrix is used for addition. Equation 3.9 shows addition in the different reference frames.

$$\omega_{BI}^B = \omega_{BO}^B + R_O^B \omega_{OI}^O \quad (3.9)$$

To establish the angular velocity, its relationship with the rotation matrix and the time derivative of the rotation matrix are considered the following. Equation 3.7 is differentiated yielding

$$\dot{R}_B^A R_A^B + R_B^A \dot{R}_A^B = 0 \quad (3.10)$$

By defining a new matrix \mathbf{S} as;

$$\mathbf{S} = \dot{\mathbf{R}}_B^A \mathbf{R}_A^B \quad (3.11)$$

and inserting \mathbf{S} matrix into equation 3.10, the expression turns into

$$\mathbf{S} + \mathbf{S}^T = 0 \quad \text{and} \quad \mathbf{S} = -\mathbf{S}^T \quad (3.12)$$

Skew symmetric form of the vector $\boldsymbol{\omega}_{AB}^A = [\omega_1 \quad \omega_2 \quad \omega_3]^T$ is written as:

$$\mathbf{S}(\boldsymbol{\omega}_{AB}^A) = \begin{bmatrix} 0 & -\omega_3 & \omega_2 \\ \omega_3 & 0 & -\omega_1 \\ -\omega_2 & \omega_1 & 0 \end{bmatrix}, \quad (3.13)$$

Thus equation 3.11 can be expressed using $\boldsymbol{\omega}_{AB}^A$

$$\mathbf{S}(\boldsymbol{\omega}_{AB}^A) = \dot{\mathbf{R}}_B^A (\mathbf{R}_B^A)^T \quad (3.14)$$

Postmultiplying both sides of above equation by \mathbf{R}_B^A gives the relationship between angular velocity and rotation matrix, and its derivative:

$$\dot{\mathbf{R}}_B^A = \mathbf{S}(\boldsymbol{\omega}_{AB}^A) \mathbf{R}_B^A \quad (3.15)$$

3.4 Attitude Representation

There are many ways to represent the attitude of the satellite in a reference frame. But frequently Euler angles and Unit Quaternions are used in many applications. We will introduce both of them but we will use unit quaternions representation in our simulations. Main reason of this is the singularity problem of the Euler angles.

Euler angles are generally used in analytical studies. However unit quaternions are widely used in simulations and data processing. In the table given below, characteristics and applications of euler angles, unit quaternions can be found [5].

Table-3.1: Comparison table of attitude representation

Attitude Representation	Parameter	Characteristics	Applications
Euler Angles	3	<ul style="list-style-type: none"> - Minimal Set - Clear Physical interpretation - Trigonometric functions in rotation matrix - No simple composition rule - Singular for certain rotations - Trigonometric functions in kinematic relation - Easy orthogonality of rotation matrix - Bilinear composition rule - Not singular at any rotation 	<ul style="list-style-type: none"> - Theoretical physics, spinning spacecraft and attitude maneuvers. - Used in analytical studies.
Unit Quaternions	4	<ul style="list-style-type: none"> - Linear kinematic equations - No clear physical interpretations - One redundant parameter - Simple kinematic relation 	<ul style="list-style-type: none"> - Widely used in simulations and data processing. - Preferred attitude representation for attitude control systems.

3.4.1 Euler Angles

Using roll (ϕ), pitch (θ) and yaw (ψ) angles the attitude can be represented by three parameters. The angles ϕ , θ and ψ represent the rotations about the x, y and z axis respectively in a rotation from one frame to another. These angles are called the Euler Angles.

$$\Theta = \begin{bmatrix} \phi \\ \theta \\ \psi \end{bmatrix} \quad (3.16)$$

The rotation matrices are given as follows:

$$R_{x,\phi} = \begin{bmatrix} 1 & 0 & 0 \\ 0 & \cos \phi & -\sin \phi \\ 0 & \sin \phi & \cos \phi \end{bmatrix} \quad (3.17)$$

$$R_{y,\theta} = \begin{bmatrix} \cos \theta & 0 & \sin \theta \\ 0 & 1 & 0 \\ -\sin \theta & 0 & \cos \theta \end{bmatrix} \quad (3.18)$$

$$R_{z,\psi} = \begin{bmatrix} \cos \psi & -\sin \psi & 0 \\ \sin \psi & \cos \psi & 0 \\ 0 & 0 & 1 \end{bmatrix} \quad (3.19)$$

The rotation matrix R_B^O is described by a rotation ψ (yaw) about the z axis, then a rotation θ (pitch) about the y axis and finally a rotation ϕ (roll) about the x axis (Figure3-5). The elements $c(\cdot)$ and $s(\cdot)$ can be used as an abbreviation for the trigonometric expressions $\cos(\cdot)$ and $\sin(\cdot)$, respectively. As a result, the rotation matrix R_B^O becomes

$$R_B^O = R_z(\psi)R_y(\theta)R_x(\phi) = \begin{bmatrix} c\psi c\theta & -s\psi c\theta + c\psi s\theta s\phi & s\psi s\theta + c\psi c\theta s\phi \\ s\psi c\theta & c\psi c\theta + s\psi s\theta s\phi & -c\psi s\theta + s\psi c\theta s\phi \\ -s\theta & c\theta s\phi & c\theta c\phi \end{bmatrix} \quad (3.20)$$

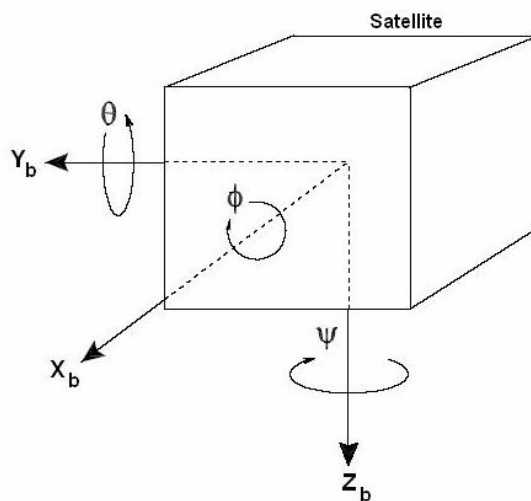


Figure3-5: Euler Angles

3.4.2 Unit Quaternions

Unit quaternions are the other way for the attitude representation. They were first described by the Irish mathematician Sir William Rowan Hamilton in 1843 and applied to mechanics in three-dimensional space. Usually unit quaternions are used in computations to overcome the singularity problem.

Quaternions have 4 dimensions (each quaternion consists of 4 scalar numbers), one real dimension and 3 imaginary dimensions. Each of these imaginary dimensions has a unit value of the square root of -1, but they are different square roots of -1 all mutually perpendicular to each other, known as i, j and k . So a quaternion can be represented as follows:

$$a + i b + j c + k d \quad (3.21)$$

While the complex numbers are obtained by adding the element i to the real numbers which satisfies $i^2 = -1$, the quaternions are obtained by adding the elements i, j and k to the real numbers which satisfy the following relations.

$$i^2 = j^2 = k^2 = -1 \quad (3.22)$$

$$i \times j = -(j \times i) = k$$

$$j \times k = -(k \times j) = i \quad (3.23)$$

$$k \times i = -(i \times k) = j$$

They have four parameters, one real part η , and three imaginary parts ε .

Unit quaternions are defined by

$$\eta = \cos \frac{\varphi}{2}, \quad \varepsilon = \begin{bmatrix} \varepsilon_1 \\ \varepsilon_2 \\ \varepsilon_3 \end{bmatrix} = \begin{bmatrix} k_x \sin(\varphi/2) \\ k_y \sin(\varphi/2) \\ k_z \sin(\varphi/2) \end{bmatrix}, \quad q = \begin{bmatrix} \eta \\ \varepsilon_1 \\ \varepsilon_2 \\ \varepsilon_3 \end{bmatrix} \quad (3.24)$$

and represent a rotation about a unit vector (k_x, k_y, k_z) through an angle φ . The unit quaternions satisfy $q^T q = 1$ which also means that $\eta^2 + \varepsilon_1^2 + \varepsilon_2^2 + \varepsilon_3^2 = 1$ (3.25)

Transformation from Euler angles to quaternion can be calculated as;

$$\begin{bmatrix} \eta \\ \varepsilon_1 \\ \varepsilon_2 \\ \varepsilon_3 \end{bmatrix} = \begin{bmatrix} \cos(\phi/2)\cos(\theta/2)\cos(\psi/2) + \sin(\phi/2)\sin(\theta/2)\sin(\psi/2) \\ \sin(\phi/2)\cos(\theta/2)\cos(\psi/2) - \sin(\phi/2)\cos(\theta/2)\sin(\psi/2) \\ \cos(\phi/2)\sin(\theta/2)\cos(\psi/2) + \sin(\phi/2)\cos(\theta/2)\sin(\psi/2) \\ \cos(\phi/2)\cos(\theta/2)\sin(\psi/2) - \sin(\phi/2)\sin(\theta/2)\cos(\psi/2) \end{bmatrix} \quad (3.26)$$

Transformation from quaternion to Euler angles can be calculated as;

$$\begin{aligned} \phi &= \text{atan}\left(2(q_2q_3 + \eta q_1), (\eta^2 - q_1^2 - q_2^2 + q_3^2)\right) \\ \theta &= \text{asin}\left(-2(q_1q_3 - \eta q_2)\right) \\ \psi &= \text{atan}\left(2(q_1q_2 + \eta q_3), (\eta^2 + q_1^2 - q_2^2 - q_3^2)\right) \end{aligned} \quad (3.27)$$

The rotation matrix can be expressed in quaternions as:

$$R_B^O(q) = R_{\eta, \varepsilon} = 1_{3 \times 3} + 2\eta S(\varepsilon) + 2S^2(\varepsilon) \quad (3.28)$$

Using equation 3.28, the rotation matrix R_B^O can be written as:

$$R_B^O = \begin{bmatrix} 1 - 2(\varepsilon_2^2 + \varepsilon_3^2) & 2(\varepsilon_1\varepsilon_2 - \varepsilon_3\eta) & 2(\varepsilon_1\varepsilon_3 + \varepsilon_2\eta) \\ 2(\varepsilon_1\varepsilon_2 + \varepsilon_3\eta) & 1 - 2(\varepsilon_1^2 + \varepsilon_3^2) & 2(\varepsilon_2\varepsilon_3 - \varepsilon_1\eta) \\ 2(\varepsilon_1\varepsilon_3 - \varepsilon_2\eta) & 2(\varepsilon_2\varepsilon_3 + \varepsilon_1\eta) & 1 - 2(\varepsilon_1^2 + \varepsilon_2^2) \end{bmatrix} \quad (3.29)$$

More frequently the rotation matrix in the opposite direction is used and according to equation 3.6 and 3.29, R_B^O is obtained as;

$$R_O^B = (R_B^O)^T = \begin{bmatrix} 1 - 2(\varepsilon_2^2 + \varepsilon_3^2) & 2(\varepsilon_1\varepsilon_2 + \varepsilon_3\eta) & 2(\varepsilon_1\varepsilon_3 - \varepsilon_2\eta) \\ 2(\varepsilon_1\varepsilon_2 - \varepsilon_3\eta) & 1 - 2(\varepsilon_1^2 + \varepsilon_3^2) & 2(\varepsilon_2\varepsilon_3 + \varepsilon_1\eta) \\ 2(\varepsilon_1\varepsilon_3 + \varepsilon_2\eta) & 2(\varepsilon_2\varepsilon_3 - \varepsilon_1\eta) & 1 - 2(\varepsilon_1^2 + \varepsilon_2^2) \end{bmatrix} \quad (3.30)$$

Now, rotation matrix R_B^O can be expressed using column vectors as;

$$R_B^O = [c_1^B \quad c_2^B \quad c_3^B] \quad (3.31)$$

where $c_i^B = [c_{ix}^B \quad c_{iy}^B \quad c_{iz}^B]^T$ are column vectors (directional cosines). c_1^B, c_2^B and c_3^B

are the projections of the x_o, y_o and z_o axes in the body frame.

$$c_1^B = \begin{bmatrix} 1 - 2(\varepsilon_2^2 + \varepsilon_3^2) \\ 2(\varepsilon_1\varepsilon_2 - \varepsilon_3\eta) \\ 2(\varepsilon_1\varepsilon_3 + \varepsilon_2\eta) \end{bmatrix} \quad c_2^B = \begin{bmatrix} 2(\varepsilon_1\varepsilon_2 + \varepsilon_3\eta) \\ 1 - 2(\varepsilon_1^2 + \varepsilon_3^2) \\ 2(\varepsilon_2\varepsilon_3 - \varepsilon_1\eta) \end{bmatrix} \quad c_3^B = \begin{bmatrix} 2(\varepsilon_1\varepsilon_3 - \varepsilon_2\eta) \\ 2(\varepsilon_2\varepsilon_3 + \varepsilon_1\eta) \\ 1 - 2(\varepsilon_1^2 + \varepsilon_2^2) \end{bmatrix} \quad (3.32)$$

3.5 The Inertia Matrix

The inertia matrix $I_o \in \mathbb{R}^{3 \times 3}$ about O (arbitrary origin) is defined according to [16] and [9]:

$$I_o = \begin{bmatrix} I_x & -I_{xy} & -I_{xz} \\ -I_{yx} & I_y & -I_{yz} \\ -I_{zx} & -I_{zy} & I_z \end{bmatrix} \quad (3.33)$$

In this equation I_x, I_y and I_z are the moments of inertia about the x_b, y_b and z_b - axes and $I_{xy} = I_{yx}$, $I_{xz} = I_{zx}$, $I_{yz} = I_{zy}$ are the products of inertia defined as:

$$I_x = \int_V (y^2 + z^2) \rho_m dV; \quad I_{xy} = I_{yx} = \int_V xy \rho_m dV \quad (3.34)$$

$$I_y = \int_V (x^2 + z^2) \rho_m dV; \quad I_{xz} = I_{zx} = \int_V xz \rho_m dV \quad (3.35)$$

$$I_z = \int_V (x^2 + y^2) \rho_m dV;; \quad I_{yz} = I_{zy} = \int_V yz \rho_m dV \quad (3.36)$$

If the axes of the body frame coincide with the principal axes of inertia, the inertia matrix reduces to:

$$\mathbf{I} = \begin{bmatrix} I_x & 0 & 0 \\ 0 & I_y & 0 \\ 0 & 0 & I_z \end{bmatrix} \quad (3.37)$$

BILSAT-1 inertia matrix parameters are $I_{xx}=9,8194 \text{ kgm}^2$; $I_{xy}=I_{yx}=0.071 \text{ kgm}^2$; $I_{xz}=I_{zx}=0,2892 \text{ kgm}^2$; $I_{yy}=9,7030 \text{ kgm}^2$; $I_{yz}=I_{zy}= 0,1011 \text{ kgm}^2$; $I_{zz}=9,7309 \text{ kgm}^2$. Diagonal terms of inertia matrix (I_{xx} , I_{yy} , I_{zz}) are larger than other components of \mathbf{I} . Throughout this thesis we neglect the off diagonal terms.

CHAPTER 4

MATHEMATICAL MODELLING

Mathematical model of dynamics and kinematics of satellite are derived in this chapter. Also satellite's environment is described in detail. The expressions are based on [6], [18] and [19].

4.1 Satellite Model

4.1.1 Dynamics for Satellite Model

The satellite is modeled as a rigid body and its dynamic model is derived using the Newton-Euler formulation. In this formulation angular momentum changes related to applied torque. General mathematical dynamic model of the satellite is obtained after some calculations.

Given the momentum p and the position vector r , the angular momentum h is

$$h = r \times p \quad (4.1)$$

Derivation of angular momentum can be done using Newton's second law together with $v \times v = 0$ and $p = mv$ [4].

$$\frac{\delta}{\delta t} h = \frac{\delta}{\delta t} r \times p + r \times \frac{\delta}{\delta t} p = v \times mv + r \times ma = r \times F = \tau \quad (4.2)$$

where v is the velocity vector and τ is the vector of all torques applied on the satellite. The angular momentum can alternatively be defined by the moment of inertia I , and the angular velocity ω of the satellite as;

$$h = I \omega \quad (4.3)$$

In equation 4.3, angular momentum was given in the \mathcal{F}_i (ECI) frame. Dynamic equation can be expressed in different frames. By using the rotation matrix, the equations given below can be derived.

$$h^B = I^B \omega_{BI}^B \quad (4.4)$$

$$R_B^I h^B = R_B^I I^B \omega_{BI}^B \quad (4.5)$$

$$h^I = R_B^I I^B \omega_{BI}^B \quad (4.6)$$

$$h^I = R_B^I I^B R_I^B \omega_{BI}^I \quad (4.7)$$

$$I^I = R_B^I I^B R_I^B \quad (4.8)$$

After differentiating equation (4.6) and applying the time derivatives of the rotation matrix, the following equation is obtained;

$$\dot{h}^I = \dot{R}_B^I I^B \omega_{BI}^B + R_B^I I^B \dot{\omega}_{BI}^B = S(\omega_{BI}^B) R_B^I I^B \omega_{BI}^B + R_B^I I^B \dot{\omega}_{BI}^B \quad (4.9)$$

In the Body frame (\mathcal{F}_b), this is expressed by postmultiplying both sides of above equation by R_I^B

$$R_I^B \dot{h}^I = R_I^B S(\omega_{BI}^B) R_B^I I^B \omega_{BI}^B + R_I^B R_B^I I^B \dot{\omega}_{BI}^B = R_I^B S(\omega_{BI}^B) R_B^I I^B \omega_{BI}^B + I^B \dot{\omega}_{BI}^B \quad (4.10)$$

Merging the equation in 4.10 with 4.2 gives;

$$\dot{h}^B = S(R_I^B \omega_{BI}^I) \mathbf{I}^B \omega_{BI}^B + \mathbf{I}^B \dot{\omega}_{BI}^B = \tau^B \quad (4.11)$$

Finally general mathematical dynamic model of the satellite is obtained as;

$$\mathbf{I}^B \dot{\omega}_{BI}^B + \omega_{BI}^B \times (\mathbf{I}^B \omega_{BI}^B) = \tau^B = \sum_k \tau_k^B \quad (4.12)$$

In the above equations;

\mathbf{I} : is the moment of inertia,

ω_{BI}^B : is the angular velocity of the body frame with respect to the inertial frame in the body frame,

τ_k^B : are the torques acting on the satellite in body frame

The torques τ_k^B are the sum of both internal torques and external torques on the satellite. Usually internal effects like fuel sloshing and thermal deformations are not

accounted when using a rigid body model. Therefore internal torques are not taken into consideration. The external torques τ_e can be separated into two groups as disturbance torques and control torques. Disturbance torques are caused by environmental effects such as gravity gradient torque, solar radiation, aerodynamic drag and etc. Control torques are intentionally applied torques from control devices such as reaction wheels, magnetic torquers and etc. Generally gravity gradient torque, magnetic torque and reaction wheel torque are considered for the total torque.

$$\tau^B = \tau_g^B + \tau_m^B + \tau_r^B \quad (4.13)$$

τ_g^B : is the gravitational torque working on the satellite body.

τ_m^B : is the torque applied by the magnetic torquer.

τ_r^B : is the torque applied by the reaction wheel.

In our simulations we will consider mainly gravity gradient torque and reaction wheel torque for the maneuver of satellite. $\tau^B = \tau_g^B + \tau_r^B$

Satellite dynamic equation in 4.12 can be alternatively expressed by using the skew-symmetric operator.

$$\mathbf{I}^B \dot{\omega}_{BI}^B + \mathbf{S}(\omega_{BI}^B) \mathbf{I}^B \omega_{BI}^B = \tau^B \quad (4.14)$$

The angular velocity of the satellite ω_{BI}^B relative to the inertial frame is expressed in the body frame as the sum of two angular velocities,

$$\omega_{BI}^B = \omega_{BO}^B + \omega_{OI}^B = \omega_{BO}^B + R_o^B \omega_{OI}^O \quad (4.15)$$

where $\omega_{OI}^O = [0 \quad -\omega_o \quad 0]^T$ is the known angular velocity of the orbit frame relative to the ECI frame, expressed in Orbit frame. Then,

$$\omega_{BI}^B = \begin{bmatrix} \omega_x \\ \omega_y \\ \omega_z \end{bmatrix} = \omega_{BO}^B - \omega_o c_2 \quad \text{with} \quad c_2 = \begin{bmatrix} 2(\varepsilon_1 \varepsilon_2 + \varepsilon_3 \eta) \\ 1 - 2(\varepsilon_1^2 + \varepsilon_3^2) \\ 2(\varepsilon_2 \varepsilon_3 - \varepsilon_1 \eta) \end{bmatrix} \quad (4.16)$$

is obtained.

4.1.2 Kinematics For Satellite Model

The satellite's orientation can be described by the kinematics. The kinematic is derived by integrating the angular velocity.

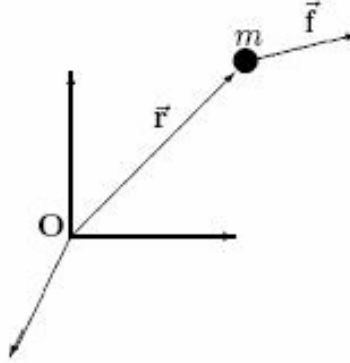


Figure4-1: Translational Motion

Translational motion of a particle of mass m is derived using Newton's second law.

$$m\ddot{r} = f \quad (4.17)$$

$$p = mv = m\dot{r} \quad (4.18)$$

$$\dot{p} = m\dot{v} = m\ddot{r} = f \quad (4.19)$$

$$\dot{r} = \frac{P}{m} \quad (4.20)$$

Here r is the position vector of the particle relative to an inertial origin O , p is the linear momentum of the particle and f is the force acting on the particle. $\dot{r} = p/m$ is known as the kinematic differential equation for the translational motion and describes how position changes for a given velocity.

For the translational motion kinematic differential equation is simple to express but for the rotational motion it is not so simple to express.

The differential equations, as given in reference [6], are;

$$\dot{\eta} = -\frac{1}{2} \epsilon^T \omega_{BO}^B \quad (4.21)$$

$$\dot{\epsilon} = \frac{1}{2} [\eta 1_{3 \times 3} + S(\epsilon)] \omega_{BO}^B \quad (4.22)$$

Hence, another way of representing Equations 4.21 and 4.22 becomes;

$$\dot{q} = \begin{bmatrix} \dot{\eta} \\ \dot{\varepsilon} \end{bmatrix} = \frac{1}{2} \begin{bmatrix} -\varepsilon^T \\ \eta \mathbf{1}_{3 \times 3} + S(\varepsilon) \end{bmatrix} \omega_{BO}^B \quad (4.23)$$

4.2 Magnetic Torque

The magnetic torquers use natural torque caused by Earth's magnetic field interacting with a magnet. The magnetic torquer produces a magnetic dipole moment when currents flow through its windings. This current is proportional to the ampere-turns and the area enclosed by the torquer.

Magnetic torques together with a gravity gradient torque can be used to obtain full three-axis stabilization. The main purpose of the actuators effect is to place the satellite in its right attitude using the magnetic field.

In the following equations; modelling of the magnetic torquers is derived [18]. Magnetic torque on a coil element in the magnetic field is given by

$$d\tau_m = ids \times B \quad (4.24)$$

On the coil element, magnetic dipole moment can be defined as $dm \cong ids$ and from a coil with windings the total dipole moment can be found by integrating over the entire coil area S as:

$$m \cong N \int_S dm \quad (4.25)$$

where N is the number of windings. Finally torque on a magnetic coil can be written as

$$\tau_m = N \int_S ids \times B = m \times B \quad (4.26)$$

which can be written relative to the body frame as

$$\tau_m^B = m^B \times B^B = \mathbf{S}(m^B) B^B = \begin{bmatrix} B_z^B m_y - B_y^B m_z \\ B_x^B m_z - B_z^B m_x \\ B_y^B m_z - B_x^B m_y \end{bmatrix} \quad (4.27)$$

In the above equation;

τ_m^B : is the torque which is generated by the magnetic torquer,

m^B : is the magnetic dipole moment generated by the torquer,

$B^B = \begin{bmatrix} B_x^B & B_y^B & B_z^B \end{bmatrix}$: is the geomagnetic field vector.

The total torque generated on the satellite by the magnetic torquers is given by the sum of all the partial torques from all the magnetic torquers.

$$\mathbf{m}^B = \begin{bmatrix} N_x i_x A_x \\ N_y i_y A_y \\ N_z i_z A_z \end{bmatrix} = \begin{bmatrix} m_x \\ m_y \\ m_z \end{bmatrix} \quad (4.28)$$

where N_k is the number of windings in the torquer on the axis in the k direction, i_k is the torquer current and A_k is the span area of the torquer, $k = x, y, z$.

Magnetic torquers were used during settling to orbit of BILSAT-1. In this thesis we are interested in maneuver of BILSAT-1. Therefore, magnetic torque from magnetic torquer is not taken into consideration in our simulations.

4.3 Reaction Wheel Torque

The main advantage of reaction wheels, compared with magnetic torquers, is the independency of satellites location for the control of the satellite. Nevertheless, weight and expenses are disadvantage of the reaction wheels. The reaction wheel equation is expressed in [23] as;

$$\boldsymbol{\tau}_r^B = \left(\frac{d\mathbf{h}_r}{dt} \right)^B + \boldsymbol{\omega}_{BI}^B \times \mathbf{h}_r - \boldsymbol{\tau}_{friction}^B \quad (4.29)$$

where $\boldsymbol{\tau}_r^B$ is the torque produced by reaction wheels in the body frame, $\mathbf{h}_r = [h_{rx} \quad h_{ry} \quad h_{rz}]^T = I_r \boldsymbol{\omega}_r$ is the angular momentum of the reaction wheels and $\boldsymbol{\tau}_{friction}^B$ is friction. The frictional torques $\boldsymbol{\tau}_{friction}^B$ is neglected in our simulations.

According to energy conservation principle, a torque rotating the reaction wheels produces a torque of the same magnitude but in different direction on the satellite. It is expressed by

$$I_r \dot{\boldsymbol{\omega}}_r = -I \dot{\boldsymbol{\omega}}_{BI}^B \quad (4.30)$$

Using $\boldsymbol{\omega}_{BI}^B = [\omega_x \quad \omega_y \quad \omega_z]^T$ in equation 4.29, the equations of reaction wheel torques are expressed as:

$$\boldsymbol{\tau}_r^B = \left(\frac{d\mathbf{h}_r}{dt} \right)^B + \boldsymbol{\omega}_{BI}^B \times \mathbf{h}_r = \begin{bmatrix} \tau_{rx} \\ \tau_{ry} \\ \tau_{rz} \end{bmatrix} = \begin{bmatrix} \dot{h}_{rx} + h_{rz} \omega_y - h_{ry} \omega_z \\ \dot{h}_{ry} + h_{rx} \omega_z - h_{rz} \omega_x \\ \dot{h}_{rz} + h_{ry} \omega_x - h_{rx} \omega_y \end{bmatrix} \quad (4.31)$$

4.4 Gravity Gradient Torque

Gravity gradient torque exists due to the variation in the gravitational field. Gravitational force varies with the inverse square of the distance from the Earth. Therefore, closer to the Earth, gravitational force is greater.

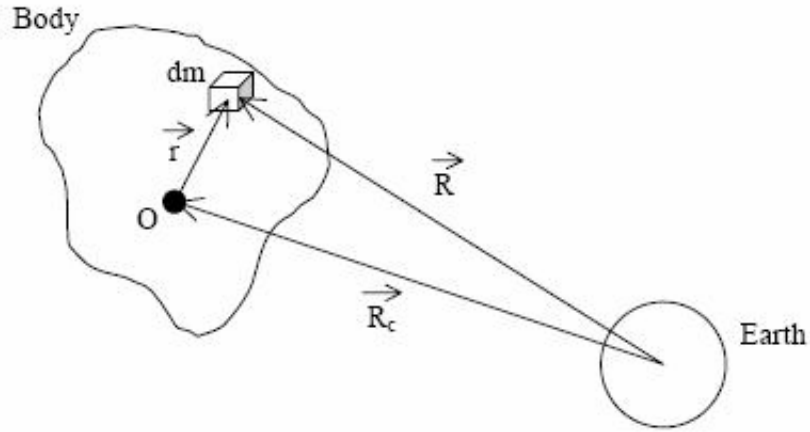


Figure4-2: Gravity gradient parameters

The force working on a mass element in the satellite is given by the gravitational law of Newton [11] as:

$$df = -\mu \frac{\vec{R}}{R^3} dm \quad (4.32)$$

where μ is the Earth's gravitational coefficient constant and equals to $\mu = GM$, G is the universal gravitational constant and M is the mass of the Earth. $R = |\vec{R}|$ is the distance from the center of the Earth to the mass element dm .

Numerical values of the constants mentioned above are:

$$M = 5.9742 * 10^{24} \text{ kg} \quad (4.33)$$

$$G = 6.6720 * 10^{-11} \text{ Nm}^2 / \text{kg}^2 \quad (4.34)$$

$$\mu = 3.986 * 10^{14} \text{ Nm}^2 / \text{kg} \quad (4.35)$$

The gravitational torque around the centre of mass of a rigid spacecraft is given by;

$$\tau_g = \int_B \vec{r} \times df = -\mu \int_B \frac{\vec{r} \times \vec{R}}{R^3} dm \quad (4.36)$$

where $r = |\vec{r}|$ is the distance from the center of mass in the satellite to the mass element dm . Here, it can be seen from figure4-2 that $\vec{R} = \vec{R}_c + \vec{r}$

Binomial series expansion of the expression R^{-3} is given in reference [18] by

$$R^{-3} = R_c^{-3} \left[1 - \frac{3(\vec{r} \cdot \vec{R}_c)}{R_c^2} + O\left(\frac{r^2}{R_c^2}\right) \right] \quad (4.37)$$

Inserting the above equation into 4.36 gravitational torque turns into

$$\tau_g = -\mu_g \int_B \frac{\vec{r} \times \vec{R}_c}{R_c^3} \left[1 - \frac{3(\vec{r} \cdot \vec{R}_c)}{R_c^2} \right] dm \quad (4.38)$$

$$\tau_g = \left(\frac{\mu_g}{R_c^3} \right) \vec{R}_c \times \int_B \vec{r} dm - \left(\frac{3\mu_g}{R_c^5} \right) \vec{R}_c \times \int_B \vec{r} \vec{r} dm \vec{R}_c \quad (4.39)$$

$$\tau_g = - \left(\frac{3\mu}{R_c^3} \right) \vec{R}_c \times \int_B \vec{r} \vec{r} dm \vec{R}_c \quad (4.40)$$

The expression $\int_B \vec{r} \vec{r} dm$ is a part of the expression of the inertial torque of the body, represented by

$$I \cong \int_B (r^2 1 - \vec{r} \vec{r}) dm \quad (4.41)$$

By defining

$$\sigma_o = \frac{\vec{R}_c}{R_c} \quad (4.42)$$

the gravitational torque for the satellite becomes

$$\tau_g = \frac{3\mu}{R_c^3} \sigma_o \times \bar{I} \sigma_o = 3\omega_o^2 \sigma_o \times \bar{I} \sigma_o \quad (4.43)$$

According to [11], ω_o is the speed of the spacecraft in a circular orbit of radius R_o . It can be said that ω_o represents the angular velocity of the orbit frame \mathcal{F}_o about its y_o axis. The gravity gradient written in the body frame is

$$\tau_g^B = 3\omega_o^2 c_3^B \times (I c_3^B) \quad , \quad \omega_o^2 = \frac{\mu}{R_c^3} \quad (4.44)$$

where c_3^B comes from the rotation matrix R_o^B and transforms the z_b axis to the z_o axis. As given before, c_3^B is:

$$c_3 = \begin{bmatrix} 2(\varepsilon_1 \varepsilon_3 - \eta \varepsilon_2) \\ 2(\varepsilon_2 \varepsilon_3 + \eta \varepsilon_1) \\ 1 - 2(\varepsilon_1^2 + \varepsilon_2^2) \end{bmatrix} \quad (4.45)$$

Another representation of the gravitational torque is;

$$\tau_g^B = 3\omega_o^2 \begin{bmatrix} (I_z - I_y) c_{23} c_{33} \\ (I_x - I_z) c_{33} c_{13} \\ (I_y - I_x) c_{13} c_{23} \end{bmatrix} = 3\omega_o^2 \begin{bmatrix} 2(I_z - I_y)(\varepsilon_2 \varepsilon_3 + \eta \varepsilon_1)(1 - 2(\varepsilon_1^2 + \varepsilon_2^2)) \\ 2(I_x - I_z)(\varepsilon_1 \varepsilon_3 - \eta \varepsilon_2)(1 - 2(\varepsilon_1^2 + \varepsilon_2^2)) \\ 4(I_y - I_x)(\varepsilon_1 \varepsilon_3 - \eta \varepsilon_2)(\varepsilon_2 \varepsilon_3 + \eta \varepsilon_1) \end{bmatrix} \quad (4.46)$$

4.5 Disturbance Torques

Several disturbance torques affects satellites. The main effective disturbance torques for satellites are described in this section. Further information can be found in reference [11].

4.4.1 Solar Radiation

Solar radiation pressure produces a force on the satellite related to its distance to the sun. Solar radiation has more effect at high altitudes. Therefore solar radiation effect is ignored in our simulations for BILSAT-1. The surface area of the satellite which faces the Sun is essential when determining the resulting acceleration caused by solar radiation.

Equation 4.47 gives the force of solar pressure;

$$P_{SR} = \frac{SF}{c} = \frac{1353}{3 \times 10^8} \frac{W / m^2}{m / s} = 4.51 \times 10^{-6} N / m^2 \quad (4.47)$$

$$SF : \text{ is the solar radiation constant } SF = 1353 W / m^2 \quad (4.48)$$

$$c : \text{ is the speed of the light } c = 3 \times 10^8 m / s \quad (4.49)$$

The torque due to the solar radiation is given by:

$$\tau_{solarradiation} = -P_{SR} * c_R * A_{\odot} * (c_{psr} - c_g) \quad (4.50)$$

where A_{\odot} is the exposed area to the Sun, c_R is the reflectivity, c_{psr} is the estimated center of pressure and c_g is the center of gravity.

4.5.2 Aerodynamic Torque

At low altitude, satellites will be influenced by the air density. The effect is dependent on the area and shape of the surface. This effect may reduce the velocity of the satellite. The aerodynamic torque is given as:

$$\boldsymbol{\tau}_{aero} = F_{aero} (\mathbf{u}_v \times (\mathbf{c}_{pa} - \mathbf{c}_g)), \quad F_{aero} = \frac{1}{2} \rho V^2 C_d A_{inc} \quad (4.51)$$

where:

ρ Atmospheric density (kg / m^3)

A_{inc} Area perpendicular to \mathbf{u}_v (m^2)

\mathbf{u}_v Unit vector in velocity direction

C_d Drag coefficient

V Velocity of satellite (m / s)

\mathbf{c}_{pa} Center of pressure

\mathbf{c}_g Center of gravity

4.6 Reference Model

Reference model generates the smooth reference trajectory for the control system to use. It operates on the reference signal so that a step in the reference will be filtered into a smooth curve. Controller then tries to follow this smooth curve. A second order or third order filter is appropriate for this aim. We simulated second order and third order filters and we saw that third order filter responds better than second order filter.

Reference vector is denoted by q_r and desired vector is denoted by q_d . Transfer function from desired reference to filtered reference was chosen as:

$$\frac{q_{d_i}}{q_{r_i}} = \frac{\omega_n^3}{(s + \omega_n)(s^2 + 2\zeta\omega_n + \omega_n^2)}, \quad i \in \{1, 2, 3, 4\} \quad (4.52)$$

The damping ratio is chosen as $\zeta = 1$ for the critical damping output from reference model. The undamped natural frequency ω_n is adjusted depending on the system requirements. We gave different value to ω_n in our simulations. Then we saw that if we increase the ω_n , settling time decreases. Nevertheless the system overshoots and required torque increases. We prefer the long settling time and low torque rather than

short settling time because of the energy consumption. In the satellite operations, energy consumption is main determining factor while designing design sub components of the satellites. In Table-4.1, the effect of ω_n to the system response is tabulated for two different values of ω_n when the controller is Sliding Mode Regulator (SMR).

Table-4.1: Effect of ω_n on system response

Parameter	$\omega_n = 0.022$ (SMR)	$\omega_n = 2$ (SMR)
Settling Time	0.09 orbits	0.01 orbits
Max. Output Torque from Regulator	4e-4 Nm	0.6 Nm
Max. Output Torque from Reaction wheel	3e-4 Nm	0.5 Nm
Response	Overdamp	Overshoot

CHAPTER 5

MODELLING of REACTION WHEELS

Mathematical model of reaction wheels is derived in this chapter. Information about tetrahedral configuration is given and equations of tetrahedral configuration are derived. Allocation problem and its solution are expressed in detail. Further information can be found in the references [3], [16] and [19]. The derivations are based on [19].

5.1 Control Allocation

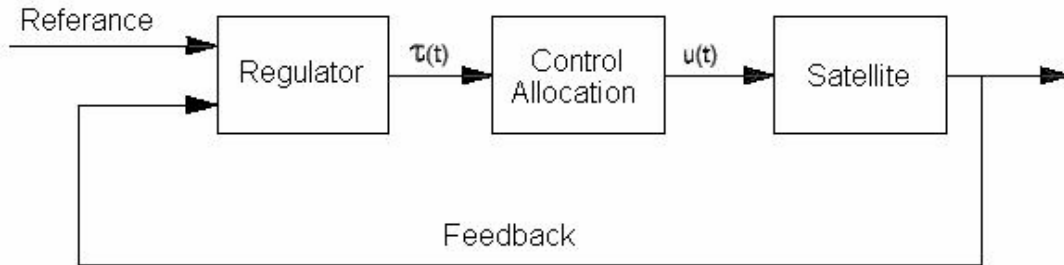


Figure-5.1: General Control Design For Reaction Wheels

In our simulations for the BILSAT-1, dimension of the controller output is $n = 3$. Nevertheless input of the actuator (reaction wheel) has the dimension $r = 4$. Therefore generalized force vector τ is distributed to input vector. According to [16] and [19] relation between force vector and input vector is given as:

$$\tau = T(\alpha) \underbrace{K}_f u, \quad (5.1)$$

where $u \in \mathbb{R}^r$ and $\alpha \in \mathbb{R}^p$ are defined as

$$\alpha = [\alpha_1, \dots, \alpha_p]^T \quad u = [u_1, \dots, u_r]^T \quad (5.2)$$

In equation 5.1, f is defined as force vector and $f = Ku \in \mathbb{R}^r$, here K is diagonal force coefficient matrix $K \in \mathbb{R}^{r \times r}$, $K = \text{diag}\{K_1, \dots, K_r\}$.

Allocation matrix $T(\alpha)$ is defined as $T(\alpha) \in \mathbb{R}^{n \times r}$, $t_i \in \mathbb{R}^n$ and $T(\alpha) = [t_1, \dots, t_r]$.

Generalized force vector τ is distributed to the input vector u by minimizing the force $f = Ku$. Minimization problem is solved as shown by equations stated below, using reference [16] and [19].

$$J = \min \{f^T W f\} \quad (5.3)$$

$$\tau - Tf = 0 \quad (5.4)$$

$$f = \underbrace{W^{-1}T^T (TW^{-1}T^T)^{-1}}_{T_\omega^\dagger} \tau \quad (5.5)$$

$$T_\omega^\dagger = W^{-1}T^T (TW^{-1}T^T)^{-1} \quad (5.6)$$

For the case where W is a unity matrix

$$T_\omega^\dagger = T^T (TT^T)^{-1} \quad (5.7)$$

Then, the actuator input vector is found as:

$$u = K^{-1}T_\omega^\dagger \tau \quad (5.8)$$

We used “alloc” command for the control allocation in the Matlab. “alloc” command was formed by Fossen and Matlab GNC Toolbox was used in our simulation sfor “alloc” command.

$$u = \text{alloc}(K, T, W, \text{tau}) \quad (5.9)$$

5.2 Control Allocation for Satellite

For the satellite, allocation problem is between the euler angles $n = 3$ (roll, pitch, yaw) and actuators $r = 4$ (reaction wheels). Allocation matrix T consists of four column vectors. Each column vector represents the distribution of the reaction wheel torques to each axis of rotation of the satellite. Allocation matrix for the satellite with four reaction wheels is given as

$$T = [t_1 \quad t_2 \quad t_3 \quad t_4] = \begin{bmatrix} r_{1,x} & r_{2,x} & r_{3,x} & r_{4,x} \\ r_{1,y} & r_{2,y} & r_{3,y} & r_{4,y} \\ r_{1,z} & r_{2,z} & r_{3,z} & r_{4,z} \end{bmatrix} \quad (5.10)$$

5.3 Configuration of Reaction Wheels

The reaction wheels of BILSAT-1 are arranged in a tetrahedral configuration. Tetrahedral configuration is used for the robust control and continuity of the control operation during failure in the any reaction wheel. The other advantage of tetrahedral configuration comes from the geometry of the location of wheels. That's, wheel assembly is capable to deliver the satellite twice as much of the maximum torque that a single wheel can supply.

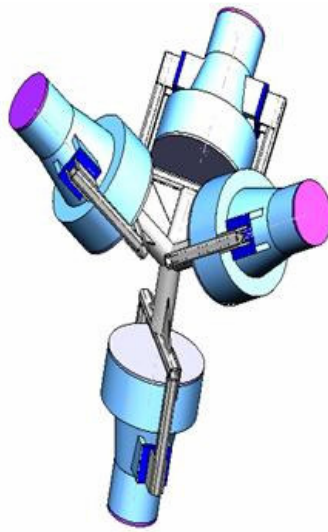


Figure-5.2: Tetrahedral Configuration of Reaction Wheels

Allocation matrix for the tetrahedral configuration can be found using equation 5.10. Equations given below are valid for each axis in equation 5.10.

$$r_{1,x} + r_{2,x} + r_{3,x} + r_{4,x} = 0 \quad (5.11)$$

$$r_{1,y} + r_{2,y} + r_{3,y} + r_{4,y} = 0 \quad (5.12)$$

$$r_{1,z} + r_{2,z} + r_{3,z} + r_{4,z} = 0 \quad (5.13)$$

These equations imply that in all axes total moment is zero. Each column vector is the unity vector, i.e.

$$\sqrt{(r_{i,x})^2 + (r_{i,y})^2 + (r_{i,z})^2} = 1, \quad i = 1, 2, 3, 4. \quad (5.14)$$

Angle between all vectors is $\varphi = 2 \cos^{-1}(1/\sqrt{3}) = 109.47^\circ$. Thus the scalar product between the two vectors is $t_i t_j = |t_i| |t_j| \cos \varphi$ where $|t_i| = |t_j| = 1$ and φ is the angle between the vectors.

t_1 , the first column of T , is replaced along the z axis as $t_1 = [0 \ 0 \ -1]$. From the equation 5.13 $r_{2,z} = r_{3,z} = r_{4,z}$ are found as $r_{2,z} = r_{3,z} = r_{4,z} = \frac{1}{3}$. Then the preliminary matrix becomes

$$T = \begin{bmatrix} 0 & r_{2,x} & r_{3,x} & r_{4,x} \\ 0 & r_{2,y} & r_{3,y} & r_{4,y} \\ -1 & \frac{1}{3} & \frac{1}{3} & \frac{1}{3} \end{bmatrix} \quad (5.15)$$

For finding t_2 , $r_{2,x} = 0$ is considered and equation 5.14 is solved for $i = 2$

$$\sqrt{(0)^2 + (r_{2,y})^2 + \left(\frac{1}{3}\right)^2} = 1 \quad (5.16)$$

$$r_{2,y} = \pm \sqrt{1 - \left(\frac{1}{3}\right)^2} \quad (5.17)$$

$$r_{2,y} = \pm \frac{2}{3} \sqrt{2} \quad (5.18)$$

If $r_{2,y} = -\frac{2}{3} \sqrt{2}$ is chosen as one of the possible solutions, application of equation

5.12 results in $r_{3,y} = r_{4,y} = \frac{1}{3} \sqrt{2}$. Thus the temporary tetrahedral matrix becomes

$$T = \begin{bmatrix} 0 & 0 & r_{3,x} & r_{4,x} \\ 0 & -\frac{2}{3} \sqrt{2} & \frac{1}{3} \sqrt{2} & \frac{1}{3} \sqrt{2} \\ -1 & \frac{1}{3} & \frac{1}{3} & \frac{1}{3} \end{bmatrix} \quad (5.19)$$

For finding t_3 and t_4 , equation 5.14 is solved for $i = 3, 4$

$$\sqrt{(r_{i,x})^2 + \left(\frac{1}{3}\sqrt{2}\right)^2 + \left(\frac{1}{3}\right)^2} = 1 \quad (5.20)$$

$$r_{i,x} = \pm \sqrt{1 - \left(\frac{1}{3}\right)^2 - \left(\frac{1}{3}\sqrt{2}\right)^2} \quad (5.21)$$

$$r_{i,x} = \pm \frac{1}{3}\sqrt{6} \quad \text{for } i = 3, 4 \quad (5.22)$$

Choosing $r_{3,x} = \frac{1}{3}\sqrt{6}$ and $r_{4,x} = -\frac{1}{3}\sqrt{6}$ (5.23)

Final tetrahedral allocation (distribution) matrix T is found as;

$$T = \begin{bmatrix} 0 & 0 & \frac{1}{3}\sqrt{6} & -\frac{1}{3}\sqrt{6} \\ 0 & -\frac{2}{3}\sqrt{2} & \frac{1}{3}\sqrt{2} & \frac{1}{3}\sqrt{2} \\ -1 & \frac{1}{3} & \frac{1}{3} & \frac{1}{3} \end{bmatrix} \quad (5.24)$$

CHAPTER 6

CONTROLLER DESIGN and SIMULATIONS

In this chapter quaternion feedback controller and sliding mode regulator for the maneuver of a small satellite using reaction wheels are described. After that their simulations in the matlab and simulink are given. Finally, the comments and discussions on the obtained responses are given.

6.1 Quaternion Feedback Controller (PD)

In quaternion feedback, attitude is controlled by calculating the attitude deviation. Suppose that the desired orientation of the body is given by a rotation matrix R_d and actual orientation is given by a rotation matrix R . In the case of rotation matrices, it does not make sense to subtract R_d from R as the result would not be a valid rotation matrix for the attitude deviation. Deviation between the desired and the actual orientation is described by the rotation matrix $\tilde{R} \in SO(3)$ defined by $\tilde{R} \triangleq R_d^T R$. $R(\tilde{q}) \triangleq R^T(q_d)R(q) = R(q_d^*)R(q)$ where q_d is the desired quaternion, q_d^* is the complex conjugate of q_d , q is actual quaternion and \tilde{q} is the actual error according to references [6] and [19]. Successive rotations in quaternion representation are expressed as $R(q_d^*)R(q) = R(q_d^* \otimes q)$, where \otimes is the quaternion product operator. Then error in unit quaternions can be written as [6], [19]

$$\tilde{q} = q_d^* \otimes q = \begin{bmatrix} \eta_d & \varepsilon_d^T \\ -\varepsilon_d & \eta_d 1_{3 \times 3} - S(\varepsilon_d) \end{bmatrix} q = \begin{bmatrix} \eta_d \eta + \varepsilon_d^T \varepsilon \\ \eta_d \varepsilon - \eta \varepsilon_d - \varepsilon_d \times \varepsilon \end{bmatrix} \quad (6.1)$$

The attitude error quaternion vector consists of the last three elements of \tilde{q} .

$$\tilde{\varepsilon} = \eta_d \varepsilon - \eta \varepsilon_d - \varepsilon_d \times \varepsilon \quad (6.2)$$

and derivative of this error is calculated as;

$$\dot{\tilde{\epsilon}} = \dot{\eta}_d \epsilon + \eta_d \dot{\epsilon} - \dot{\eta} \epsilon_d - \eta \dot{\epsilon}_d - \dot{\epsilon}_d \times \epsilon - \epsilon_d \times \dot{\epsilon} \quad (6.3)$$

Nonlinear proportional and derivational (PD) controller is constituted using 6.2 and 6.3.

$$u = -K_p \tilde{\epsilon} - K_d \dot{\tilde{\epsilon}} \quad (6.4)$$

where u is the torque vector K_p is positive definite proportional gain constant and K_d is positive definite derivative gain constant. Notice that, although it is a PD controller in terms of quaternion and its derivative, it is a nonlinear controller in terms of Euler angles which are the actual variables that are controlled.

6.1.1 Stability Analysis

Stability analysis of the quaternion feedback controller is based on the Lyapunov candidate function (LCF). The total energy of the satellite can be chosen as the LCF. Energy equations and lyapunov analysis are given below.

6.1.2 Energy Considerations

The total energy of the satellite can be divided into kinetic and potential energy. Kinetic energy of the satellite is a result of the rotation in the orbit frame. On the other hand gravity gradient and gyro effects due to revolution about the Earth are the main sources of the potential energy.

6.1.2.1 Kinetic Energy

The kinetic energy is given in body frame with respect to the orbit frame as

$$E_{kin} = \frac{1}{2} (\omega_{BO}^B)^T \mathbf{I} \omega_{BO}^B \quad (6.5)$$

6.1.2.2 Potential Energy

Equation 6.6 represents the potential energy due to the gravity gradient and equation 6.7 represents the potential energy due to revolution of the satellite about the Earth.

$$E_{gg} = \frac{3}{2} \omega_o^2 ((\mathbf{c}_3^B)^T \mathbf{I} \mathbf{c}_3^B - I_z) \quad (6.6)$$

$$E_{gyro} = \frac{1}{2} \omega_o^2 (I_x - (\mathbf{c}_1^B)^T \mathbf{I} \mathbf{c}_1^B) \quad (6.7)$$

6.1.2.3 Total Energy

Total energy of the satellite is computed as the sum of kinetic and potential energy.

$$E_{tot} = E_{kin} + E_{gg} + E_{gyro} \quad (6.8)$$

Distinct form of equation 6.8 is:

$$E_{tot} = \frac{1}{2}(\boldsymbol{\omega}_{BO}^B)^T \mathbf{I} \boldsymbol{\omega}_{BO}^B + \frac{3}{2} \omega_o^2 ((\mathbf{c}_3^B)^T \mathbf{I} \mathbf{c}_3^B - I_z) + \frac{1}{2} \omega_o^2 (I_x - (\mathbf{c}_1^B)^T \mathbf{I} \mathbf{c}_1^B) \quad (6.9)$$

$$\text{Using } \mathbf{c}_i^B = [c_{1i}^B \ c_{2i}^B \ c_{3i}^B]^T \text{ and } (\mathbf{c}_i^B)^T \mathbf{I} \mathbf{c}_i^B = I_x c_{1i}^2 + I_y c_{2i}^2 + I_z c_{3i}^2 \quad (6.10)$$

equation 6.9 turns into the following:

$$E_{tot} = \frac{1}{2}(\boldsymbol{\omega}_{BO}^B)^T \mathbf{I} \boldsymbol{\omega}_{BO}^B + \frac{3}{2} \omega_o^2 (I_x c_{13}^2 + I_y c_{23}^2 + I_z (c_{33}^2 - 1)) + \frac{1}{2} \omega_o^2 (I_z c_{31}^2 + I_y c_{21}^2 + I_x (c_{11}^2 - 1)) \quad (6.11)$$

In chapter 3 equation 3.5 states that R_O^B is orthogonal. This means that:

$$c_{11}^2 + c_{21}^2 + c_{31}^2 = 1 \text{ and } c_{13}^2 + c_{23}^2 + c_{33}^2 = 1 \quad (6.12)$$

Using above identities in equation 6.11, one gets

$$E_{tot} = \frac{1}{2}(\boldsymbol{\omega}_{BO}^B)^T \mathbf{I} \boldsymbol{\omega}_{BO}^B + \frac{3}{2} \omega_o^2 ((I_x - I_z) \mathbf{c}_{13}^2 + (I_y - I_z) \mathbf{c}_{23}^2) + \frac{1}{2} \omega_o^2 ((I_x - I_y) \mathbf{c}_{21}^2 + (I_x - I_z) \mathbf{c}_{31}^2) \quad (6.13)$$

as the total energy. The Lyapunov candidate function is chosen as

$$V(\mathbf{x}) = E_{tot} \quad (6.14)$$

In this equation E_{tot} satisfies the properties given below:

$$V(0) = 0 \quad (6.15)$$

$$V(\mathbf{x}) > 0 \quad \forall \mathbf{x} \neq 0 \quad (6.16)$$

From equation 6.13 it is clear that

$$\mathbf{x} = [\boldsymbol{\omega}_{BO}^B, c_{21}, c_{31}, c_{13}, c_{23}]^T \quad (6.17)$$

and if $\mathbf{x} = 0$ then $V(0) = 0$.

For ensuring that the energy function is positive definite $V(\mathbf{x}) > 0 \quad \forall \mathbf{x} \neq 0$, inertial constraint required is $I_x > I_y > I_z$. In BILSAT-1 this constraint is not satisfied.

However, when we have investigated the energy function using Matlab, we have seen that energy function was positive definite. Therefore we have used total energy

function to show stability analysis of quaternion feedback controller.

The derivative of the Lyapunov function is given in [9] and [19] as

$$\dot{V} = (\omega_{BO}^B)^T \tau^B \quad (6.18)$$

Refreshing the fact that quaternion feedback controller was

$$u = -K_p \tilde{\epsilon} - K_d \dot{\tilde{\epsilon}} \quad (6.19)$$

with u being the torque applied to the system, \dot{V} becomes;

$$\dot{V} = (\omega_{BO}^B)^T \tau^B = (\omega_{BO}^B)^T (-K_p \tilde{\epsilon} - K_d \dot{\tilde{\epsilon}}) \quad (6.20)$$

Using equations 6.2 and 6.3 in equation 6.20, the new expression given below is obtained.

$$\begin{aligned} \dot{V} = & (\omega_{BO}^B)^T (-K_p (\eta_d \epsilon - \eta \epsilon_d - \epsilon_d \times \epsilon) \\ & - K_d (\dot{\eta}_d \epsilon + \eta_d \dot{\epsilon} - \dot{\eta} \epsilon_d - \eta \dot{\epsilon}_d - \dot{\epsilon}_d \times \epsilon - \epsilon_d \times \dot{\epsilon})) \end{aligned} \quad (6.21)$$

Making use of kinematic equations of the satellite, derivative of the energy function can be expressed as;

$$\begin{aligned} \dot{V} = & (\omega_{BO}^B)^T (-K_p (\eta_d \epsilon - \eta \epsilon_d - \epsilon_d \times \epsilon) - K_d (\dot{\eta}_d \epsilon + \eta_d (\frac{1}{2}(\eta 1 + S(\epsilon)) \omega_{BO}^B) \\ & - (-\frac{1}{2} \epsilon^T \omega_{BO}^B) \epsilon_d - \eta \dot{\epsilon}_d - \dot{\epsilon}_d \times \epsilon - \epsilon_d \times (\frac{1}{2}(\eta 1 + S(\epsilon)) \omega_{BO}^B))) \end{aligned} \quad (6.22)$$

Using skew symmetric matrix expression for the cross products in equation 6.22, one gets

$$\begin{aligned} \dot{V} = & (\omega_{BO}^B)^T (-K_p (\eta_d \epsilon - \eta \epsilon_d - S(\epsilon_d) \epsilon) - K_d (\dot{\eta}_d \epsilon + \eta_d (\frac{1}{2}(\eta 1 + S(\epsilon)) \omega_{BO}^B) \\ & - (-\frac{1}{2} \epsilon^T \omega_{BO}^B) \epsilon_d - \eta \dot{\epsilon}_d - S(\dot{\epsilon}_d) \epsilon - S(\epsilon_d) (\frac{1}{2}(\eta 1 + S(\epsilon)) \omega_{BO}^B))) \end{aligned} \quad (6.23)$$

From equation 6.23 it is not easy to predict that $\dot{V} < 0$. Some steps for further simplification should be taken.

For the sake of simplicity, if reference is taken as zero, equation 6.20 changes into

$$\dot{V} = (\omega_{BO}^B)^T (-K_p \epsilon - K_d \dot{\epsilon}) \quad (6.24)$$

By adding a new term to Lyapunov function in equation 6.9 one gets

$$\begin{aligned} V = & \frac{1}{2} (\omega_{BO}^B)^T I \omega_{BO}^B + \frac{3}{2} \omega_o^2 ((c_3^B)^T I c_3^B - I_z) + \\ & \frac{1}{2} \omega_o^2 (I_x - (c_1^B)^T I c_1^B) + K_p (\epsilon^T \epsilon + (1 - \eta)^2) \end{aligned} \quad (6.25)$$

where $K_p (\epsilon^T \epsilon + (1 - \eta)^2)$ is the new added term. By using the property $\epsilon^T \epsilon + \eta^2 = 1$

this new term can be further simplified as:

$$K_p(\boldsymbol{\varepsilon}^T \boldsymbol{\varepsilon} + 1 - 2\eta + \eta^2) = 2K_p(1 - \eta) \quad (6.26)$$

Derivative of this equation is;

$$-2K_p \dot{\eta} \quad (6.27)$$

From equation 4.21 $\dot{\eta}$ expression is added, and this results in;

$$K_p \boldsymbol{\varepsilon}^T \boldsymbol{\omega}_{BO}^B \quad (6.28)$$

After that, the derivative of the new Lyapunov function can be expressed as;

$$\dot{V} = (\boldsymbol{\omega}_{BO}^B)^T (\boldsymbol{\tau}_r^B + K_p \boldsymbol{\varepsilon}) \quad (6.29)$$

Putting torque expression $\boldsymbol{\tau}_r^B$ for the zero reference results in;

$$\dot{V} = (\boldsymbol{\omega}_{BO}^B)^T (-K_p \boldsymbol{\varepsilon} - K_d \dot{\boldsymbol{\varepsilon}} + K_p \boldsymbol{\varepsilon}) \quad (6.30)$$

$$\dot{V} = (\boldsymbol{\omega}_{BO}^B)^T (-K_d \dot{\boldsymbol{\varepsilon}}) \quad (6.31)$$

Now it is required to show that equation 6.31 is negative definite. Inserting equation 4.22 for the $\dot{\boldsymbol{\varepsilon}}$ term gives;

$$\dot{V} = (\boldsymbol{\omega}_{BO}^B)^T (-K_d (\frac{1}{2}(\boldsymbol{\eta} \mathbf{1}_{3 \times 3} + \mathcal{S}(\boldsymbol{\varepsilon}))) \boldsymbol{\omega}_{BO}^B) \quad (6.32)$$

Then, with zero reference, it is seen that the system will be stable provided that $(\boldsymbol{\eta} \mathbf{1}_{3 \times 3} + \mathcal{S}(\boldsymbol{\varepsilon}))$ term is positive definite. For positive definiteness of this 3×3 matrix, the leading principal minors should be positive. i.e. $\boldsymbol{\eta} > 0, \boldsymbol{\eta}^2 + \boldsymbol{\varepsilon}_3^2 > 0$ and $\boldsymbol{\eta}(\boldsymbol{\eta}^2 + \boldsymbol{\varepsilon}_1^2 + \boldsymbol{\varepsilon}_2^2 + \boldsymbol{\varepsilon}_3^2) > 0$. This shows that \dot{V} is negative definite provided that $\boldsymbol{\eta} > 0$.

In equation 3.24 $\boldsymbol{\eta}$ was given as $\boldsymbol{\eta} = \cos \frac{\boldsymbol{\varphi}}{2}$, therefore $\boldsymbol{\varphi}$ must be in an interval $-\pi < \boldsymbol{\varphi} < \pi$ for it to be positive. So, as a result, one can state that the method works properly, provided the inertial constraints stated are satisfied. Once the stability is guaranteed, one can choose proper K_p and K_d values for better system performance.

6.2 Sliding Mode Regulator

The sliding mode regulator idea is based on bringing the system states to a manifold or surface where the states stay for all time. The sliding manifold is designed such that once the system states are on the sliding manifold, states will converge to the desired states. Sliding mode controller has the ability to deal with parameter variations in the original nonlinear system (Robustness).

Satellite dynamic model was given in equation 4.12 as

$$\mathbf{I}^B \dot{\boldsymbol{\omega}}_{BO}^B = -\boldsymbol{\omega}_{BO}^B \times (\mathbf{I}^B \boldsymbol{\omega}_{BO}^B) + \boldsymbol{\tau}^B \quad (6.33)$$

By defining a new matrix $M(q)$ as

$$M(q) = \eta \mathbf{1}_{3 \times 3} + S(\boldsymbol{\varepsilon}) \quad (6.34)$$

$$M(q) = \begin{bmatrix} \eta & -\varepsilon_3 & \varepsilon_2 \\ \varepsilon_3 & \eta & -\varepsilon_1 \\ -\varepsilon_2 & \varepsilon_1 & \eta \end{bmatrix} \quad (6.35)$$

the kinematic equations in 4.23 can be rewritten as:

$$\dot{\eta} = -\frac{1}{2} \boldsymbol{\varepsilon}^T \boldsymbol{\omega}_{BO}^B \quad (6.36)$$

$$\dot{\boldsymbol{\varepsilon}} = \frac{1}{2} M(q) \boldsymbol{\omega}_{BO}^B \quad (6.37)$$

The task of the sliding mode controller is formulated as to bring the limit of the norm of quaternion error to zero. $\boldsymbol{\varepsilon}_e(t) = \boldsymbol{\varepsilon}_d(t) - \boldsymbol{\varepsilon}(t)$

$$\lim_{t \rightarrow \infty} \|\boldsymbol{\varepsilon}_d(t) - \boldsymbol{\varepsilon}(t)\| = 0 \quad (6.38)$$

where $\boldsymbol{\varepsilon}_d(t)$ is the desired quaternion, $\boldsymbol{\varepsilon}(t)$ is the actual quaternion and $\boldsymbol{\varepsilon}_e(t)$ is the quaternion error. According to reference [22], a suitable sliding manifold $\boldsymbol{\sigma}$ is chosen such that it is reached in finite time and is maintained thereafter.

$$\boldsymbol{\sigma}(\boldsymbol{\varepsilon}) = \dot{\boldsymbol{\varepsilon}}_e + K \boldsymbol{\varepsilon}_e = 0 \quad (6.39)$$

where K is a diagonal positive matrix and

$$\dot{\boldsymbol{\varepsilon}}_e = \dot{\boldsymbol{\varepsilon}}_d - \dot{\boldsymbol{\varepsilon}} \quad (6.40)$$

Using equation 6.37 in 6.40 one gets

$$\dot{\boldsymbol{\varepsilon}}_e = \dot{\boldsymbol{\varepsilon}}_d - \frac{1}{2} M(q) \boldsymbol{\omega}_{BO}^B \quad (6.41)$$

Derivative of sliding manifold, as derived in reference [22], is given as:

$$\dot{\boldsymbol{\sigma}} = \left[\ddot{\boldsymbol{\varepsilon}}_d - \frac{1}{2} \dot{\eta} \boldsymbol{\omega}_{BO}^B + \frac{1}{2} M \mathbf{I}^{-1} S(\boldsymbol{\omega}_{BO}^B) \mathbf{I} \boldsymbol{\omega}_{BO}^B - \frac{1}{2} M \mathbf{I}^{-1} \boldsymbol{\tau}^B + K \dot{\boldsymbol{\varepsilon}}_e \right] \quad (6.42)$$

Lyapunov candidate function is chosen as:

$$V = \frac{1}{2} \boldsymbol{\sigma}^T M \mathbf{I}^{-1} \boldsymbol{\sigma} > 0 \quad \text{and} \quad \dot{V} = \frac{1}{2} \boldsymbol{\sigma}^T M \mathbf{I}^{-1} \dot{\boldsymbol{\sigma}} \quad (6.43)$$

where $M \mathbf{I}^{-1}$ is a symmetric positive definite matrix. Then, \dot{V} becomes

$$\dot{V} = \boldsymbol{\sigma}^T \left[-\frac{1}{2} M \mathbf{I}^{-1} \dot{\eta} \boldsymbol{\omega}_{BO}^B + \frac{1}{2} S(\boldsymbol{\omega}_{BO}^B) \mathbf{I} \boldsymbol{\omega}_{BO}^B + M \mathbf{I}^{-1} \ddot{\boldsymbol{\varepsilon}}_d + M \mathbf{I}^{-1} K \dot{\boldsymbol{\varepsilon}}_e - \frac{1}{2} \boldsymbol{\tau}^B + M \mathbf{I}^{-1} \boldsymbol{\sigma} \right] \quad (6.44)$$

Control law is chosen as $\tau = u_{eq} + \rho \text{sign}(\sigma)$ where proper control torque u_{eq} cancels out all the terms in the derivative of V, and $\rho \text{sign}(\sigma)$ guarantees that it is less than zero at all times. After the substitution, the derivative of V being negative definite shows the existence of a sliding mode controller that is asymptotically stable.i.e

$$u_{eq} = -IM^{-1}\dot{\eta}\omega_{BO}^B + S(\omega_{BO}^B)I\omega_{BO}^B + 2IM^{-1}\ddot{\epsilon}_d + 2IM^{-1}K\dot{\epsilon}_e + 2IM^{-1}\sigma \quad (6.45)$$

$$\dot{V} = -\sigma^T \rho \text{sign}(\sigma) = -\sigma^T \rho \sum_{i=1}^3 |\sigma_i| \quad (\rho > 0) \quad (6.46)$$

U_{eq} is costly for implementation and the sign function causes chattering problem, To overcome these difficulties discontinuous control law is implemented satisfying all requirements for stability with the following discontinuous control law .

$$\tau_i = u_i^{\max} \text{sat}\left(\frac{\sigma_i}{\Phi}\right) \quad i = 1, 2, 3 \quad (6.47)$$

where Φ is the sliding boundary layer (thickness) and

$$u_i^{\max} \geq |u_{i_{eq}}| + \rho \quad , \quad (\rho > 0) \quad (6.48)$$

u_i^{\max} was taken as maximum torque of reaction wheels and equation 6.47 was realized as controller torque in our simulations. Saturation function is used to help mediate the chattering problem that occurs with the sign function. Saturation function ($\text{sat}(\cdot)$) is given as

$$\text{sat}\left(\frac{\sigma_i}{\Phi}\right) = \begin{cases} 1 & \text{for } \sigma_i > \Phi \\ \frac{\sigma_i}{\Phi} & \text{for } |\sigma_i| \leq |\Phi| \\ -1 & \text{for } \sigma_i < -\Phi \end{cases} \quad (6.49)$$

The saturation function becomes the sign function when sliding boundary layer approaches zero.

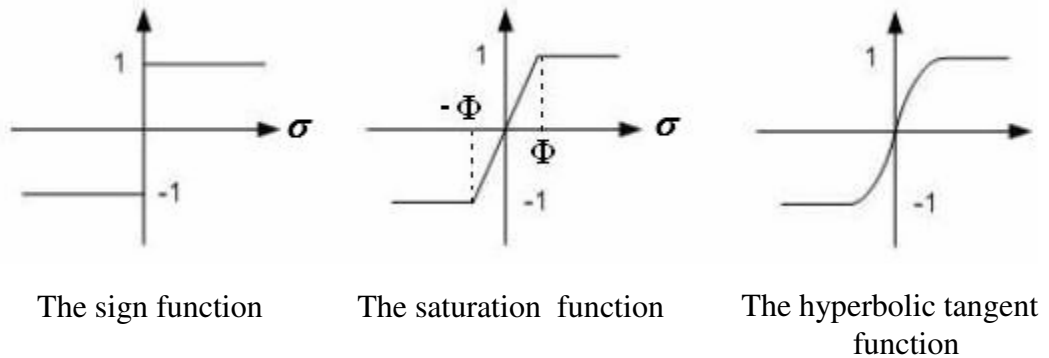


Figure-6.1: Functions

6.3 Simulations

Based on the information and derivations done in previous chapters controllers are designed and simulated using Matlab and Simulink software. General BILSAT-1 parameters which are used in the simulations are given in the table below.

Table-6.1: General BILSAT-1 parameters

Parameter	Value
Weight	120 kg
Inertia Moment	$I_x = 9.8194, I_y = 9.7030, I_z = 9.7309 \text{ kgm}^2$
Orbit	686 km
Orbit Period	97.7 Min

6.3.1 Quaternion Feedback Controller (PD)

Quaternion feedback controller is investigated for the BILSAT-1 satellite. Reaction wheels are considered as actuator for maneuver of the satellite.

Simulation parameters are as shown in table below.

Table-6.2: Simulation parameters of Quaternion Feedback Controller

Initial Angular Velocity:	$\omega_{BO}^B = [0 \ 0 \ 0]^T$
Initial Euler Angles:	$[\phi \ \theta \ \psi] = [0 \ 0 \ 0]$
Proportional Gain Parameter K_p:	0.5
Derivative Gain Parameter K_d:	2.5
Desired Euler Angles:	$[\phi \ \theta \ \psi] = [20 \ 40 \ 60]$
Max Torque of Wheels:	1 Nm
Aerodynamic Torque:	$3.4245e-7$

K_p and K_d values are chosen empirically (trial and error) regarding best tuning. It is noticed that if K_p is decreased, the frequency of oscillations decreases. If K_d is increased, the system damps faster. Simulations in this section are repeated for several cases. In all cases aerodynamic torque is taken into consideration.

In case 1, four reaction wheels are applied as the actuators and noise effect is not considered.

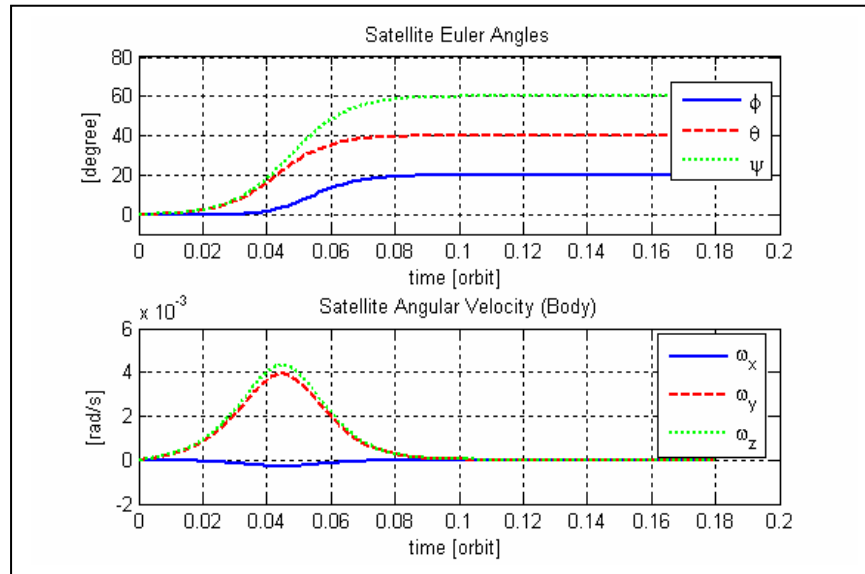


Figure-6.2: System response of QFC without noise

The system is overdamped with long rise time and settling time. Rise time is 0.04 orbits and settling time is 0.09 orbits. The angles reach their final value at 0.1 orbits.

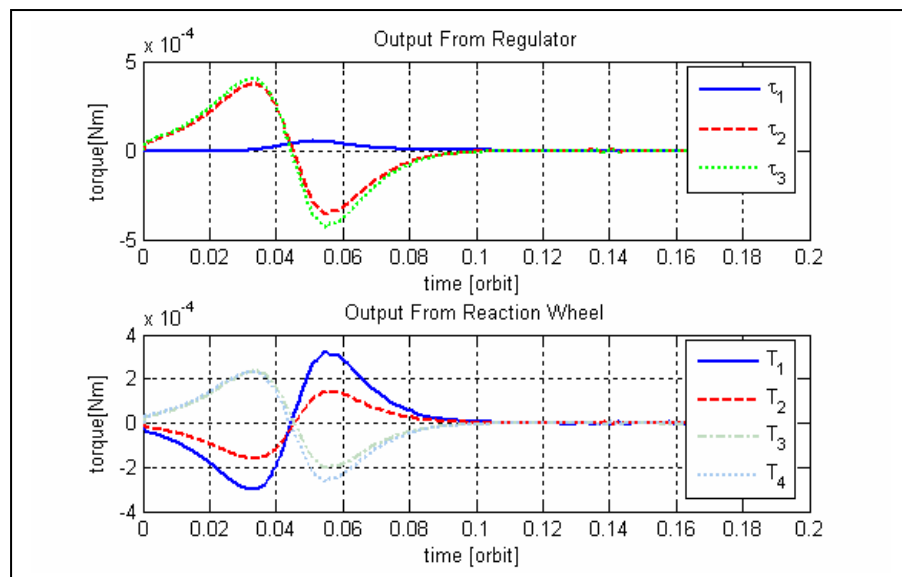


Figure-6.3: Output from regulator and wheels without noise

The upper graph in Figure-6.3 shows the output torque of the controller before the allocation process. The (3×1) output matrix is converted to the (4×1) reaction wheel torque matrix by the allocation command and the lower graph in Figure-6.3 shows this output matrix. The output of the reaction wheels reaches to zero after 0.11 orbits.

In case 2, four reaction wheels are applied as the actuators and uniformly distributed noise effect is considered.

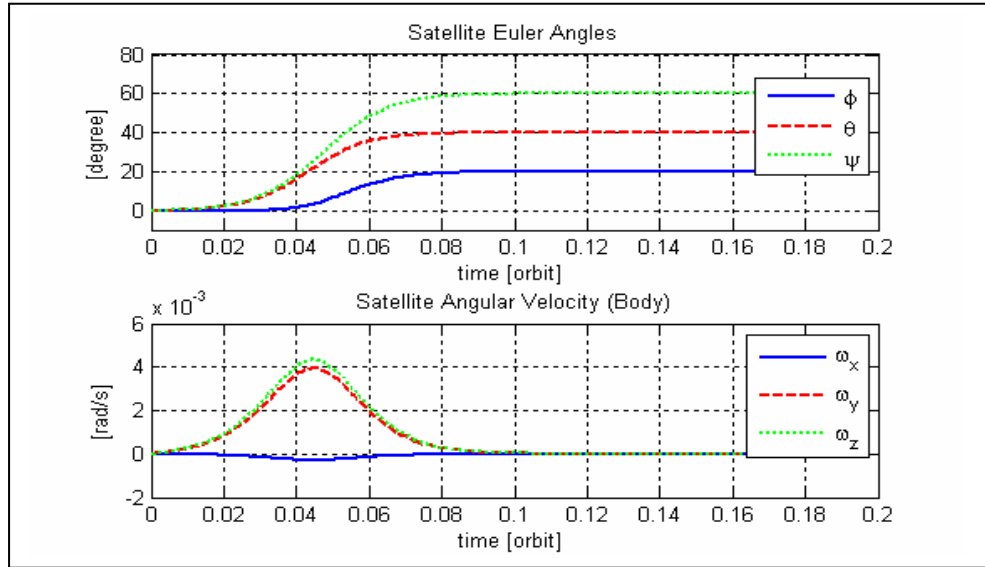


Figure-6.4: System response for QFC with noise

Noise does not affect the euler angle response and angular velocity too much. Using reference model for the filtering is the main reason of this response.

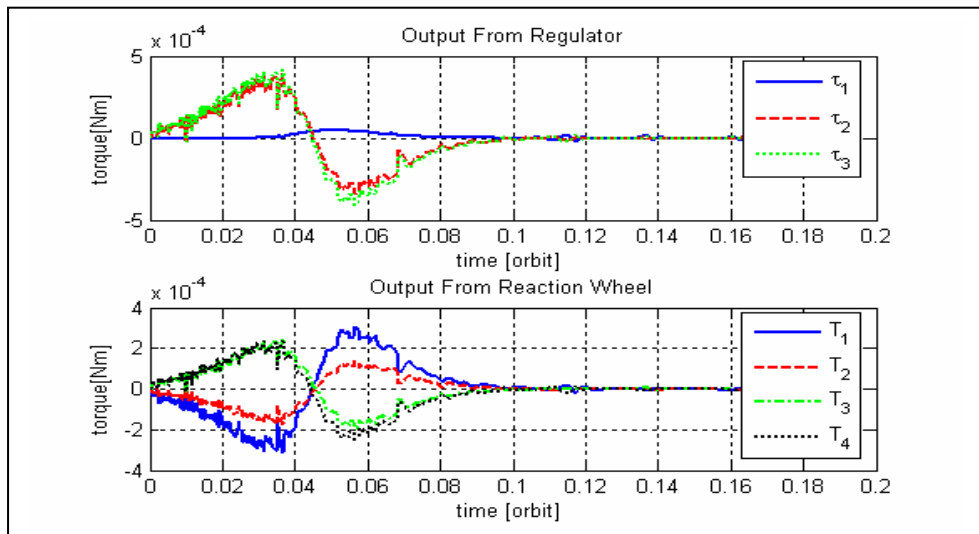


Figure-6.5: Output from regulator and wheels with noise

Compared to case 1, noise affects the torque obtained from the controller output. The affected output from regulator causes the torque coming from reaction wheels to oscillate as it behaves as the input of the allocation process. Output of the reaction wheel does not converge to zero completely but this does not affect the behavior of the overall system.

In case3, the second reaction wheel is disabled in order to show that system still works in case of loss of one reaction wheel. Noise effect is not considered.

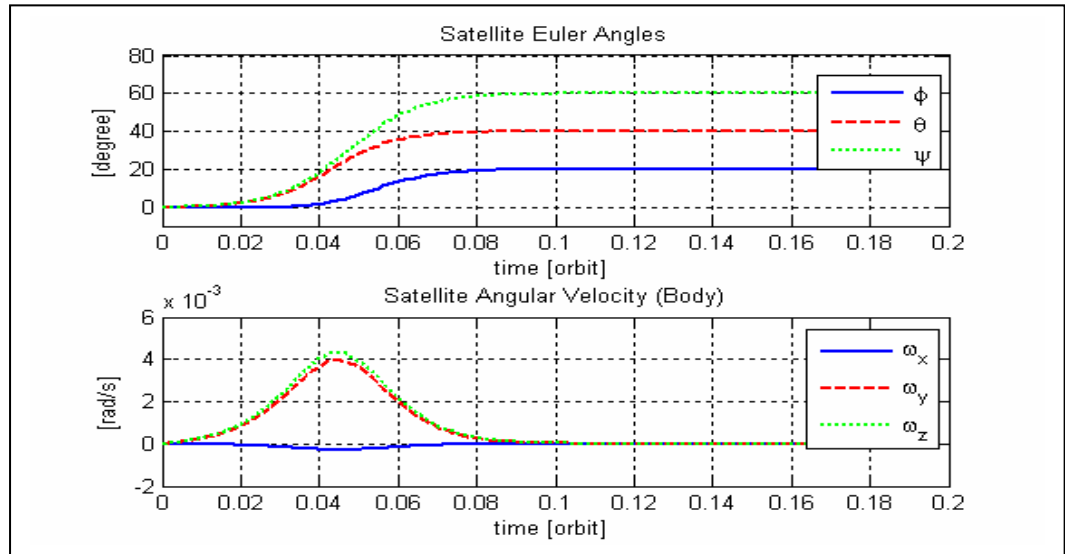


Figure-6.6: System response for the QFC without noise and reaction Wheel-2 was disabled

Disabling the 2nd wheel doesn't effect either settling time or rise time of the satellite euler angles. This is mainly because of the tetrahedral configuration of the reaction wheels.

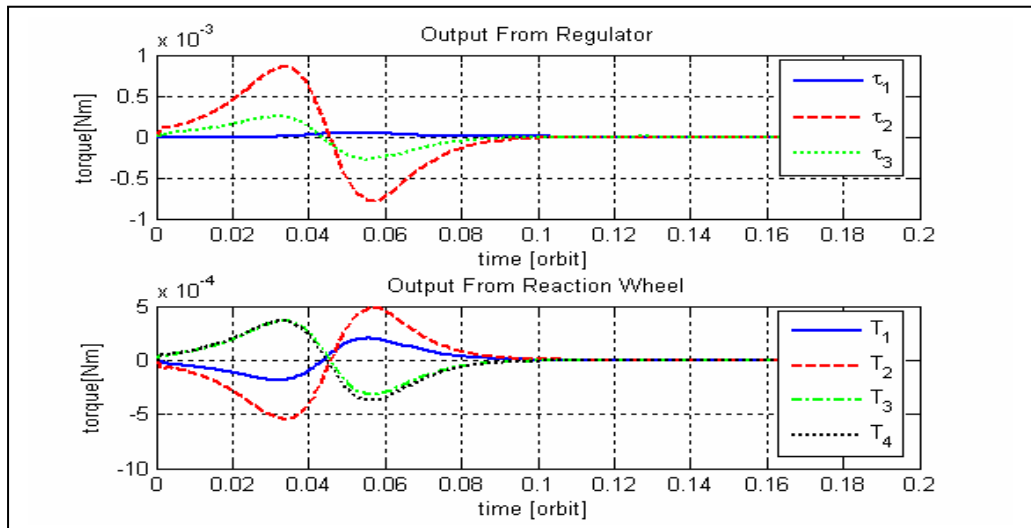


Figure-6.7: Output from regulator and wheels without noise and reaction Wheel-2 was disabled

As can be seen from Figure-6.7 the second reaction wheel is inactive thus produces no torque.

In case 4, the second and fourth reaction wheels are disabled in order to investigate the performance of the system in the case of a loss of two reaction wheels. Noise effect is not considered.

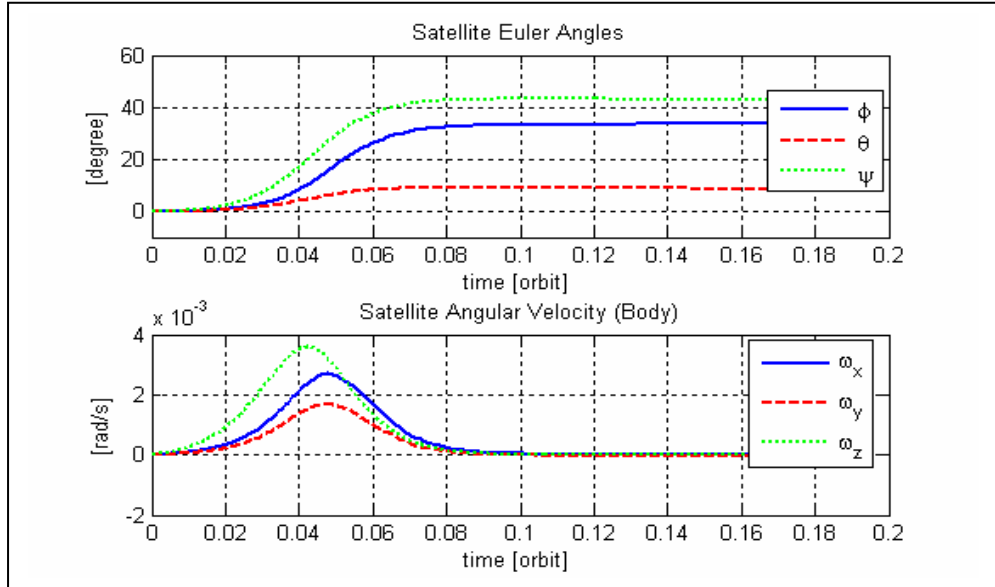


Figure-6.8: System response for the QFC without noise and reaction wheels-2, 4 were disabled

As can be seen from the Figure-6.8, the disabling of the two wheels results in not being able to obtain the desired angles. None of the angles reaches the desired values. It can be concluded that tetrahedral configuration does not compensate for the loss of 2 wheels, but at least the system does not become unstable.

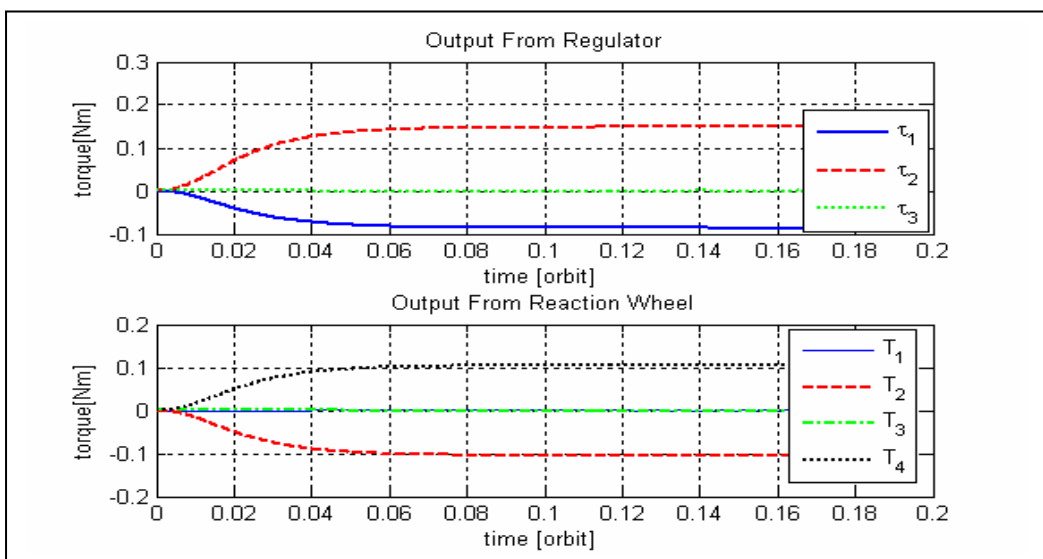


Figure-6.9: Output from regulator and wheels without noise and reaction wheels-2, 4 were disabled

In case 5, Maneuvering of the small satellite in one direction (pitch axis) is simulated. Desired pitch angle is taken as 30° . Noise effect is not considered.

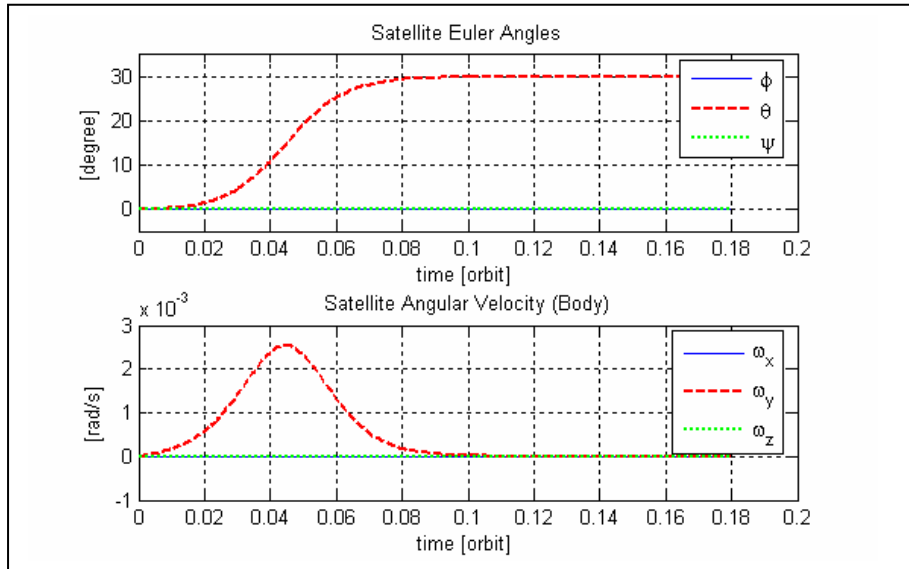


Figure-6.10: System response for the QFC without noise and desired euler angles are $[\phi \ \theta \ \psi] = [0 \ 30 \ 0]$

Rise time is 0.04 orbits and settling time is 0.09 orbits. The pitch angle reaches its final value at 0.1 orbits.

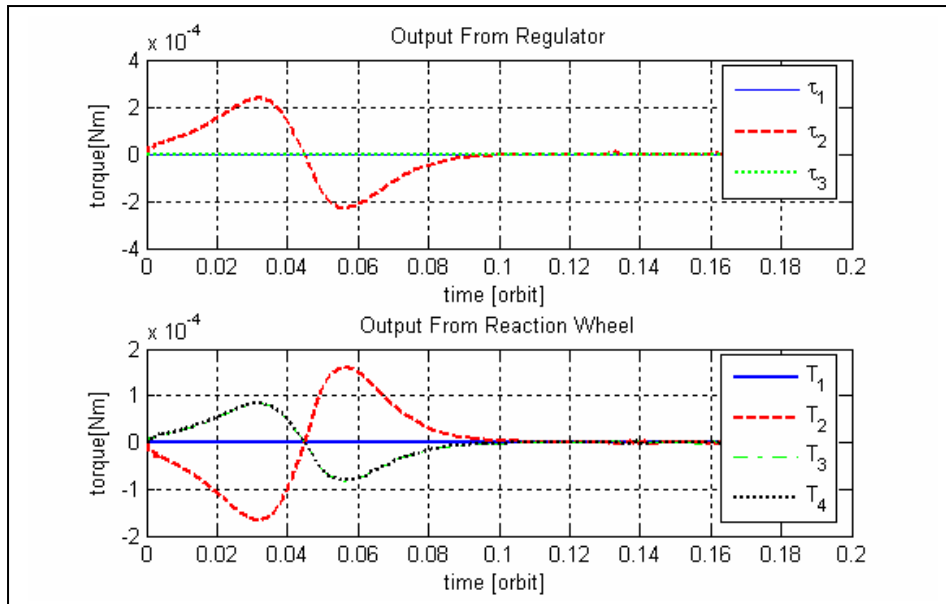


Figure-6.11: Output from regulator and wheels without noise desired euler angles are $[\phi \ \theta \ \psi] = [0 \ 30 \ 0]$

6.3.2 Sliding Mode Regulator

Sliding mode regulator is investigated for the BILSAT-1 satellite. Reaction wheels are considered as actuator for maneuver of the satellite.

Simulation parameters are taken as shown in table below.

Table-6.3: Simulation parameters of the Sliding Mode Regulator

Initial Angular Velocity:	$\omega_{BO}^B = [0 \ 0 \ 0]^T$
Initial Euler Angles:	$[\phi \ \theta \ \psi] = [0 \ 0 \ 0]$
K:	$0.2 * 1_{3 \times 3}$
Φ:	0.002
Desired Euler Angles:	$[\phi \ \theta \ \psi] = [20 \ 40 \ 60]$
Max Torque of Wheels:	1 Nm
Aerodynamic Torque:	$3.4245e-7$

Sliding boundary layer (thickness) Φ was chosen empirically. In case 7, effect of K was investigated. In this case it was seen that if K is increased, oscillation is constituted in the output. Simulations in this section are repeated for several cases as done in previous section. In all cases aerodynamic torque is taken into consideration without case 6.

In case 1, four reaction wheels are applied as the actuators and noise effect is not considered.

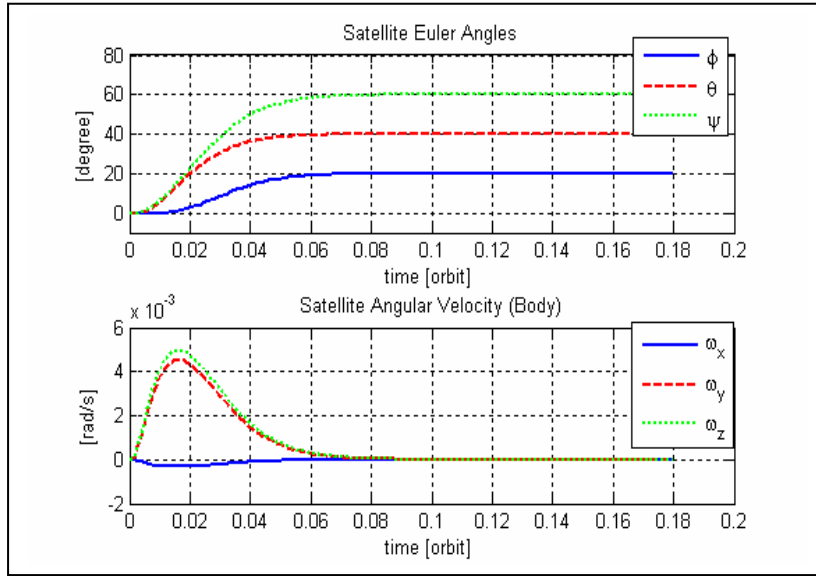


Figure-6.12: System response for the SMR without noise

The system responds faster than QFC. Rise time is 0.04 orbits and settling time is 0.07 orbits. The angles reach their final value at 0.08 orbits.

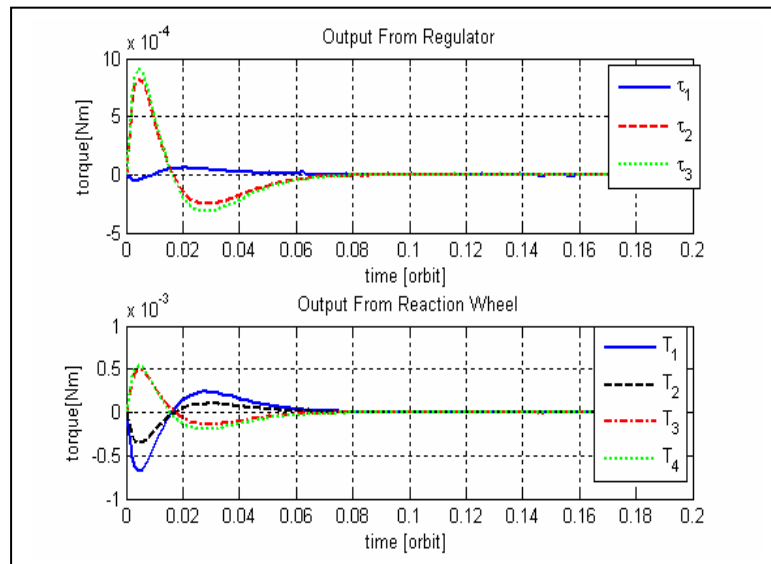


Figure-6.13: Output from regulator and wheels without noise

The upper graph in Figure-6.13 shows the output torque of the controller before the allocation process. The (3×1) output matrix is converted to the (4×1) reaction wheel torque matrix by the allocation command and the lower graph in Figure-6.13 shows this output matrix. The output of the reaction wheels reaches to zero after 0.08 orbits.

In case 2, four reaction wheels are applied as the actuators, noise effect is considered.

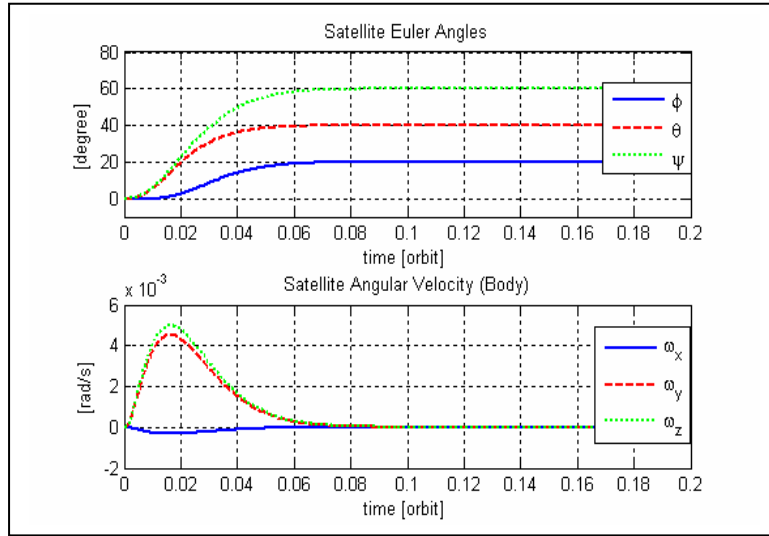


Figure-6.14: System response for the sliding mode regulator with noise

Like QFC, noise does not affect the euler angle response and angular velocity too much.

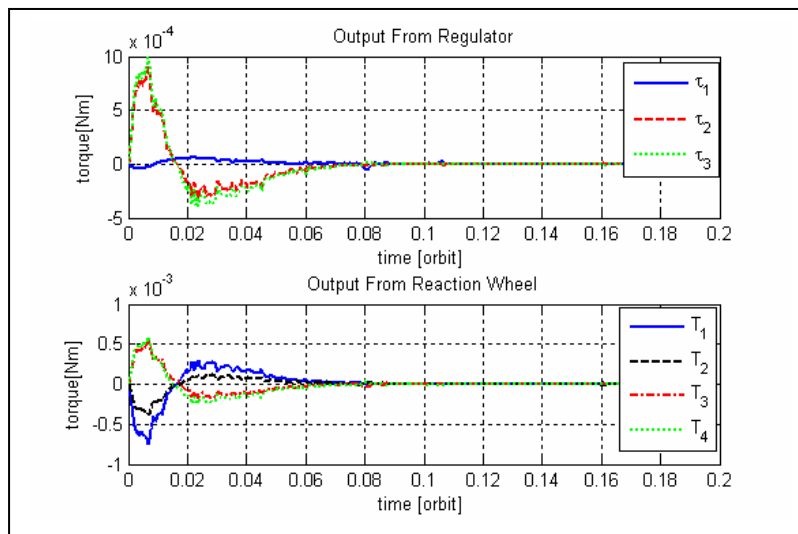


Figure-6.15: Output from regulator and wheels with noise

Noise effects the torque obtained from the controller output. The affected output from regulator causes the torque coming from reaction wheels to oscillate as it behaves as the input of the allocation process. The output reaction wheel does not converge to zero completely but this does not affect the behavior of the overall system. SMR shows better performance than QFC as it can be seen from the comparison of Figure-6.15 and Figure-6.5.

In case 3, the second reaction wheel is disabled in order to show that system still works in case of loss of one reaction wheel. Noise effect is not considered.

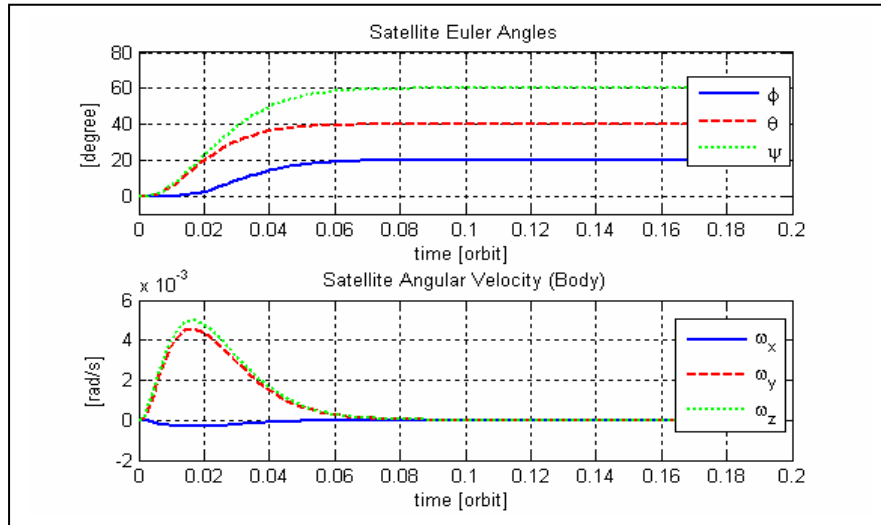


Figure-6.16: System response for the SMR without noise and reaction wheel-2 was disabled

Disabling the 2nd wheel doesn't effect either settling time or rise time of the satellite euler angles. This is mainly because of the tetrahedral configuration of the reaction wheels.

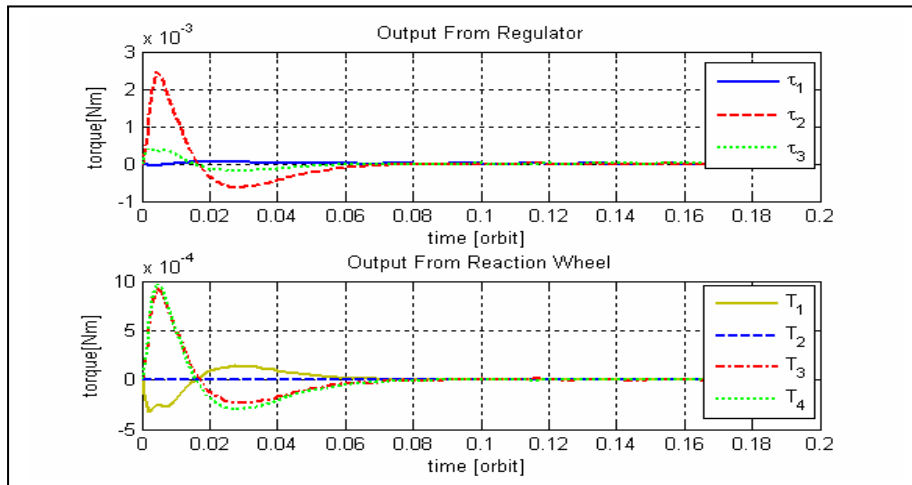


Figure-6.17: Output from regulator and wheels without noise and reaction Wheel-2 was disabled

As can be seen from figure-6.17 the second reaction wheel is inactive thus produces no torque.

In case 4, the second and fourth reaction wheels are disabled in order to investigate the performance of the system in the case of a loss of two reaction wheels. Noise effect is not considered.

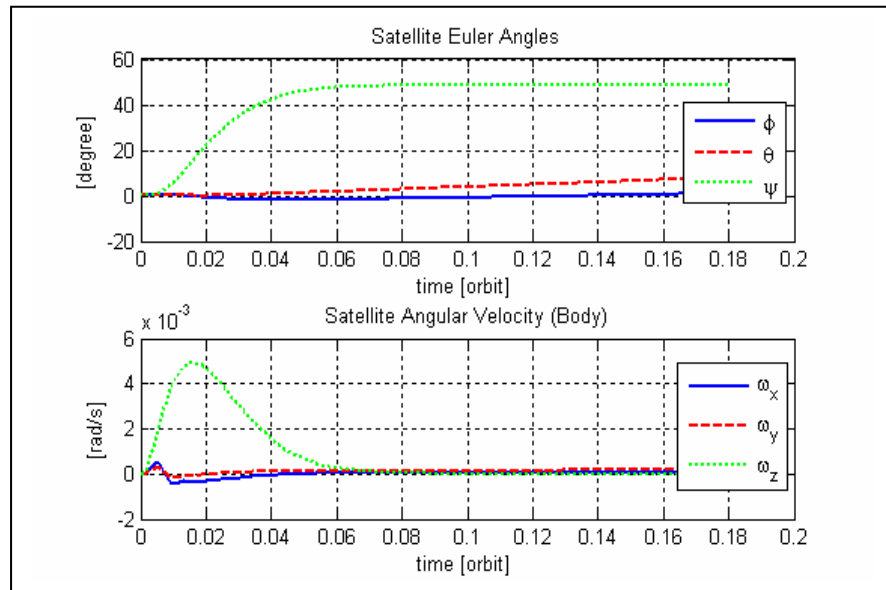


Figure-6.18: System response for the sliding mode regulator without noise and reaction wheel-2, 4 were disabled

As can be seen from the Figure-6.18, the disabling of the two wheels results in not being able to obtain the desired angles. None of the angles reaches the desired values. It can be concluded that tetrahedral configuration does not compensate for the loss of 2 wheels, but at least the system does not become unstable.

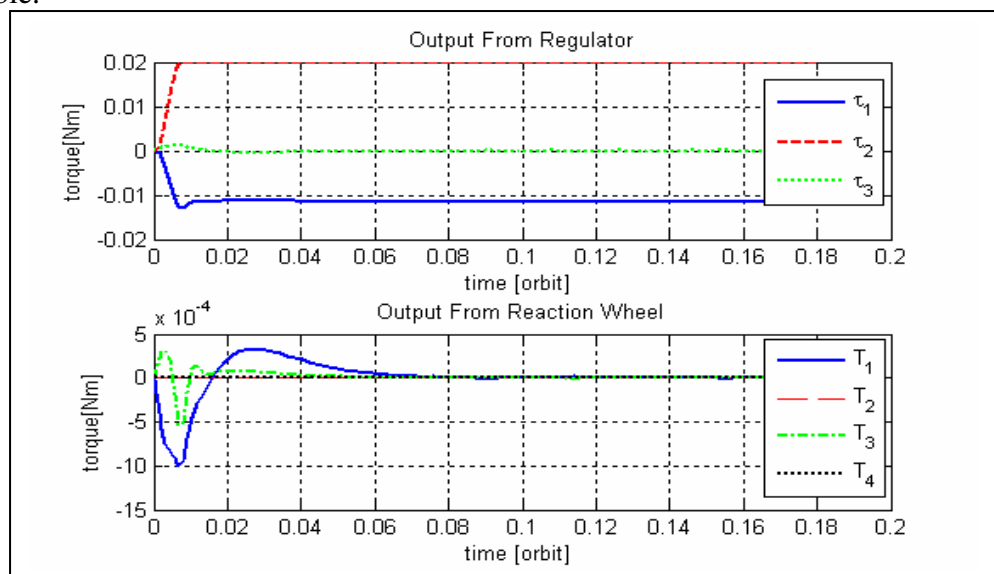


Figure-6.19: Output from regulator and wheels without noise and reaction Wheel-2, 4 were disabled

In case 5, maneuvering of the small satellite in one direction (pitch axis) is simulated. Desired pitch angle is taken as 30° . Noise effect is not considered.

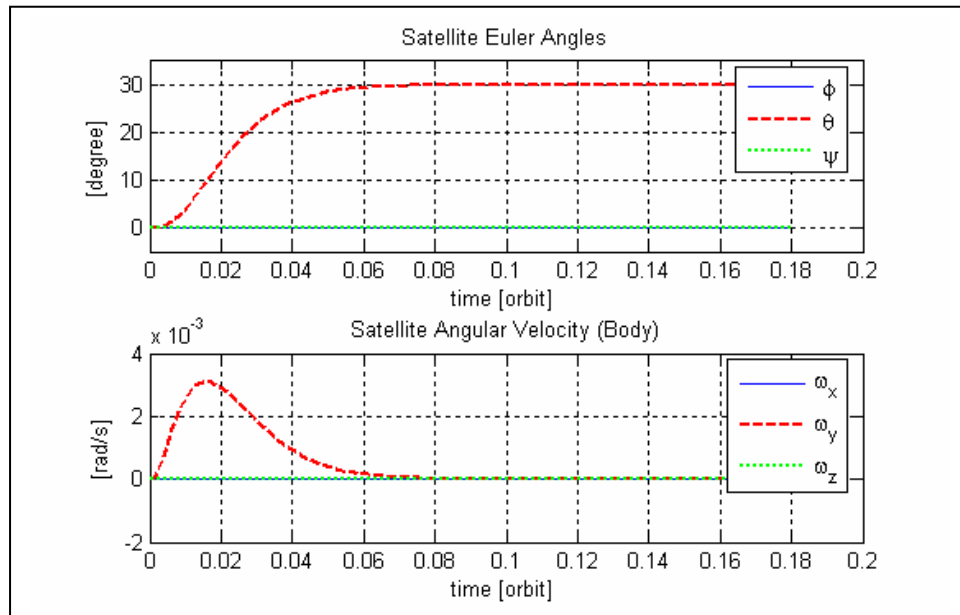


Figure-6.20: System response for the sliding mode regulator without noise and desired euler angles are $[\phi \ \theta \ \psi]=[0 \ 30 \ 0]$

Rise time is 0.04 orbits and settling time is 0.07 orbits. The pitch angle reaches its final value at 0.08 orbits.

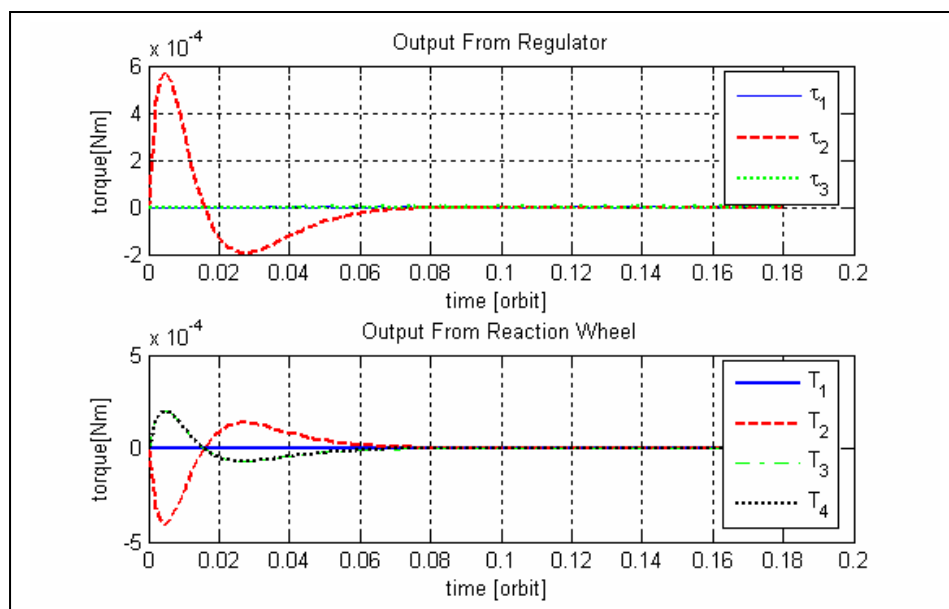


Figure-6.21: Output from regulator and wheels without noise desired euler angles are $[\phi \ \theta \ \psi]=[0 \ 30 \ 0]$

In case 6, four reaction wheels are applied as the actuators, noise effect and aerodynamic torque are not considered. Effect of aerodynamic torque on controller can be seen in this case.

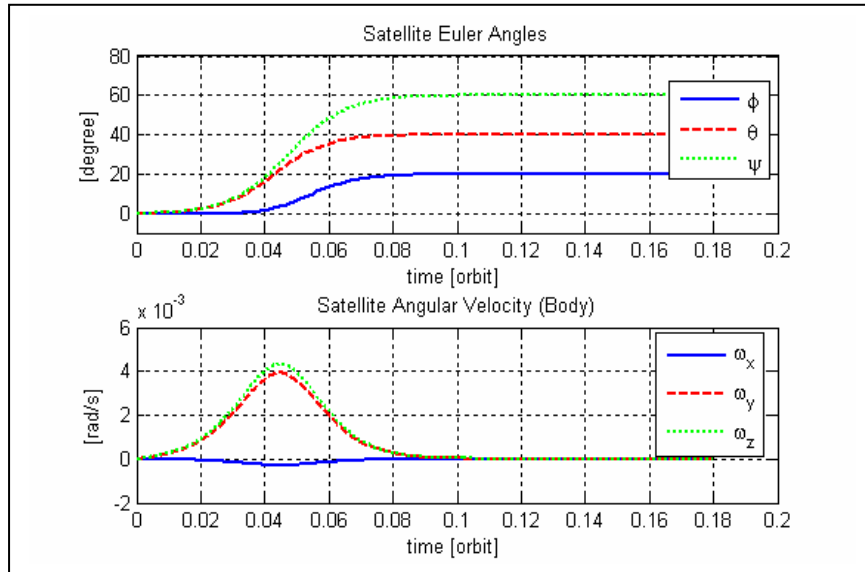


Figure-6.22: System response of SMR without aerodynamic torque

It can be seen from Figure-6.22 that magnitude of aerodynamic torque is very small ($3.4245e-7$) regarding to output torque from regulator ($5.0e-4$). Therefore aerodynamic torque does not change the total torque substantially. Euler angles and angular velocity results without aerodynamic torque almost identically with the case 1. Nonetheless aerodynamic torque is considered to simulate space conditions in all case simulations except case 6.

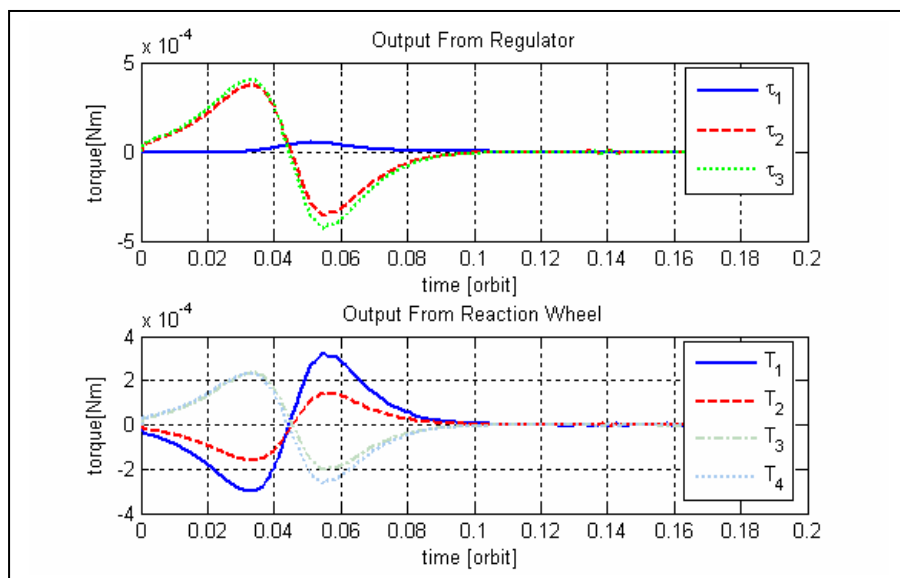


Figure-6.23: Output from regulator and wheels without aerodynamic torque

In case 7, four reaction wheels are applied as the actuators, noise effect is not considered. Effect of K value used for calculation of sliding manifold is investigated in this case. K is taken as $2 * 1_{3 \times 3}$ instead of $0.2 * 1_{3 \times 3}$.

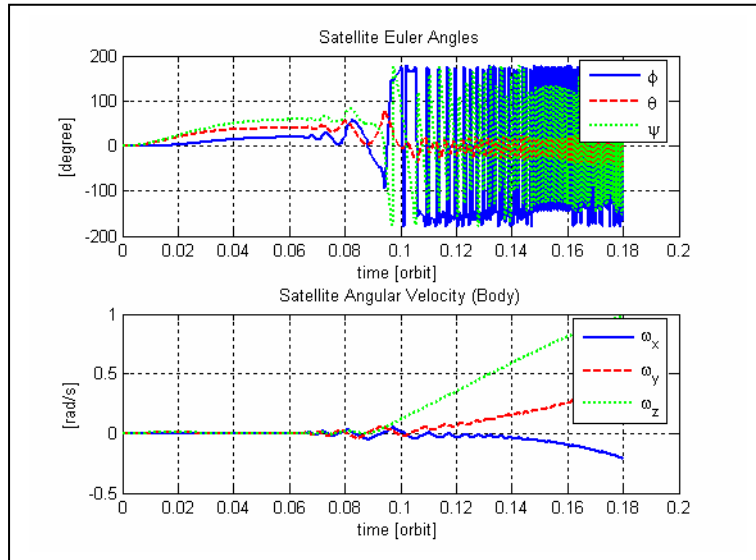


Figure-6.24: System response of SMR with $K = 2 * 1_{3 \times 3}$

Increasing the value of K effects response of SMR in desired values. SMR does not approach to desired value. Therefore in our simulations value of K was chosen as $0.2 * 1_{3 \times 3}$ after giving different value to K.

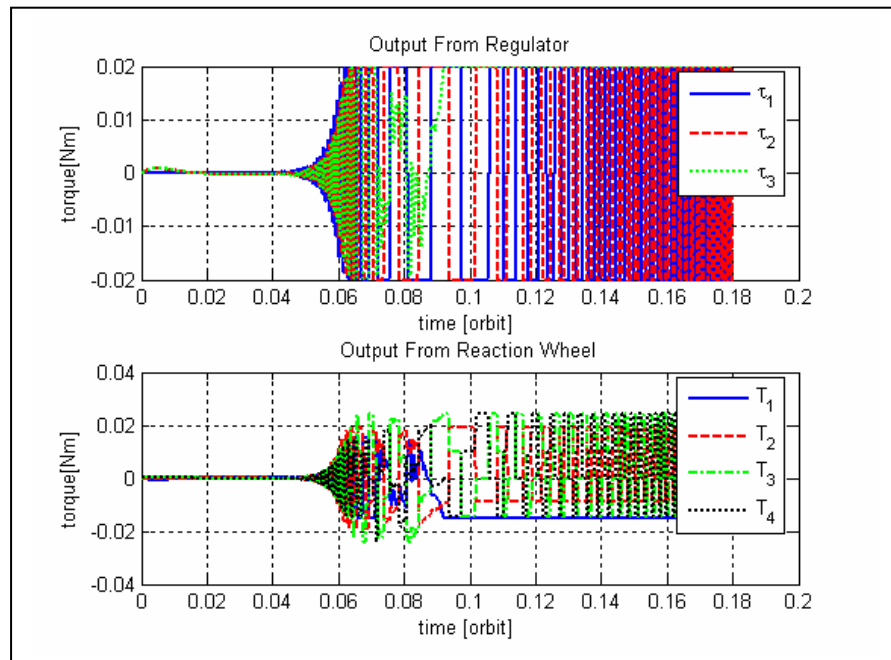


Figure-6.25: Output from regulator and wheels with $K = 2 * 1_{3 \times 3}$

6.3.3 Actual Results Taken from BILSAT-1

We used the actual results taken from Tübitak-Bilten for BILSAT-1 in pitch direction to compare our results with actual response of BILSAT-1. Data taken from Tübitak-Bilten is obtained according to time and command given in table 6.4

Table-6.4: Time and command table for the BILSAT-1

20 March 2006 02:22:00 UTC	Pitch=+30 degree command
20 March 2006 02:37:00 UTC	Pitch=0 degree command
20 March 2006 02:52:00 UTC	Pitch=+30 degree command
20 March 2006 03:07:00 UTC	Pitch=0 degree command
20 March 2006 04:02:00 UTC	Pitch=-30 degree command
20 March 2006 04:17:00 UTC	Pitch=0 degree command
20 March 2006 04:32:00 UTC	Pitch=-30 degree command
20 March 2006 04:47:00 UTC	Pitch=0 degree command
20 March 2006 05:37:00 UTC	Pitch=-30 degree command
20 March 2006 05:52:00 UTC	Pitch=0 degree command
20 March 2006 06:07:00 UTC	Pitch=+30 degree command
20 March 2006 06:22:00 UTC	Pitch=0 degree command

According to commands in table 6.4 obtained response of BILSAT-1 is given in figure 6.26. In this figure horizontal axis denotes time and vertical axis denotes pitch axis. Zoom is required to investigate behavior of BILSAT-1. 06:00:00 UTC - 06:25:00 UTC time segment is chosen and result is plotted in figure 6.27.

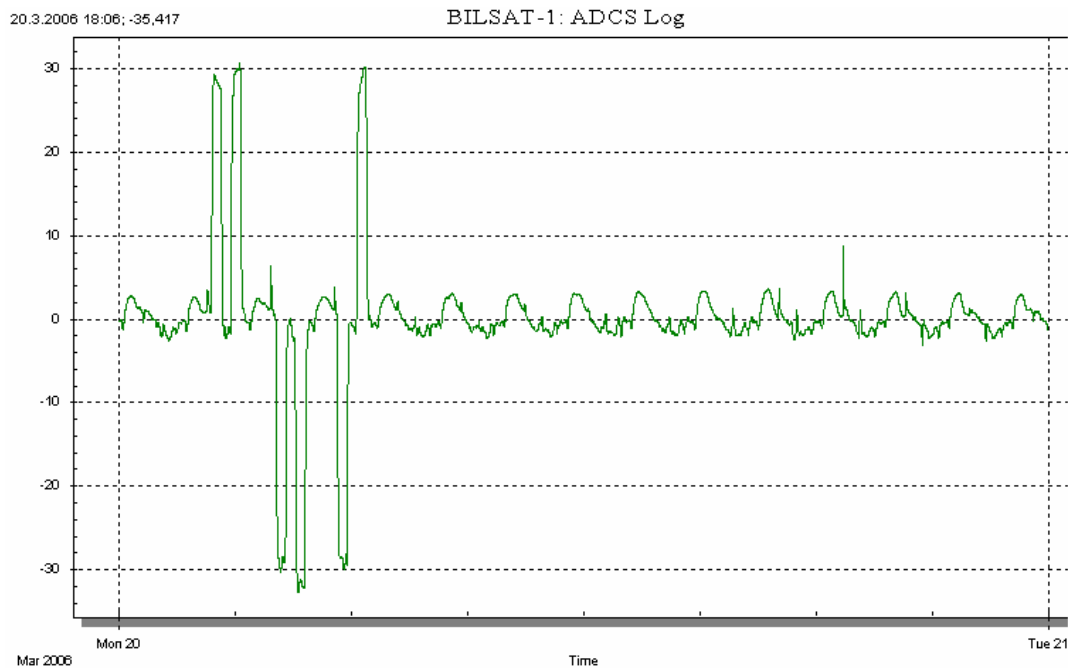


Figure-6.26: Actual pitch axis maneuver of BILSAT-1

Pitch= $+30^\circ$ degree command is given at 06:07:00 UTC and BILSAT-1 reaches desired value at 06:19:00 UTC. If we express the horizontal axis in orbit domain, settling time is 0.124 orbits for BILSAT-1. It can be said that this result is very close to our simulation results.

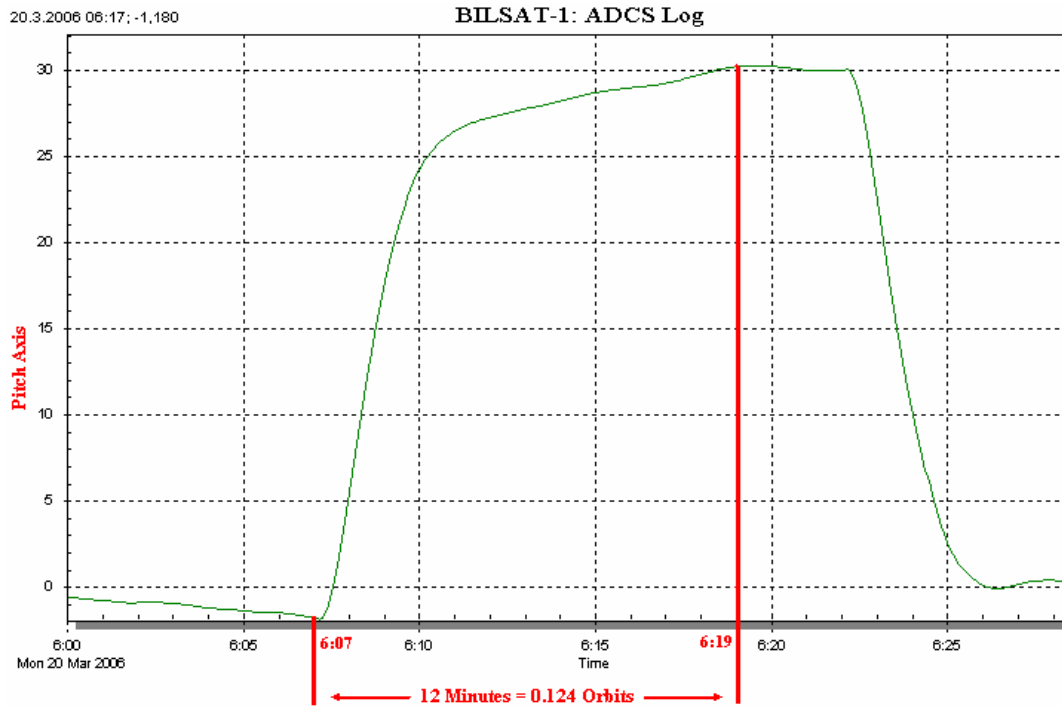


Figure-6.27: Actual pitch axis maneuver of BILSAT-1 (Zoomed)

CHAPTER 7

CONCLUSIONS and FUTURE WORK

In this chapter brief summary and conclusions on the results obtained in previous chapters are given. Controllers used in this thesis are compared with those of reference [20]. Recommendations and suggestions are given for future work.

In this thesis, nonlinear attitude control techniques for Low Earth Orbit small satellites are investigated. Sensors which are used for attitude determination and actuators which are used for attitude control are briefly introduced. Nonlinear mathematical model of a satellite is derived and BILSAT-1's parameters are applied in the model used for simulations.

Firstly, literature on attitude dynamics and control of satellite are studied. Nonlinear control techniques are chosen as the scope of this thesis. On the other hand linear control techniques are studied in reference [20]. Quaternion Feedback Controller (PD) and Sliding Mode Regulator are simulated for maneuver of satellite in our work. Reaction wheels are considered as actuators in attitude maneuver mode. These controllers are also examined in [8], [19] and [22]. Instead of Euler angle representation, unit quaternions are selected for attitude representation. Thus singularity problem is prevented. Gravity gradient torque and aerodynamic torque are taken into consideration in our simulations. Tetrahedral configuration is used in locating the reaction wheels. So that in case one of the reaction wheels is disabled, attitude control process continues without any problem. An other reason of using tetrahedral configuration is that twice the value of the torque that can be obtained from one reaction wheel can be obtained along any of the three directions. In stabilization analysis of Quaternion Feedback Controller, total energy of the satellite is chosen as Lyapunov candidate function. For the Sliding Mode Regulator, Lyapunov candidate function is chosen according to the suggestions of references [19] and [22]. The simulation results for both the Quaternion

Feedback Controller and Sliding Mode Regulator are given in Chapter 6.

In reference [20], linear controller is applied for the attitude maneuvering by the use of reaction wheels as actuators. When we compare our results with those of reference [20], it can be said that sliding mode results are similar with linear controller results. In both simulations when the all reaction wheels are enabled, settling time is 0.07 orbits, rise time is 0.04 orbits and euler angles reach their desired value nearly at about 0.08 orbits. In case that two reaction wheels are disabled, linear controller response is better than sliding mode controller. However, linear controller needs more torque than sliding mode regulator. When we compare nonlinear Quaternion Feedback Controller (PD) with linear controller, Euler angles reach their desired value at about 0.1 orbits in nonlinear QFC controller. This means that QFC spends more time than other controllers to reach desired values. The controller parameters of QFC can be changed to obtain shorter settling time. But this operation increases power consumption of the satellite. Also we compared the simulation results taken from Tübitak-Bilten for BILSAT-1 in pitch direction with our results. BILSAT-1 reaches to the desired value at about 0.124 orbits and it can be said that this result is very close to our simulation results.

Table-7.1: Simulation result of controllers

	Rise Time	Settling Time	Max Torque
QFC	0.04 orbits	0.09 orbits	4e-4
SMR	0.04 orbits	0.07 orbits	8e-4
LR	0.04 orbits	0.07 orbits	12e-4
BILSAT-1	0.06 orbits	0.12 orbits	Not applicable*

* Not applicable as they use a different method in applying torques.

Uniformly distributed noise (10% noise of torque) was applied to actuator torque to observe behaviour of controllers. QFC and SMR successfully tolerated noise. It was seen that noise effected torques output from controller and reaction wheels. Nonetheless it didn't affect Euler angles and angular velocity too much. Magnitude of noise was increased and deviation of Euler angles from desired angles was seen. As a conclusion, it can be said that QFC and SMR are robust controller for the acceptable range of noise (10% noise of torque).

For future work, it is suggested to design nonlinear controller using magnetic torquer for attitude stabilization of the satellite. Moreover, different allocation methods for reaction wheel torques can be investigated. Inertia matrix is taken in diagonal form in our thesis. The effect of using a nondiagonal inertia matrix on the system performance for different

controllers used is also worth studying.

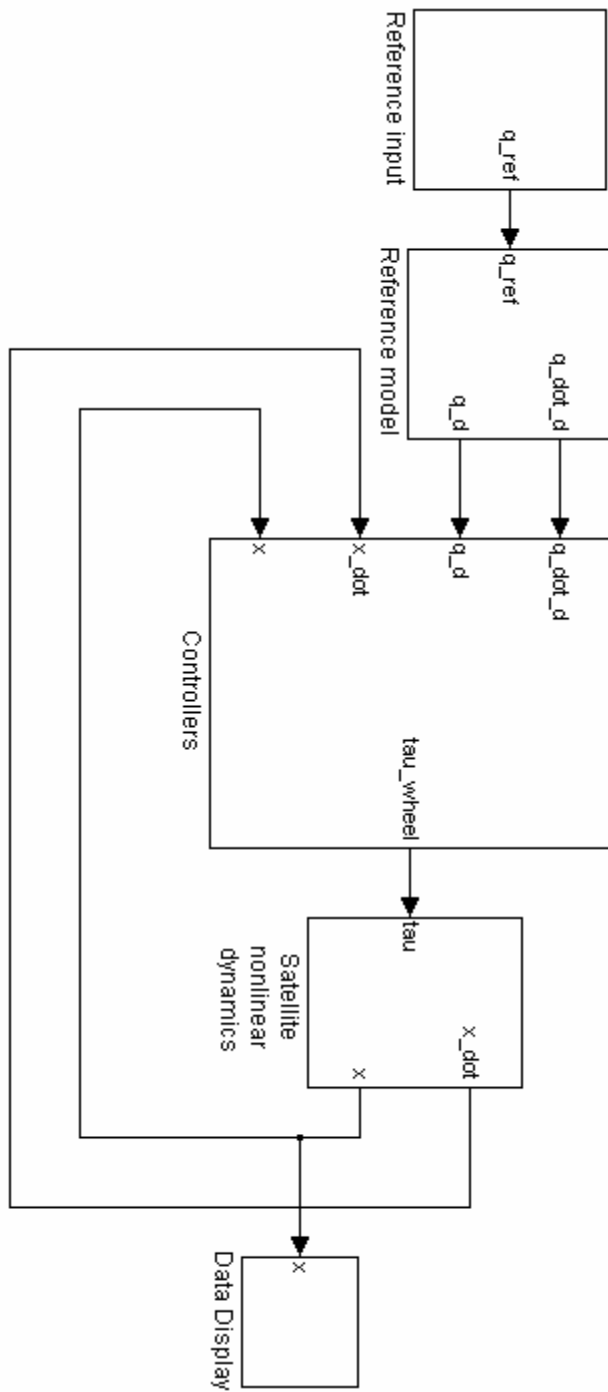
REFERENCES

- [1] <http://www.bilten.metu.edu.tr/bilsat>
- [2] L.M. Gomes, G. Yuksel, A.S. Curiel, A. Bradford, M. Sweeting. BILSAT: Advancing Small-Sat Capabilities, SS C03-VI-4, 17th AIAA/USU Conference on Small Satellites
- [3] J.R. Wertz, and W.J. Larson, (editors). Space mission analysis and design. Kluwer academic publishers, 1999
- [4] K. Svartveit. Attitude determination of the NCUBE satellite. Department of engineering cybernetics, NTNU, 2003
- [5] T. Bak. Spacecraft Attitude Determination- a Magnetometer Approach. Ph.D. thesis. Aalborg University, Denmark, 2002
- [6] Egeland, Olav and Gravdahl, J. Tommy. Modeling and simulation for control. Department of Engineering Cybernetics, NTNU, 2001
- [7] S. Ose. Attitude determination for the Norwegian student satellite nCube, Department of Engineering Cybernetics, NTNU, 2004
- [8] O. Hegrenes. Attitude control by means of explicit model predictive control, via multi-parametric quadratic programming, Department of Engineering Cybernetics, NTNU, 2004
- [9] J. E. Overby. Attitude control for the Norwegian student satellite nCube, Department of Engineering Cybernetics, NTNU, 2004
- [10] F. M. Indergaard. Design and implementation of a gravity boom for the Norwegian nano satellite NCUBE. Master Thesis, NTNU 2003
- [11] P. C. Hughes. Spacecraft Attitude Dynamics. USA: John Wiley & Sons. Inc. 1986
- [12] R. Wisniewski. Satellite Attitude Control Using Only Electromagnetic Actuation. Ph.D. Thesis, Department Of Control Engineering. Aalborg University. Denmark. 1996
- [13] B. E. Busterud. Orienteringsregulering av microsatelliter. Master Thesis, NTNU 2003
- [14] H. K. Khalil. Nonlinear Systems. Upper Saddle River, New Jersey, USA. 2000
- [15] M. Vidyasagar. Nonlinear Systems Analysis. Prentice-Hall, Inc. 1993
- [16] T. I. Fossen. Marine Control Systems. Trondheim, Norway. Marine Cybernetics. 2002

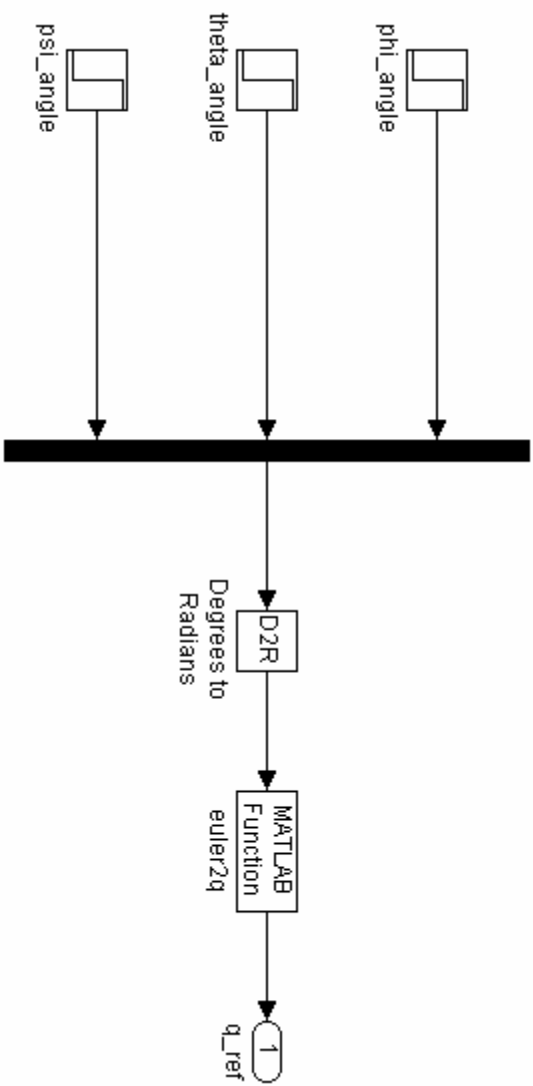
- [17] S. Skogestad and I. Poslethwaite. Multivariable feedback control. (1996)
- [18] R. Kristiansen. Attitude Control Of a Microsatellite. Master Thesis, Department of Engineering Cybernetics, NTNU, 2000
- [19] G. Ytrehus. Styring av mikrosatellitt med reaksjonshjul i tetraeder. Master thesis, NTNU 2003
- [20] C. Kaplan. LEO Satellite, Attitude determination and control components, some linear control methods, MSc. thesis, METU 2006
- [21] K. L. Makovec. A nonlinear magnetic controller for three axis stability of nanosatellites. Master thesis, Virginia 2001
- [22] J. H. McDuffie and Y. B. Shtessel. A de-coupled Sliding Mode Controller and observer for satellite attitude control. IEEE 29th symposium on system theory. March 9-11. 1997 pg-92.
- [23] M. H. Kaplan. Modern spacecraft dynamics and control. John Wiley & Sons, New York (1976)
- [24] C. D. Hall, P. Tsiotras, H. Shen. Tracking rigid body motion using thrusters and momentum wheels. Journal of the Astronautical Sciences, Vol. 50, No. 3, 2002.
- [25] <http://www.sstl.co.uk>
- [26] O. Uslu. Orbit dynamics, attitude dynamics and control investigation into possible application to TURKSAT, MSc. Thesis in Aeronautical Engineering. Middle East Technical University, Ankara, 1997.
- [27] H. O. Derman. 3-Axis attitude control of a geostationary satellite, MSc. Thesis in Aeronautical Engineering, Middle East Technical University, Ankara, 1999.

APPENDIX A – SIMULINK DIAGRAMS

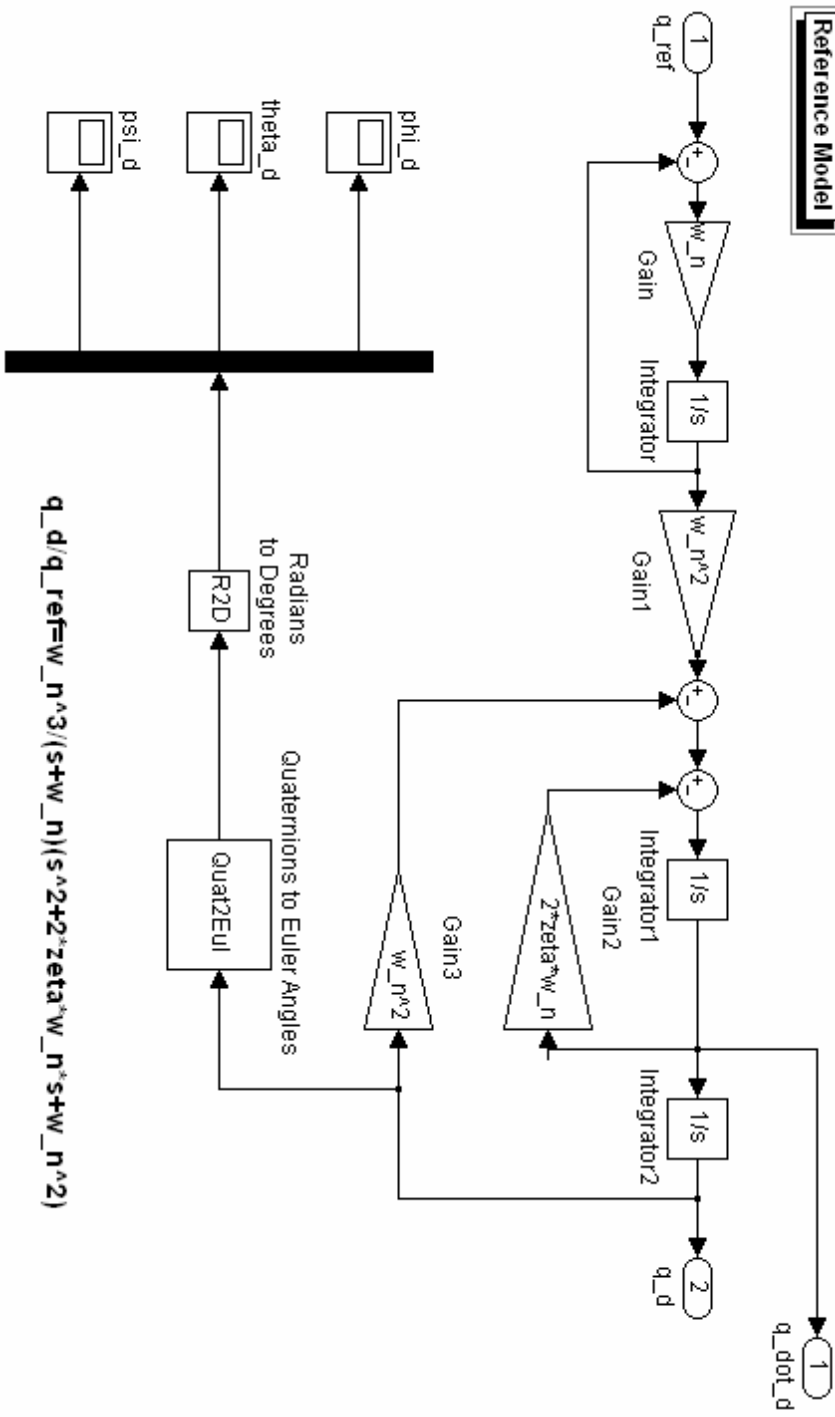
Satellite Control Model



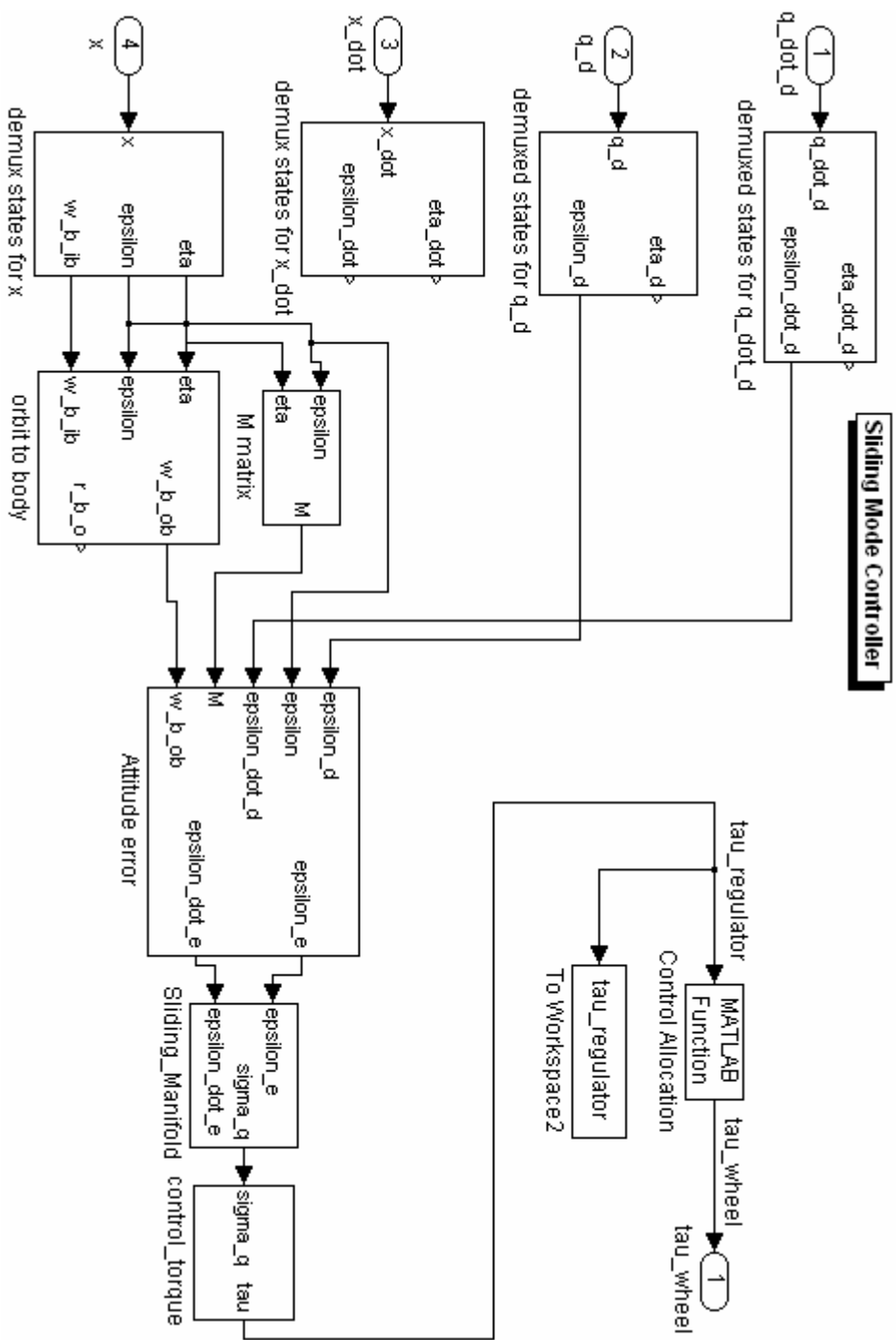
Reference Input Angles



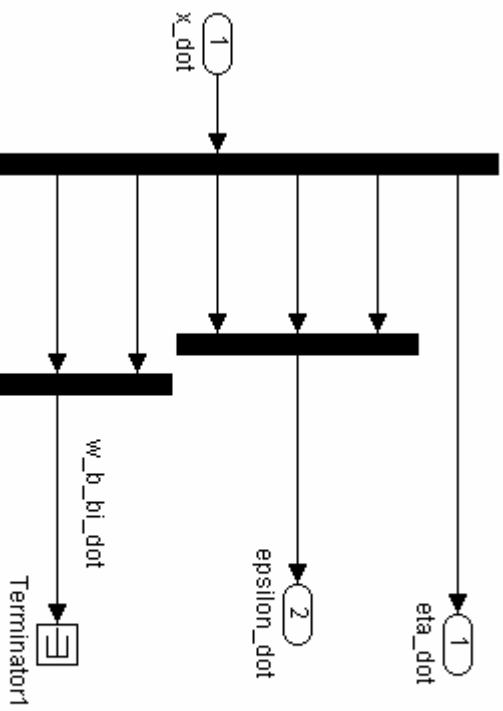
Reference Model



$$q_d/q_{ref} = w_n^3 / (s + w_n)(s^2 + 2 \cdot \zeta \cdot w_n \cdot s + w_n^2)$$

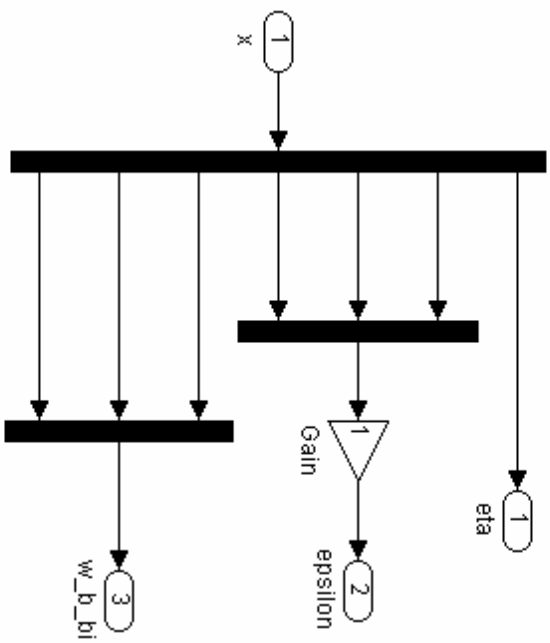


Demuxed states for x_{dot}

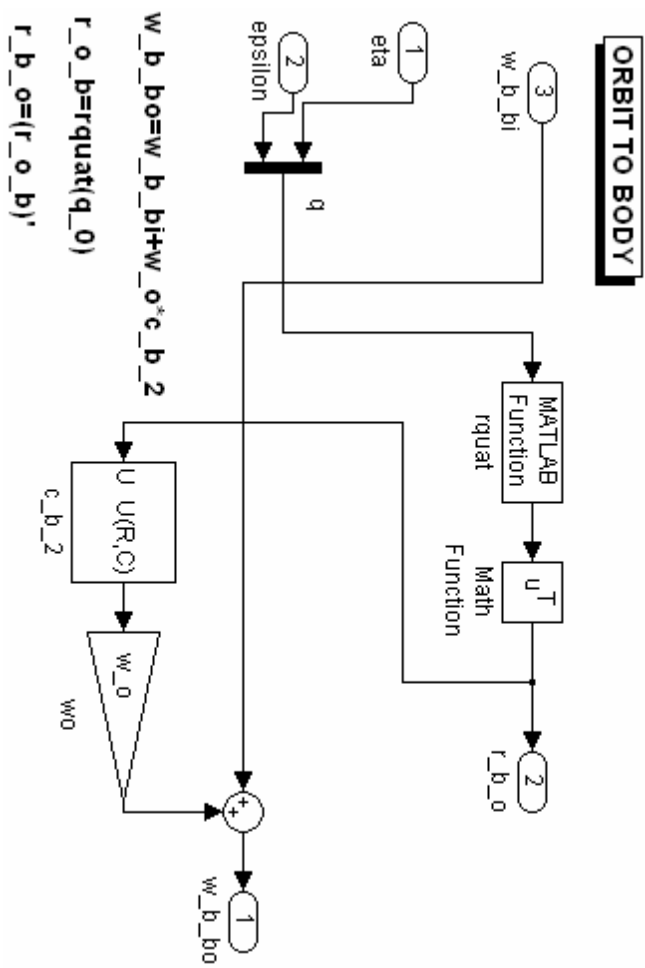
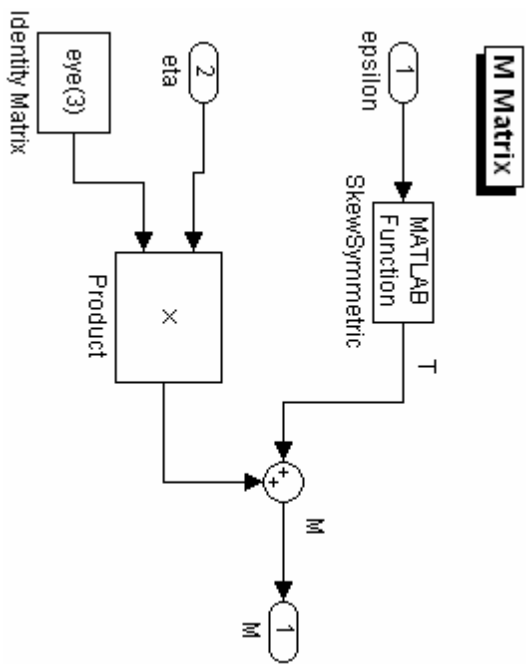


```
x_dot=[eta_dot;epsilon_dot_1;epsilon_dot_2;epsilon_dot_3;
w_b_bi_dot_1;w_b_bi_dot_2;w_b_bi_dot_3]
```

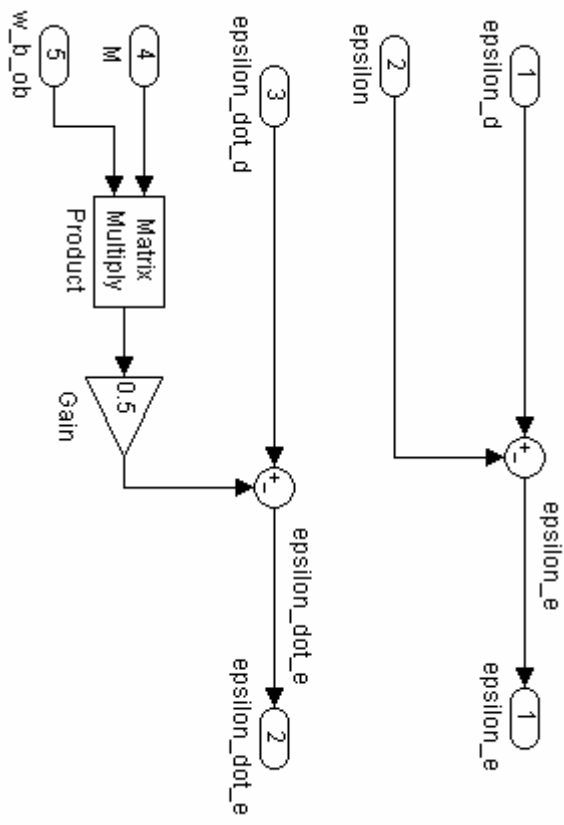
Demuxed states for x



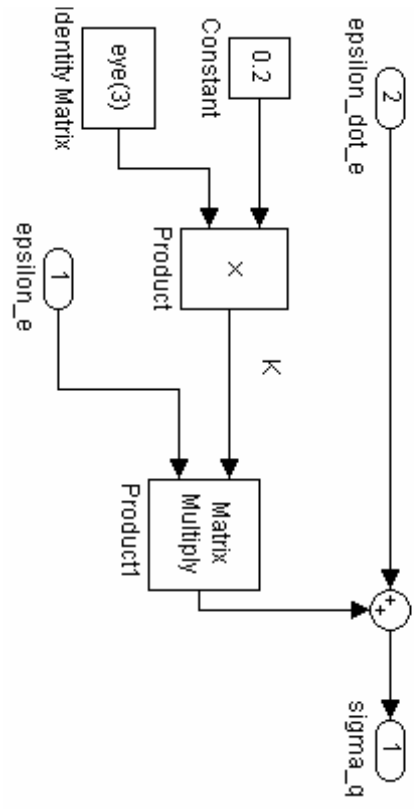
```
x=[eta;epsilon_1;epsilon_2;epsilon_3;
w_b_bi_1;w_b_bi_2;w_b_bi_3]
```

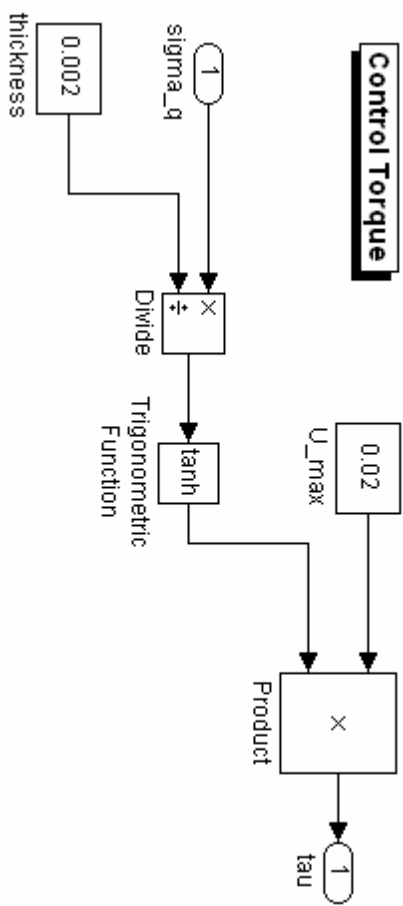


Attitude Error

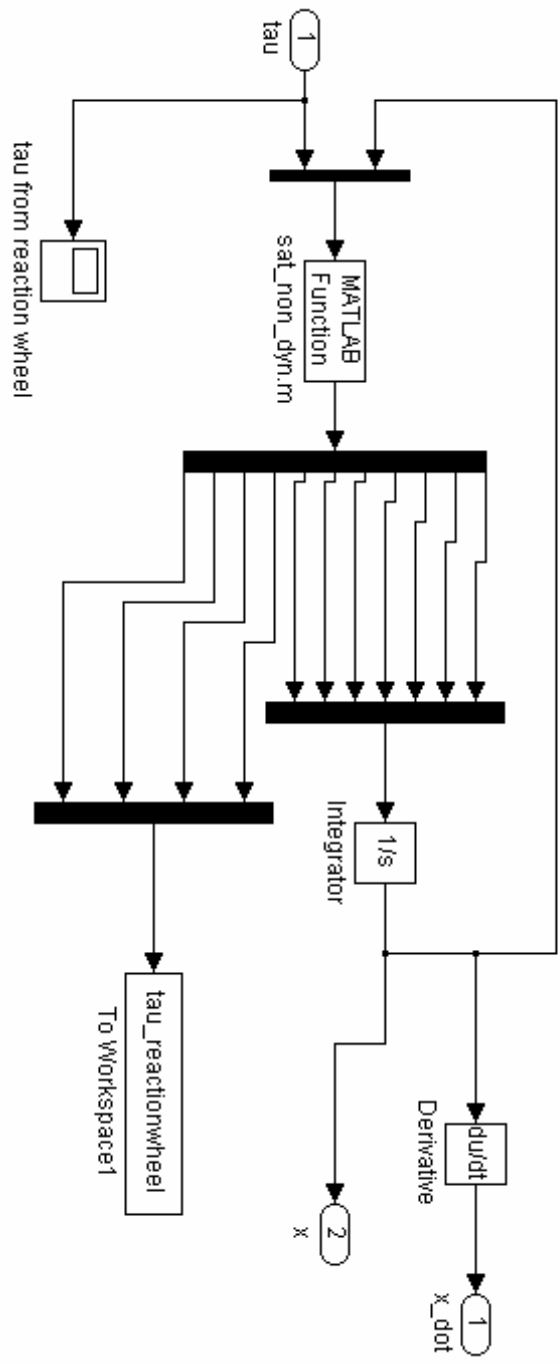


Sliding Manifold



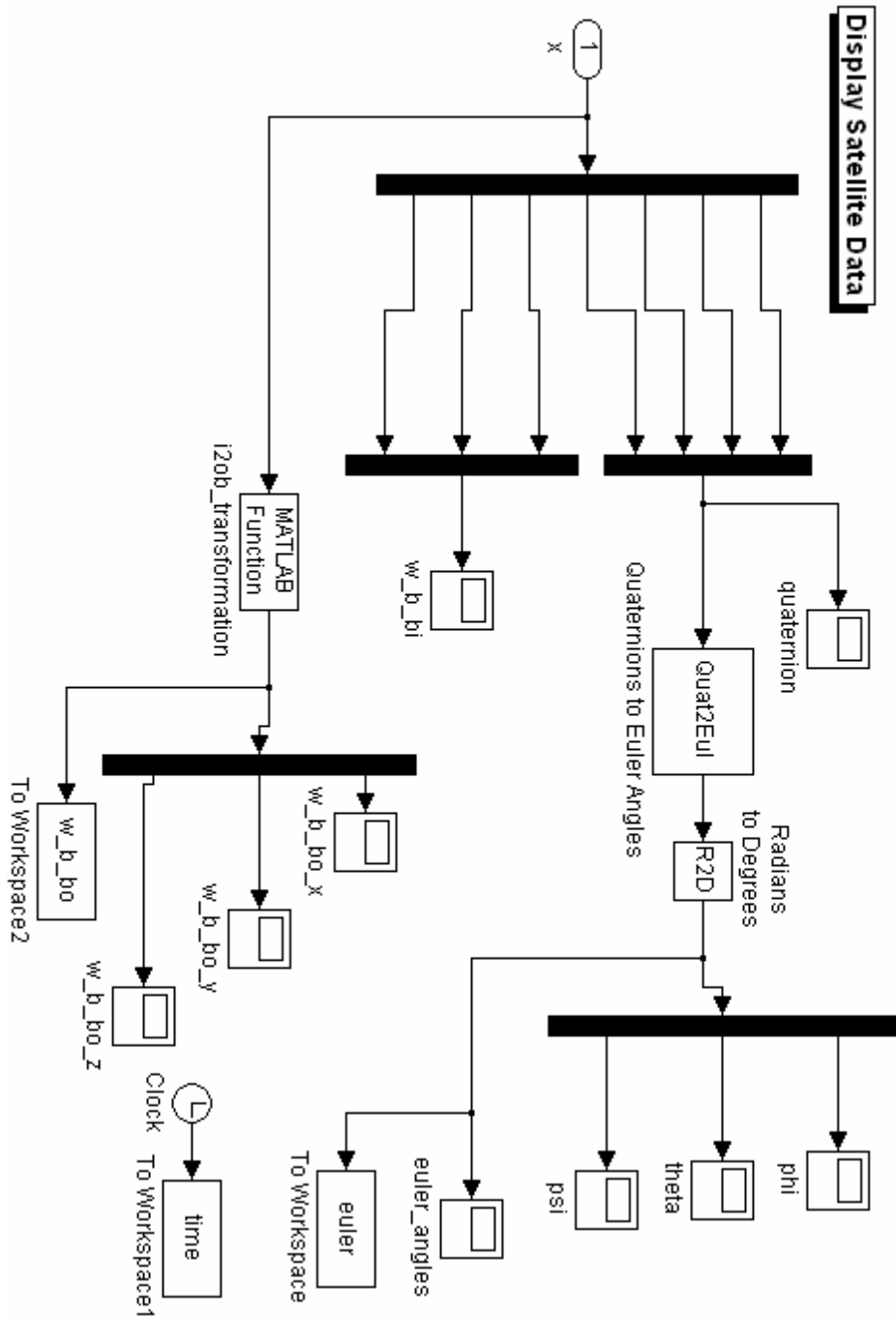


Satellite Nonlinear Dynamic

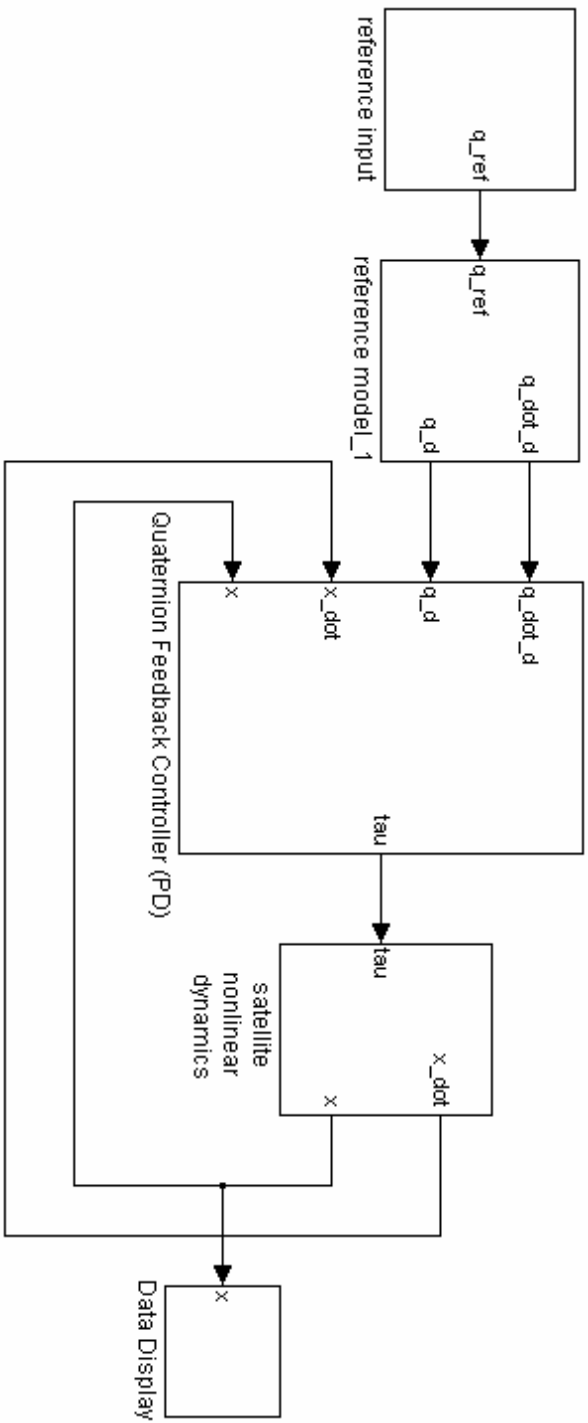


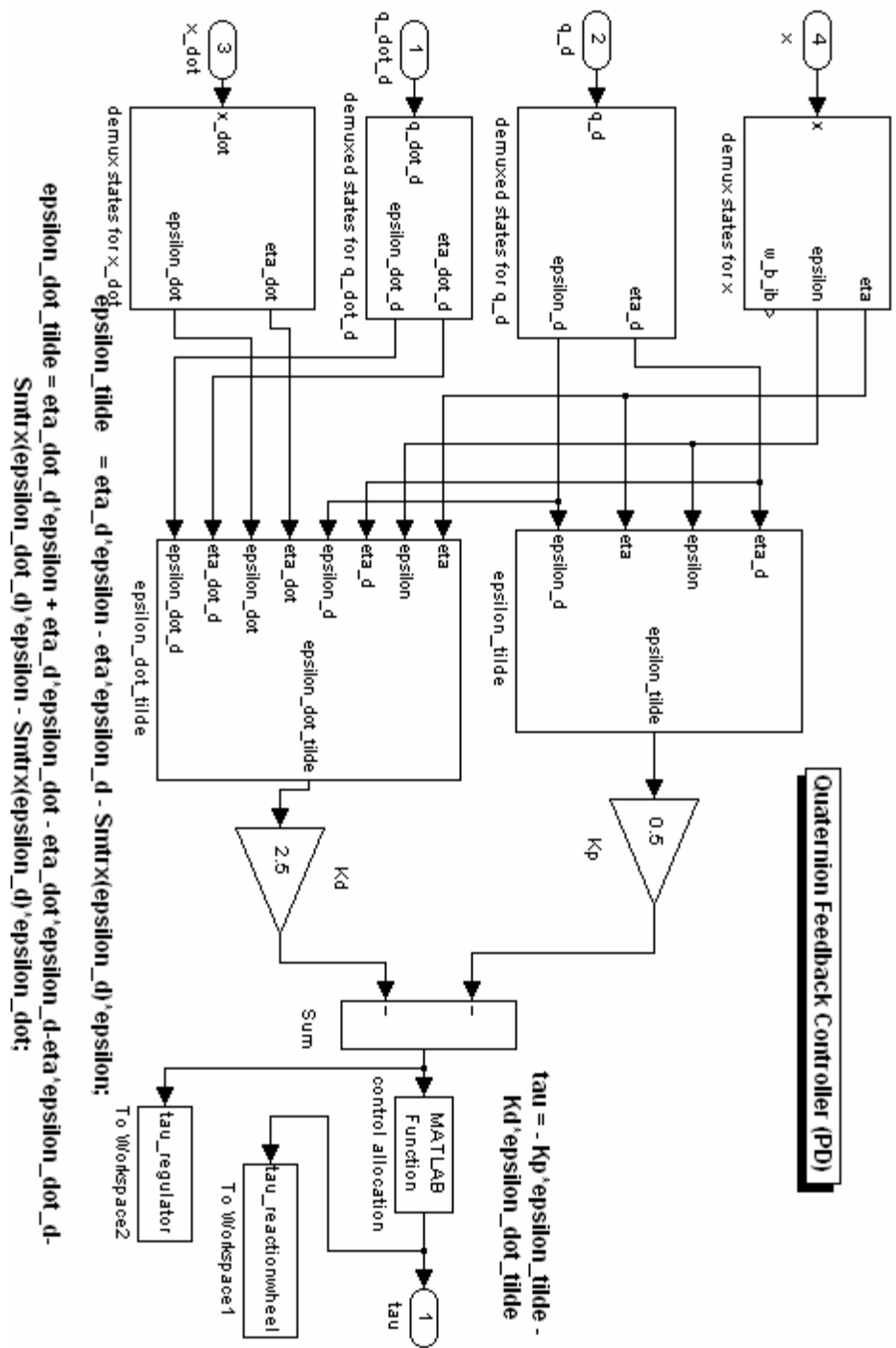
$$g_B = \text{Smtx}(3 \times w_0 \times 2 \times R_B_0(:,3)) \times I \times R_B_0(:,3);$$

$$w_B_BI_dot = \text{lmv}() \times (\text{tau} + g_B - \text{Smtx}(w_B_BI) \times I \times w_B_BI)$$

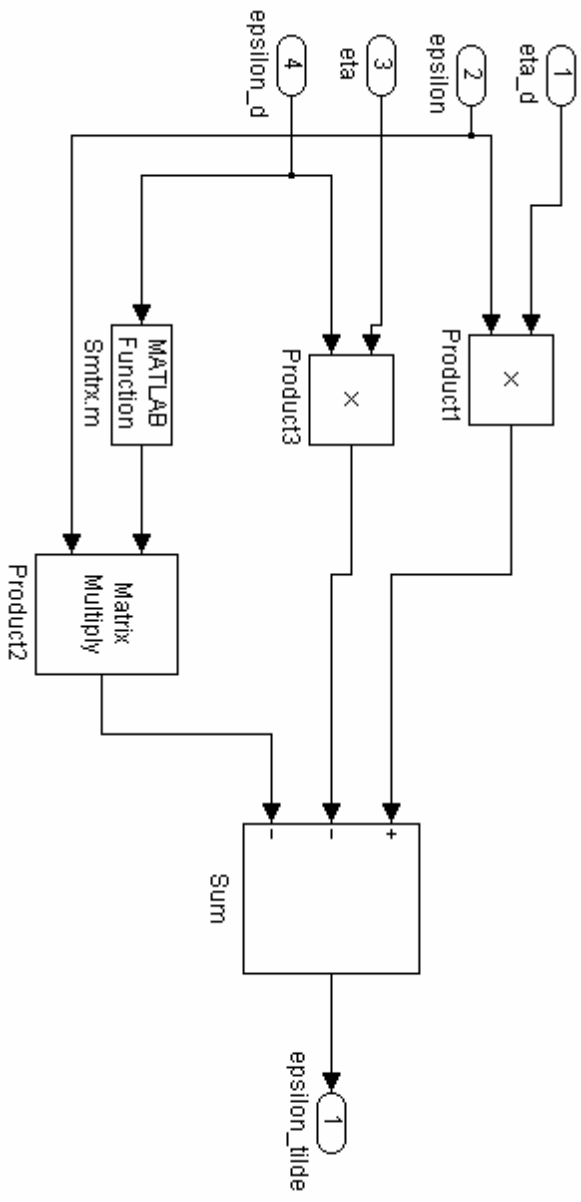


Satellite Control Model

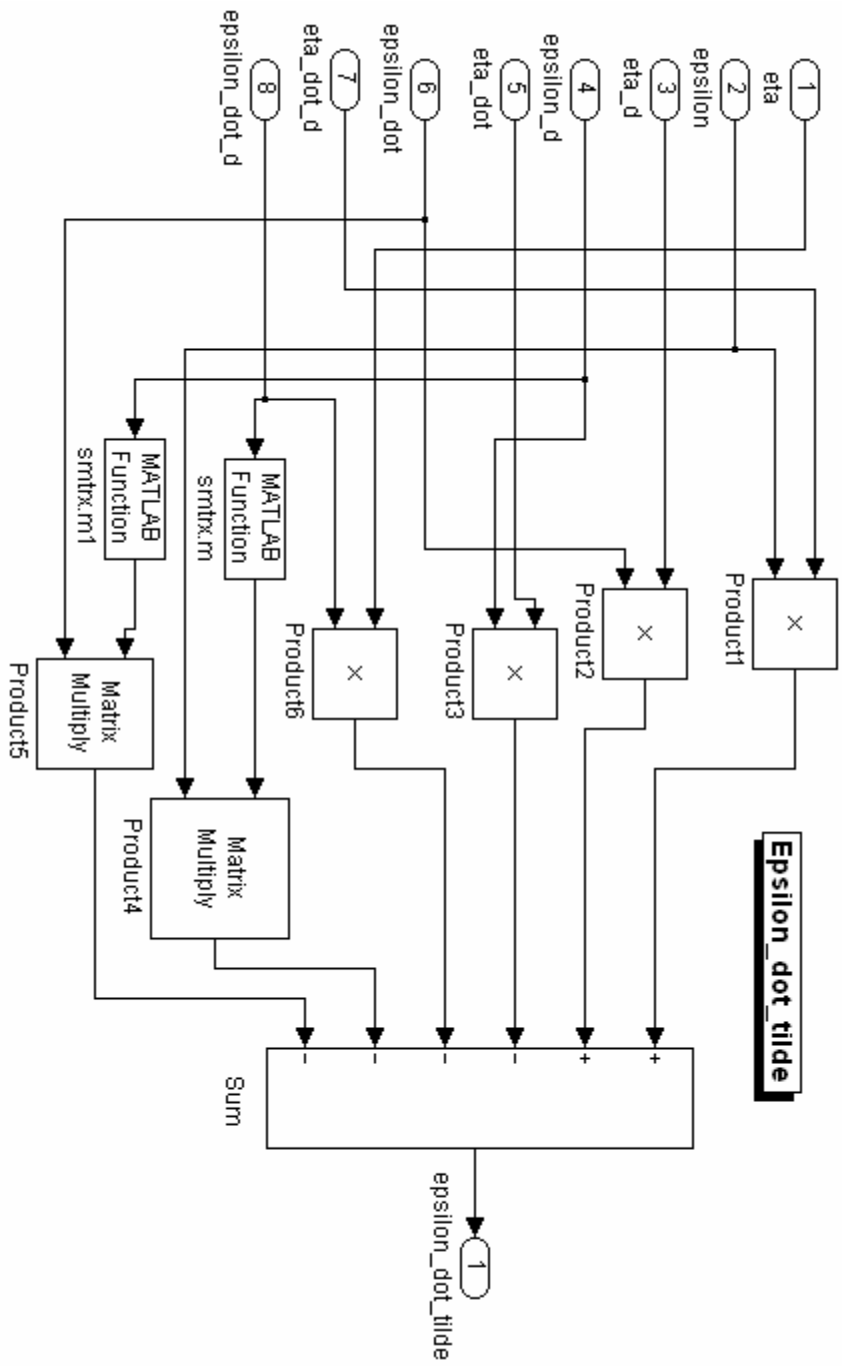




Epsilon_tilde



$\epsilon_{\tilde{}} = \eta_d \epsilon - \eta \epsilon_d - \text{SmtrX}(\epsilon_d) \epsilon$



$\epsilon_{\dot{t}} = \epsilon_{\dot{t}} + \epsilon_{\dot{t}} \epsilon_{\dot{t}} + \epsilon_{\dot{t}} \epsilon_{\dot{t}} - \epsilon_{\dot{t}} \epsilon_{\dot{t}} - \epsilon_{\dot{t}} \epsilon_{\dot{t}} - \epsilon_{\dot{t}} \epsilon_{\dot{t}} - \epsilon_{\dot{t}} \epsilon_{\dot{t}} - \epsilon_{\dot{t}} \epsilon_{\dot{t}}$

APPENDIX B – MATLAB SOURCE CODES

```
%euler2q.m
%*****
%File euler2q.m
%Function that transforms Euler angles to quaternion parameters
%Written by Ceren KAPLAN and Soner KARATAS
%December 2005
%*****
function q_0 = euler2q(e)

e1=0.5*e(1,:);
e2=0.5*e(2,:);
e3=0.5*e(3,:);

u(1)=sin(e1);
u(2)=sin(e2);
u(3)=sin(e3);

u(4)=cos(e1);
u(5)=cos(e2);
u(6)=cos(e3);

q0=(u(1)*u(2)*u(3))+u(4)*u(5)*u(6);
q1=(-u(2)*u(3)*u(4))+u(1)*u(5)*u(6);
q2=(u(1)*u(5)*u(3))+u(2)*u(4)*u(6);
q3=(u(3)*u(4)*u(5))-u(1)*u(2)*u(6);

q_0=[q0;q1;q2;q3];

end
```

```

%*****
%figures. m
%A file to plot euler,w_b_bo,tau_regulator and tau_reactionwheel
%Writteb by Ceren KAPLAN and Soner KARATAS
%December 2005
%*****

global euler time t_o
%Plotting the simulated trajectories
t=time/t_o;

figure(1);
plot(t,euler(:,1),'b-', t,euler(:,2),'r--', t,euler(:,3),'g:');
grid;
legend('\phi','\theta','\psi');
xlabel('time [orbit] ');
ylabel('[degree]');
Title('Satellite Euler Angles');

figure(2);
plot(t,w_b_bo(1,:),'b-', t,w_b_bo(2,:),'r--', t,w_b_bo(3,:),'g:');
grid;
legend('\omega_x','\omega_y','\omega_z');
xlabel('time [orbit] ');
ylabel('[rad/s]');
Title('Satellite Angular Velocity (Body)');

figure(3);
plot(t,tau_regulator(1,:),'b-', t,tau_regulator(2,:)...
     ,t,tau_regulator(3,:),'g:');
grid;
legend('\tau_1','\tau_2','\tau_3');
xlabel('time [orbit] ');
ylabel('torque[Nm]');
Title('Output From Regulator');

figure(4);
plot(t,tau_reactionwheel(:,1),'b-...'
     ,t,tau_reactionwheel(:,2),'k--'...'
     ,t,tau_reactionwheel(:,3),'r-'...'
     ,t,tau_reactionwheel(:,4),'g:');

grid;
legend('T_1','T_2','T_3','T_4');
xlabel('time [orbit] ');
ylabel('torque[Nm]');
Title('Output From Reaction Wheel');

```

```

%*****
%Rquat.m
%A file to transform quaternion matrix to rotation matrix
%Written modified by Ceren KAPLAN and Soner KARATAS
%December 2005
%*****
function R = Rquat(q)
n=q(1,:);
e1=q(2,:);
e2=q(3,:);
e3=q(4,:);
d11=(n^2+e3^2-e2^2-e1^2);
d12=2*(e1*e2+n*e3);
d13=2*(e1*e3-n*e2);
d21=2*(e1*e2-n*e3);
d22=(n^2-e3^2+e2^2-e1^2);
d23=2*(e2*e3+n*e1);
d31=2*(e1*e3+n*e2);
d32=2*(e2*e3-n*e1);
d33=(n^2-e3^2-e2^2+e1^2);
R=[d11,d12,d13;d21,d22,d23;d31,d32,d33];
end

```

```

%*****
%sat_non_dyn.m
%A file to calculate the nonlinear satellite dynamic equations
%Written by Geir Ytrehus , modified by Ceren KAPLAN and Soner KARATAS
%December 2005
%*****

function xdot = sat_non_dyn(input)
global I w_o TD I_o K1

% The state space variables
q = input(1:4);
w_b_bi = input(5:7);

% The system input from the controller after actuator allocation
u = input(8:11)

% Normalizing the quaternions - necessary due to numerical inaccuracy
q = q/(q'*q);
eta = q(1) ;
epsilon = q(2:4);

% Transforming from w_b_ib to w_b_ob for use in the dynamical model update
r_o_b = Rquat(q);
r_b_o = r_o_b';
c2 = r_b_o(:,2);
w_b_bo = w_b_bi+w_o *c2;
%w_b_bo = w_b_bi+w_o *c2;

% Reaction wheels in a tetrahedral
T = TD
%T(1,:) = zeros(1,3); % Disabling wheel 1
%T(2,:) = zeros(1,3); % Disabling wheel 2
%T(3,:) = zeros(1,3); % Disabling wheel 3
%T(4,:) = zeros(1,3); % Disabling wheel 4
%u(1) = 0; %Disabling wheel 1
%u(2) = 0; %Disabling wheel 2
%u(3) = 0; %Disabling wheel 3
%u(4) = 0; %Disabling wheel 4

% Maximum torque available is 0.01 [Nm]
% u_max = 0.01;
u_max = 1;
for i = 1:4
if abs(u(i))>u_max
u(i)= sign(u(i))*u_max;
end;
end;

```

```

tau = T'*K1*u;

% Uniformly distributed noise
% The expression sign((2*rand(2)-1)) ensures that the noise is either
% area -1 or 1 of the actuator torque because rand(1) gives numbers in
% the area [0.0 1.0]. Multiplying with a percentage of the produced torque
% gives a realistic disturbance effect.
%p = 0.4; % 40% noise added to the actuator torque
%noise=p*(sign(2*rand(1)-1))*[tau(1); tau(2); tau(3)];
%tau = tau + r_b_o*(noise) ;

% Gravity gradient torque
g_B = Smtrx(3*w_o^2*r_b_o(:,3))*I*r_b_o(:,3);

% Aerodynamic torque
t_aero = 3.4245e-7;

% The dynamical equations
eta_dot = -(1/2)*epsilon*w_b_bo;
epsilon_dot = (1/2)*(eta*eye(3) + Smtrx(epsilon))*w_b_bo;
w_b_bi_dot = inv(I)*(tau + g_B + t_aero - Smtrx(w_b_bi)*(I*w_b_bi));

x_dot = [eta_dot; epsilon_dot; w_b_bi_dot;u];

```

```

%*****
%Simulationsetup.m
%A file to setup the MATLAB/Simulink BILSAT-1 reaction wheel simulation
%For linear,nonlinear and sliding mode controllers.
%Written by Geir Ytrehus , modified by Ceren KAPLAN and Soner KARATAS
%December 2005
%*****

clear all;
global I w_o TD K I_o K1 W

%*****
%Inertia Matrix
%*****

Ixx = 9.8194; Ixy = 0.0721; Ixz = 0.2893; Iyx = 0.0721; Iyy = 9.7030;
Iyz = 0.1011; Izx = 0.2892; Izy = 0.1011; Izz = 9.7309; %BILSAT-1 inertia matrix
InertialMatrix=[Ixx 0 0; 0 Iyy 0; 0 0 Izz];
%InertialMatrix=[Ixx Ixy Ixz; Iyx Iyy Iyz; Izx Izy Izz];
I=InertialMatrix;

% Some useful definitions
kx = (Iyy - Izz)/Ixx;
ky = (Ixx - Izz)/Iyy;
kz = (Iyy - Ixx)/Izz;

% Tetrahedral distribution matrix
% All reaction wheels are taken as identical if desired
% they can be scaled by the motor gains

TD = [0 0 -1;
0 -sqrt(6*3*4)/9 sqrt(4)/6;
1/6*sqrt(6*4) sqrt(6*3*4)/18 sqrt(4)/6;
-1/6*sqrt(6*4) sqrt(6*3*4)/18 sqrt(4)/6 ]

%force matrix
k1 = 1;
k2 = 1;
k3 = 1;
k4 = 1;
K1 = [k1 0 0 0
0 k2 0 0
0 0 k3 0
0 0 0 k4]

```

```

%weight matrix
w1 = 1;
w2 = 1;
w3 = 1;
w4 = 1;
W = [w1 0 0 0
     0 w2 0 0
     0 0 w3 0
     0 0 0 w4]

%*****
%Initial Values
%*****

m = 120; % [kg] Mass of Satellite
M = 5.9742e24; % [kg] Mass of Earth
gamma = 6.6720e-11; % [] Gravity constant
my_g = gamma*M; % [kg] Earth gravity constant
re_e = 6.378137e6; % [m] Equatorial radius of Earth
rp_e = 6.356752e6; % [m] Polar radius of Earth
eccentricity = sqrt(1- (rp_e/re_e)^2); % Eccentricity of the ellipsoid
h_s = 600e3; % [m] Satellite orbit
r_total = re_e + h_s; % [m] Distance from satellite to
%Earth center
t_e = round (8.6164130e4); % [s] Integer length of sidereal day
w_e = 2*pi/(t_e); % [rad/s] Earth Angular Velocity
w_o = sqrt( my_g/( r_total^3)); % [rad/s] Satellite Angular Velocity
t_o = 2*pi/w_o; % [s] Satellite Orbit Period
v_o = h_s*w_o; % [m/s] Satellite Velocity

%*****
%Reference Model Parameters
%*****

w_n = 0.022;
zeta =1;

%*****
% Initial attitude in Euler angles
%*****

deg_0 = (pi/180)* [0; 0; 0] ;

% Initial attitude in Euler parameters (quaternions)
q_0 = euler2q(deg_0);

%*****
% Transforming from w_B_BO to w_B_BI
%*****

```

```

r_o_b = Rquat(q_0);
r_b_o = r_o_b';
c2 = r_b_o(:,2);
w_b_bo = [0; 0; 0] ;
w_b_bi = w_b_bo - w_o*c2;

% The initial state vector
x0 = [q_0(1); q_0(2); q_0(3); q_0(4); w_b_bi(1); w_b_bi(2); w_b_bi(3)];

%*****
% The linearized system matrices
%*****

A = [0 1 0 0 0 0;
-4*kx*w_o^2 0 0 0 0 (1 - kx)*w_o;
0 0 0 1 0 0;
0 0 -3*ky*w_o^2 0 0 0;
0 0 0 0 0 1;
0 -(1 - kz)*w_o 0 0 -kz*w_o^2 0
];
B = [0 0 0
1/(2*Ixx) 0 0;
0 0 0;
0 1/(2*Iyy) 0;
0 0 0;
0 0 1/(2*Izz)
];
C = [1 0 0 0 0 0;
0 0 1 0 0 0;
0 0 0 0 1 0
];

```

```

%Smtrx.m
%*****
%File Smtrx.m
%Function that takes skew symmetric matrix of input
%Written by Ceren KAPLAN and Soner KARATAS
%December 2005
%i denotes the input matrix
%*****

function S = Smtrx(i)
S =[0 -i(3) i(2)
    i(3) 0 -i(1)
    -i(2) i(1) 0];

```

```

%*****
%t_aero.m
%A file to calculate the aerodynamic torque
%Written by Ceren KAPLAN and Soner KARATAS
%December 2005
%*****

function torque = t_aero

% torque = [(1/2)*rho*Cd*A*v*v]*rt;
% torque = F_aero*rt;
% F_aero=[(1/2)*rho*Cd*A*v*v]

MU=3.986e14;    %MU [m^3/s^2]:gravitational parameter for the central body
re_e = 6.378137e6; %re_e [m]:Equatorial radius of Earth
h_s = 686e3;    %h_s [m]:Satellite orbit
r=re_e+h_s;    %r [m]:Distance from satellite to Earth center
a=r;          %a [m]:semimajor axis of the orbit
              %when the orbit was taken circular

v = sqrt((2*MU/r) - (MU/a)); %v [m/s]:the velocity of the spacecraft
              %(velocity at perigee)

rho=2.89*10^-13; %rho [kg/m^3]:Atmospheric density
Cd=2;          %Cd :the coefficient of drag on the spacecraft
A=0.42;       %A [m^2]:Projection area

F_aero = (1/2)*rho*Cd*A*v*v; %F_aero [N]:aerodynamic drag force

rt=0.05;      %rt [m]:(c_pa-c_g)the moment arm for the drag force
              %(center of pressure -center of mass)

torque = F_aero*rt; % aerodynamic torque [N*m]

```

APPENDIX C – TETRAHEDRAL CONFIGURATION ANGLE

Figure C.1 shows the general form of the tetrahedral configuration.

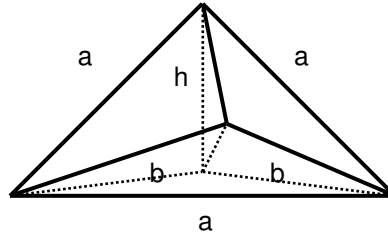


Figure C.1 : Tetrahedral Configuration.

Using the model given in equation C.1 tetrahedral configuration angle can be calculated.

By using cosine theorem, the relationship between a and b sides can be derived as,

$$a^2 = b^2 + b^2 - 2b^2 \cos(120^\circ) \quad (C.1)$$

Then,

$$a^2 = 2b^2 \left(1 + \frac{1}{2}\right) \Rightarrow b = \frac{a}{\sqrt{3}} \quad (C.2)$$

Also,

$$h^2 + b^2 = a^2 \Rightarrow h^2 = a^2 - \frac{a^2}{3} \Rightarrow h = a\sqrt{\frac{2}{3}} \quad (C.3)$$

Figure C.2 shows the geometric relationship between the angle φ and the sides of the tetrahedral configuration (a, b, h and x).

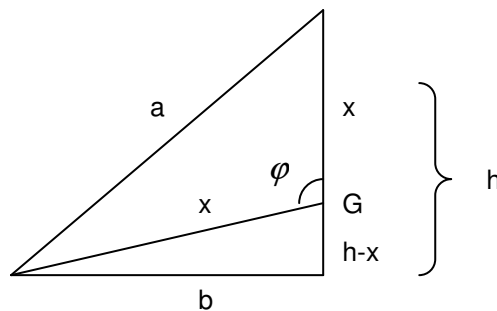


Figure C.2: Geometric Relationship between the Angle φ and sides.

Following equations are derived according to Figure C.2,

$$x^2 = b^2 + (h - x)^2 \quad (\text{C.4})$$

Then,

$$x = \frac{b^2 + h^2}{2h} \quad (\text{C.5})$$

Equations C.2 and C.3 are applied to C.5, and x can be found as,

$$x = \frac{\frac{a^2}{3} + 2\frac{a^2}{3}}{2a\sqrt{\frac{2}{3}}} \Rightarrow x = a\sqrt{\frac{3}{8}} \quad (\text{C.6})$$

Again using cosine law,

$$x^2 + x^2 - 2x^2 \cos \varphi = a^2 \quad (\text{C.7})$$

Equation C.6 to Equation C.7 are applied, and the angle φ is found as,

$$\cos \varphi = -\frac{1}{3} \Rightarrow \varphi = \cos^{-1}\left(-\frac{1}{3}\right) \Rightarrow \varphi = 109.47^\circ \quad (\text{C.8})$$